

An Adaptive Orthogonal Frequency Division Multiplexing Baseband Modem for Wideband Wireless Channels

by

Jit Ken Tan

B.S., Carnegie Mellon University (2003)

Submitted to the Department of Electrical Engineering and Computer Science

in partial fulfillment of the requirements for the degree of

Master of Science

at the

MASSACHUSETTS INSTITUTE OF TECHNOLOGY

May 2006

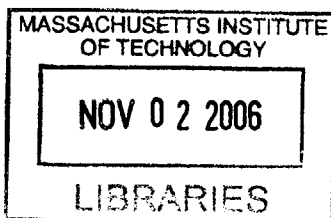
© Massachusetts Institute of Technology 2006. All rights reserved.

Author
Department of Electrical Engineering and Computer Science
May 12, 2006

Certified by
Charles G. Sodini
Professor
Thesis Supervisor

Accepted by
Arthur C. Smith

Chairman, Department Committee on Graduate Students



An Adaptive Orthogonal Frequency Division Multiplexing Baseband Modem for Wideband Wireless Channels

by

Jit Ken Tan

Submitted to the Department of Electrical Engineering and Computer Science
on May 12, 2006, in partial fulfillment of the
requirements for the degree of
Master of Science

Abstract

This thesis shows the design of an Orthogonal Frequency Division Multiplexing baseband modem with Frequency Adaptive Modulation protocol for a wideband indoor wireless channel. The baseband modem is implemented on a Field Programmable Gate Array and uses 294,939 2-input NAND gates with a clock frequency of 128 MHz. The Frequency Adaptive Modulation algorithm is 6% of the entire baseband modem which means that it is of low complexity.

The baseband modem is then integrated with a RF Front End. The maximum transmit power of the RF Front End is 7.5 dBm. This prototype takes 128 MHz of bandwidth and divides it into 128 1-MHz bins. The carrier frequency is at 5.25 GHz. Measurements are taken with this prototype to investigate the concept of Frequency Adaptive Modulation. With a target uncoded Bit Error Rate of 10^{-3} , it is found at distances of 1.0m to 10.8m, the data rate varies from 355 Mbps to 10 Mbps. The average data rate of this system is 2.57 times the average data rate without Frequency Adaptive Modulation. The fact that a Rayleigh channel is decomposed into Gaussian sub-channels through Frequency Adaptive Modulation is also verified.

Thesis Supervisor: Charles G. Sodini
Title: Professor

Acknowledgments

I would like to thank the following: my advisor Charlie Sodini for his tutorage - I am fortunate to have an advisor who fosters both intellectual and professional development; Team members Farinaz Edalat, Nir Matalon, Khoa Nguyen and Albert Jerng who make the project I am working on possible; Undergraduate research assistants, Raymond Wu, Justin Pun and Indy Yu for their help in the project; Mark Spaeth for consultation on the practical aspects of putting a prototype together; Professor Sodini and Professor Lee's research group who enrich the intellectual environment in the office and making the office a fun place to work; Rhonda Maynard for her administrative help; My family who has emotionally and financially supported me undertaking my education here away from home; and God who has blessed me with this opportunity to be here.

This material is based upon work supported by the National Science Foundation under Grant No. ANI-0335256. Any opinions, findings, and conclusions or recommendations expressed in this material are those of the author(s) and do not necessarily reflect the views of the National Science Foundation.

Contents

1	Introduction	15
1.1	Wideband Transceivers	15
1.2	Use of OFDM in Wideband Transceivers	16
1.3	Frequency Adaptive Modulation	17
1.4	MIT WiGLAN Node	20
1.5	Outline of Thesis	22
2	Wireless Gigabit Local Area Network	23
2.1	Indoor Channel Model	23
2.2	CP Requirement	24
2.2.1	Mathematical Form of OFDM with CP	26
2.2.2	CP Length	28
2.3	Frequency Diversity Order of WiGLAN	29
2.4	N_{FFT} based on Frequency Diversity Order and CP length	30
2.5	Key Parameters in the WiGLAN	31
2.6	Summary	32
3	An OFDM Baseband Transceiver	35
3.1	Effect of RF Front End on sub-carrier usage	36
3.2	QAM	38
3.3	Practical Transmission Model	42
3.3.1	Effects of Carrier and Sampling Frequency Offsets	43
3.3.2	Effects of Phase Noise	47

3.3.3	Bit Resolution of ADC and DAC	47
3.4	Receiver Design	48
3.4.1	Packet Detection	49
3.4.2	CFO Estimation and Correction	51
3.4.3	Channel Estimation and Correction	53
3.4.4	Phase Tracking	55
3.5	OFDM Transmitter	58
3.5.1	Clipper	61
3.5.2	PA Control at the Transmitter	64
3.6	Summary	65
4	Frequency Adaptive Modulation	67
4.1	Networking Aspects on the WiGLAN	68
4.1.1	Integration of the Physical Layer with the MAC layer	68
4.1.2	Bit Error Rate	68
4.2	Step 1: SNR Estimation	69
4.2.1	SNR Estimation	71
4.2.2	Sub-carrier Modulation Assignment	74
4.3	Step 2: CSI Feedback	76
4.4	Step 3: Data	78
4.5	Summary	79
5	Results and Analysis	81
5.1	Logic Utilization of the WiGLAN Baseband Node	81
5.2	Measurement Test setup	87
5.3	Channel Measurements	88
5.4	Analysis	89
5.4.1	Path Loss Exponent In the Lab	97
5.4.2	Decomposition of Rayleigh Channel to Gaussian sub-carriers .	98
5.4.3	Data Rate of the WiGLAN ignoring Frequency Adaptive Modulation Overhead	100

5.4.4	Data Rate of WiGLAN with Frequency Adaptive Modulation Overhead	102
5.4.5	Data Rate of a normal OFDM System	104
5.4.6	Comparison of WiGLAN to a normal OFDM system	105
5.5	Summary	107
6	Conclusions and Future Research	109
6.1	Conclusions	109
6.2	Future Research	111
6.2.1	Adaptive CP	111
6.2.2	Reduction of PAPR	112
6.2.3	Adaption of Pilot Sub-carriers	113
6.2.4	Development of Better SNR Estimation Scheme	113
6.2.5	Use of OOK	114
A	Acronyms	115

List of Figures

1-1	Spectral Efficiency Through Overlap and Orthogonality of the subcarriers	17
1-2	BER Performance for BPSK under Rayleigh and Gaussian Conditions	18
1-3	Frequency Adaptive Modulation Used: Optimization of Data Rate . .	19
1-4	Measurement: Frequency Adaptive Modulation In Action	19
1-5	RF Front End Schematic	21
1-6	WiGLAN Node	21
2-1	Need of a CP in a Wireless Channel	25
2-2	Simple Implementation of OFDM Baseband Modem	27
2-3	Example of the excess delay spread on a Power Delay Profile	28
3-1	Entire OFDM Baseband Transceiver	35
3-2	Ease of Reconstruction Filter based on number of subcarriers used .	37
3-3	Different in Constellations with same maximum power and same average power	40
3-4	QAM Constellation Map	41
3-5	Complete baseband transmission model	43
3-6	Subcarrier symbol rotation due to SFO and CFO	44
3-7	ICI resulting from CFO δf	45
3-8	OFDM symbol window drift due to sampling frequency offset	46
3-9	Receiver Design	48
3-10	Double Sliding Window Packet Detection Algorithm	50
3-11	WiGLAN Implementation of Packet Detection	52

3-12	Implementation of CFO Estimator and Corrector	53
3-13	Implementation of Channel Estimator and Corrector	56
3-14	Insertion of pilot subcarriers to estimate time-varying phase rotation	58
3-15	Implementation of Phase Tracking Module	59
3-16	OFDM Transmitter	60
3-17	Rare Occurrence of Large Peaks in OFDM Signal	62
3-18	Clipper Implementation	65
4-1	Protocol for Frequency Adaptive Modulation	68
4-2	Packet Structure during SNR Estimation	69
4-3	SNR Margin	73
4-4	Adaptive Modulation Assignment with target BER of 10^{-3}	75
4-5	Packet Structure during CSI Feedback	77
4-6	Packet Structure during Data Transmission	78
5-1	Baseband Modem Implementation on FPGA	82
5-2	Location of transmitter-receiver pair in the Lab	86
5-3	Measurements for Location A-B	90
5-4	Measurements for Location C-D	91
5-5	Measurements for Location D and E	92
5-6	Measurements for Location F and G	93
5-7	Measurements for Location H and I	94
5-8	Measurements for Location J and K	95
5-9	Mean SNR vs $-10\log_{10}(d)$	99
5-10	Rayleigh Fading Channel decomposed to Gaussian sub-carriers (System BER $\geq 2.4 \times 10^{-6}$ and Sub-carrier BER $\geq 2.2 \times 10^{-4}$ shown) . . .	100
5-11	Data Rate vs Link Distance	101
5-12	Effective Data Rate vs. Link Distance	103

List of Tables

1.1	Summary of RF Front End Specifications	22
1.2	Summary of Baseband Specifications	22
2.1	Coherence Bandwidth in Indoor Conditions	30
2.2	Summary of Indoor Channel Characteristics for Link Distance up to 10m	32
2.3	Summary of Key System Parameters based on the Channel	32
3.1	Modulation dependent variables	38
3.2	BPSK Encoding Table	38
3.3	4-QAM Encoding Table	38
3.4	16-QAM Encoding Table	39
3.5	64-QAM Encoding Table	39
3.6	256-QAM Encoding Table	39
4.1	$SNR_{margin}(dB)$ for different N given $\chi = 7^{-6}$	73
4.2	Making Modulation Assignment based on $\hat{\sigma}_k^2$	76
5.1	Number of 2-input NAND gates of Transmitter and Receiver	83
5.2	Number of 2-input NAND gates of IFFT/FFT Module	83
5.3	Estimated Number of 2-input NAND gates of Transceiver	83
5.4	Number of 2-input NAND gates of Frequency Adaptive Modulation blocks	84
5.5	Link Distance for various measurements	85
5.6	Adaptive Modulation Assignment for Location A to D	89

5.7	Adaptive Modulation Assignment for Tx Location E to H	96
5.8	Adaptive Modulation Assignment for Tx Location I to L	96
5.9	Measured Mean SNR and System BER of a normal OFDM System in various locations ($\text{BER} \geq 2.4 \times 10^{-6}$ shown)	97
5.10	WiGLAN Data Rate for location A to L	101
5.11	Effective WiGLAN Data Rate And Data Loss from Overhead for loca- tion A to K	104
5.12	Finding the highest QAM modulation that yield a $\text{BER} \leq 10^{-3}$ for a normal OFDM System at Locations A to L (BPSK $\text{BER} \geq 2.4 \times 10^{-6}$ shown)	105
5.13	Data Rate for normal OFDM System at location A to K	106
5.14	Throughput gain of WiGLAN compared to Normal OFDM System .	107
6.1	Summary of Baseband Specifications	110
6.2	Summary of RF Front End Specifications	110

Chapter 1

Introduction

The Wireless Gigabit Local Area Network (WiGLAN) project [1] at MIT seeks to prototype a baseband modem that utilizes a combination of 1) Wide bandwidth 2) Orthogonal Frequency Division Multiplexing (OFDM) and 3) Frequency adaptive modulation to drive data rate up in a wireless indoor environment. The focus of this thesis is to document the implementation of this prototype and the analysis of indoor measurements using this prototype with a radio-frequency (RF) Front End.

1.1 Wideband Transceivers

The Shannon-Hartley Capacity Theorem states that the capacity C of the channel is the following function of the signal bandwidth W and the average signal-to-noise ratio (SNR)

$$C = W \log_2 (1 + SNR) \quad (1.1)$$

Hence there is a natural tendency to increase the bandwidth W in today's pursuit of achieving higher data rate. Examples of this occurrence are manifested in the following wireless standards:

- Local Area Networks: The most well-known wireless standard would be 802.11a [2] with a bandwidth of 20 MHz and an uncoded data rate of 72 Mbps. There is a new 802.11n proposal [3] to combine a bandwidth increase of 40 MHz together

with multiple antennas to drive the uncoded data rate up to 720 Mbps.

- Personal Area Networks: There is an ultra-wideband proposal [4] to use 528 MHz bandwidth to achieve an uncoded data rate of 640 Mbps.

1.2 Use of OFDM in Wideband Transceivers

Increasing the signal bandwidth W for a data signal on a single carrier might be problematic if the frequency selective fading condition occurs

$$W \gg W_c \quad (1.2)$$

where W_c is defined as the coherence bandwidth of the channel.

Definition 1.2.1. The coherence bandwidth, W_c , is a statistical measure of the range of frequencies over which the channel can be considered flat (i.e. a channel which passes all spectral components with approximately equal gain and linear phase) [5].

If frequency selective fading occurs, a complex multi-tap equalizer is required. One method of mitigating frequency selective fading while maintaining a large bandwidth is OFDM. In OFDM, the entire channel bandwidth is divided into several narrow sub-bands where each sub-band will experience flat fading. The flat fading condition is favored in communication systems because it reduces the complex multi-tap equalizer in the frequency selective fading case to a simple one-tap equalizer.

In addition, OFDM is a spectral efficient modulation scheme as there is spectral overlap with the sub-carriers as seen in Figure 1-1. Recovery of data despite of spectral overlap is possible because each sub-channel is orthogonal to each other. Currently, the use of OFDM is quite pervasive in the today's wireless standards [2, 3, 4]

However the use of OFDM has its disadvantages:

1. The peak-to-average power ratio (PAPR) of the transmitted signal is very high. Distortion from non-linearity will result unless a power backoff of the power

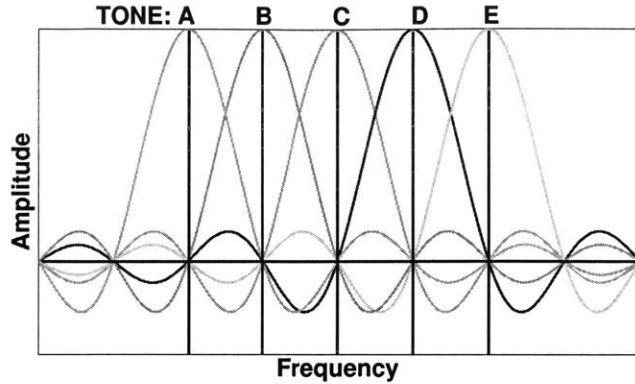


Figure 1-1: Spectral Efficiency Through Overlap and Orthogonality of the sub-carriers

amplifier (PA) is exercised. This leads to a situation where there is a tradeoff between power efficiency of the PA and non-linear distortion.

2. Due to the spectral overlap of the sub-channels, OFDM is sensitive to mismatches in the transmit-receive oscillators, phase noise and Doppler effects.

More details about OFDM systems will be provided in Chapter 3.

1.3 Frequency Adaptive Modulation

In today's wireless standards [2, 3, 4], there is a rate adaptation mechanism where the modulation scheme is changed subject to the constraint that this modulation scheme is the same for all OFDM sub-carrier. This is optimal provided that all the sub-carriers are highly correlated (i.e. if one channel can support a particular modulation scheme, all the other sub-carriers would be able to support it too).

Let's examine the ramifications of keeping the modulation scheme in each OFDM sub-carrier constant when each sub-carrier is independent. Independence of sub-carriers is typical in wideband communication where each sub-carrier is sufficiently spaced apart. In this scenario, it could make sense to estimate the SNR on each sub-carrier and adapt the modulation scheme on a sub-carrier basis. This enables each sub-carrier to be fully utilized hence the throughput of the system should increase as a result of performing adaptive modulation on a per sub-carrier basis.

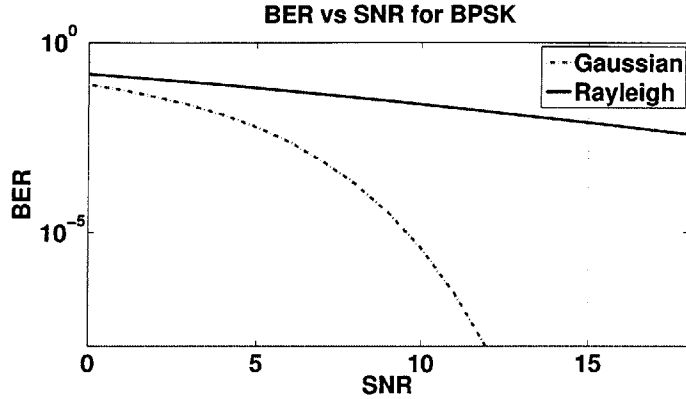


Figure 1-2: BER Performance for BPSK under Rayleigh and Gaussian Conditions

Under the same scenario where each sub-carrier is independent, the attenuation on each sub-carrier can be modeled as Independently and Identically Distributed (iid) random variables drawn from a Rayleigh distribution. If all the sub-carriers use the same modulation scheme, it can be said that Rayleigh fading across the frequency dimension is experienced by the system. The defining characteristic of this Rayleigh fading is having data transmission even on sub-carriers experiencing deep fades. Frequency Adaptive Modulation can be used to counter this Rayleigh fading. The sub-carriers experiencing deep fades are not used. Essentially, the Frequency Adaptive Modulation has reduced the Rayleigh fading channel to independent Gaussian sub-channels. The Bit Error Rate (BER) performance of a Rayleigh Channel and a Gaussian channel for Binary Phase-Shift Keying (BPSK) is shown in Figure 1-2. Also note that channel coding performs better in a Gaussian channel compared to a Rayleigh channel [6]. When channel coding is applied to a system, greater gain is derived when Frequency Adaptive Modulation is used.

Having examined two extreme scenarios where all the sub-carriers are either correlated or independent, it can be inferred that the goodness of Frequency Adaptive Modulation is related to the frequency diversity order of the system. The frequency diversity order can be defined as the number of independently fading propagation frequency paths. This can be expressed as a ratio of the signal bandwidth W to

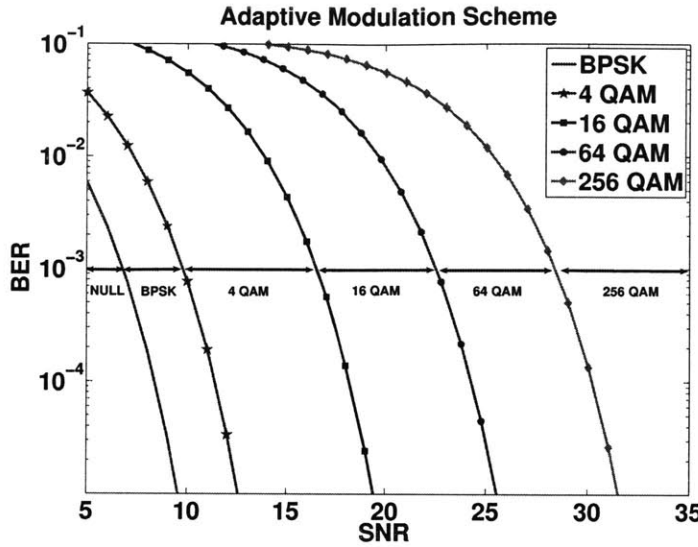


Figure 1-3: Frequency Adaptive Modulation Used: Optimization of Data Rate

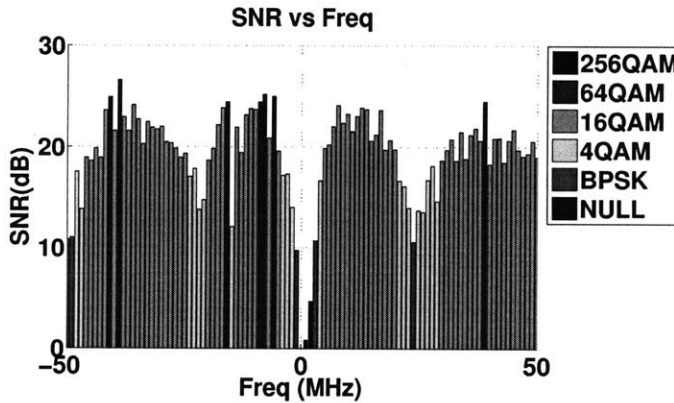


Figure 1-4: Measurement: Frequency Adaptive Modulation In Action

coherence bandwidth of the channel.

$$\text{Frequency Diversity Order} = \frac{W}{W_c} \quad (1.3)$$

Chapter 5 will explore empirically the goodness of adaptive modulation under various indoor channel conditions. When performing Frequency Adaptive Modulation, the criterion of optimization can be one of the following:

1. Data Rate.
2. Average Transmitting Energy.

3. BER.

In this project, the goal is to optimize the data rate of the system while keeping the average transmitting energy constant and the BER of the system below a particular threshold. Specifically, the WiGLAN scheme adopted maximizes data rate by using the most efficient modulation in each sub-channel allowed by its SNR while maintaining an uncoded BER less than 10^{-3} . This is shown in Figure 1-3. In Figure 1-4, the scheme is applied to an actual channel and the resulting adaption is shown.

It should be noted that Frequency Adaptive Modulation requires significant channel knowledge at the transmitter hence synchronization between the transmitter and receiver is required. The effective data rate can be expressed in the following equation

$$R_{eff} = \frac{R * T_{data}}{T_{data} + T_{sync}} \quad (1.4)$$

where

- R_{eff} is the effective data rate.
- R is the data rate during the payload.
- T_{data} is the length of the payload.
- T_{sync} is the time needed for synchronization between transmitter and receiver.

According to Equation 1.4, R_{eff} is optimized when T_{data} is large. However, T_{data} is limited by the expiration time to the channel knowledge acquired by the transmitter. In an indoor environment, the throughput gain of Frequency Adaptive Modulation is best appreciated as the channel is static for a relatively long time such as 10ms. Characteristics of the indoor channel will be explored in Chapter 2. In Chapter 5, the effective throughput gain is quantified with respect to Equation 1.4.

1.4 MIT WiGLAN Node

The WiGLAN Node is the prototype transceiver shown in Figure 1-6, used to conduct indoor channel experiments. The transceiver consists of two portions:

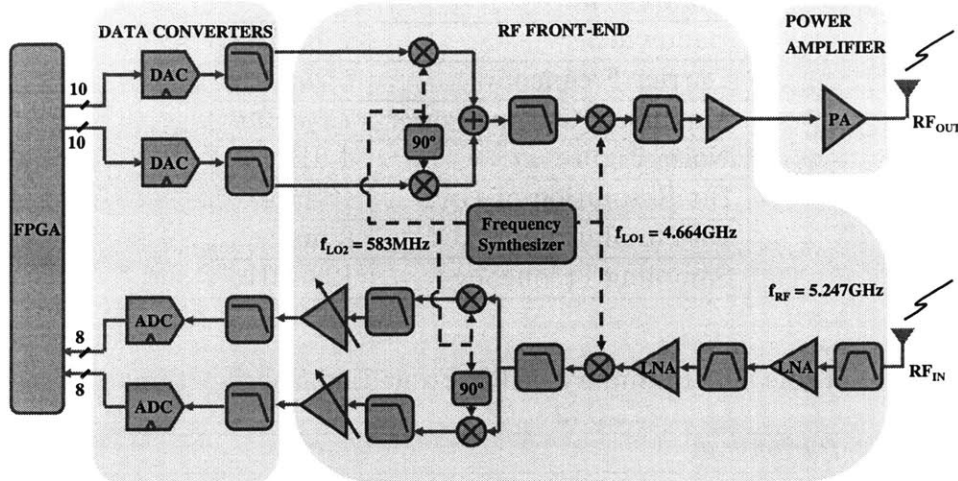


Figure 1-5: RF Front End Schematic

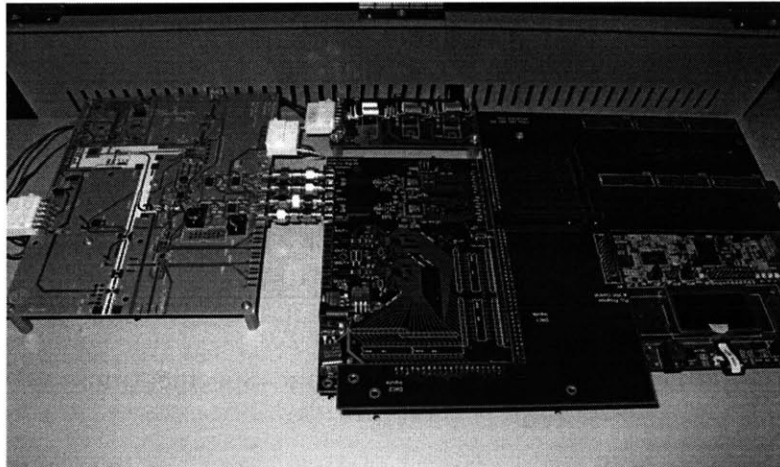


Figure 1-6: WiGLAN Node

1. *Baseband Modem:* This is extensively documented in this thesis.
2. *RF Front End:* The RF Front End is a custom system made with discrete components. The RF Front End Node Schematic can be found in Figure 1-5. More details can be found in [7]. A summary of this RF Front End specifications can be found in Table 1.1.

The summary of specifications for baseband modem can be found in Table 1.2. The baseband modem is implemented on a Xilinx SX35 Field Programmable Gate Array (FPGA) mounted on an Avnet Evaluation Board. System Generator for DSP

<i>Parameter</i>	<i>Value</i>
Bandwidth	128 MHz
Carrier Frequency	5.25 GHz
Maximum Output Power	7.5 dBm
Noise Figure	4 dB
Bit Resolution of DAC	10 bits
Bit Resolution of ADC	8 bits
Sampling Frequency	128 MHz

Table 1.1: Summary of RF Front End Specifications

<i>Parameter</i>	<i>Value</i>
Sampling Frequency	128 MHz
Sub-carrier Frequency Spacing	1 MHz
Number of data sub-carriers	119
Number of pilot sub-carriers	8
IFFT/FFT Period	1 μ s
Cyclic Prefix (CP)	.2 μ s
Symbol Period	1.2 μ s
Uncoded BER	10^{-3}
Modulation Per Bin	BPSK, 4, 16, 64, 256 QAM
Max Link Distance	10 m

Table 1.2: Summary of Baseband Specifications

is the software tool utilized to generate the Register Transfer Level (RTL) code for the FPGA.

1.5 Outline of Thesis

Chapter 2 describes the indoor channel model and its effects on the system. Chapter 3 reviews the basic OFDM transceiver architecture and implementation. Chapter 4 delves into the adaptive modulation scheme. Chapter 5 documents the indoor channel measurements and analyzes it. Chapter 6 concludes and provides directions for further work.

Chapter 2

Wireless Gigabit Local Area Network

In this chapter, the Wireless Gigabit Local Area Network (WiGLAN) specifications affected by the characteristics of the indoor environment are discussed, namely the Cyclic Prefix (CP), the system bandwidth and number of sub-carriers available for use.

2.1 Indoor Channel Model

In the wireless environment, the signal at the transmitter can travel on multiple paths to reach the receiver. The signal seen at the receiver will be the sum of the transmitted signal from multiple paths characterized with different amplitude and phase. In a wireless environment where motion is prevalent, the multiple paths taken by the transmitted signal to receiver will change over time.

Mathematically, the channel can be modeled as a Finite Impulse Response (FIR) filter with time-varying tap values.

$$h(\tau, t) = \sum_i h_i(t) \cdot \delta(\tau - \tau_i) \quad (2.1)$$

If data transmission is confined to the coherence time T_c of the channel, the channel

can be modeled as a linear and time-invariant (LTI) system

$$h(t) = \sum_i h_i \cdot \delta(t - t_i) \quad (2.2)$$

Definition 2.1.1. The coherence time, T_c is a statistical measure of the time duration over which the channel impulse response is essentially invariant [5].

$$\begin{aligned} T_c &= \sqrt{\frac{9}{16\pi f_m^2}} \\ f_m &= v/\lambda \end{aligned} \quad (2.3)$$

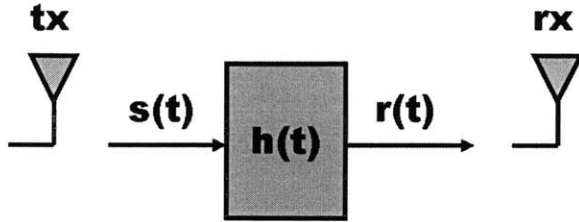
where

- v is the maximum velocity of transceiver.
- λ is the wavelength of the carrier frequency.

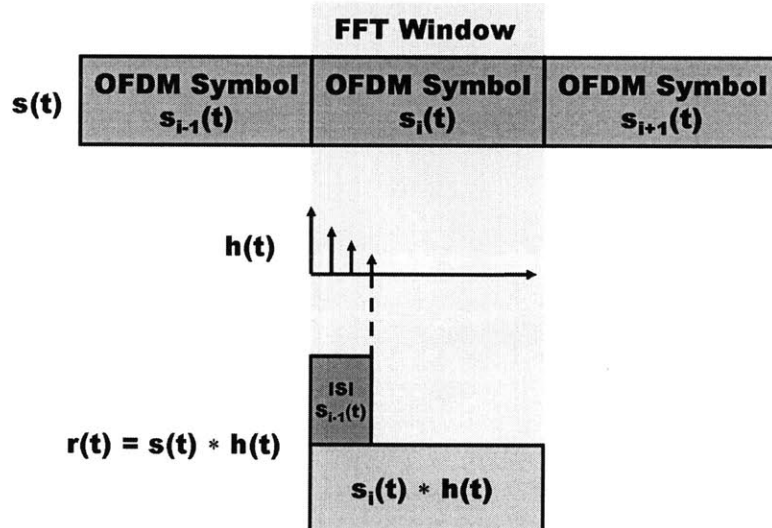
In the context of the WiGLAN project with a carrier frequency of 5.25 GHz and the maximum velocity v of 1 m/s (walking speed) in an indoor environment, T_c as computed by Equation 2.3 is 24 ms. For the rest of the thesis, the channel will be modeled as an LTI system as the assumption is made that continuous data transmission for the WiGLAN project will not exceed 10 ms.

2.2 CP Requirement

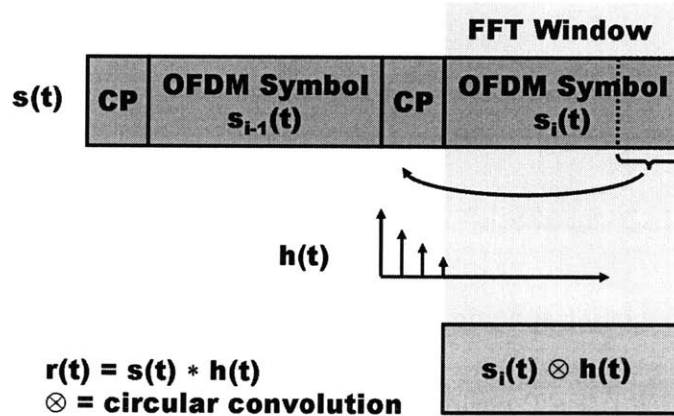
When transmitting in the wireless channel, the received Orthogonal Frequency Division Multiplexing (OFDM) signal can be modeled as shown in Figure 2-1a. In this situation, Inter-symbol Interference (ISI) occurs between successive OFDM symbols as seen in Figure 2-1b. A CP can be inserted to avoid ISI as depicted in Figure 2-1c. Note that the length of the CP should be longer than the length of the channel impulse response for the condition of no ISI to hold true.



(a) Received signal model in a wireless channel



(b) Channel Causes ISI without CP



(c) Having CP prevents ISI

Figure 2-1: Need of a CP in a Wireless Channel

The next two sub-sections will express the mathematical form of an OFDM signal and find the length of the CP based on the length of the channel impulse response.

2.2.1 Mathematical Form of OFDM with CP

With the insertion of the CP, the mathematical form of the transmitted signal $s(t)$ looks like the following

$$s(t) = \frac{1}{\sqrt{T_{FFT}}} \sum_{i=-\infty}^{+\infty} \sum_{k=-K/2}^{K/2-1} X_{i,k} e^{j2\pi k \Delta_f (t - T_{CP} - iT_{SYM})} u(t - iT_{SYM}) \quad (2.4)$$

$$u(t) = \begin{cases} 1 & 0 \leq t < T_{FFT}, \\ 0 & \text{else.} \end{cases} \quad (2.5)$$

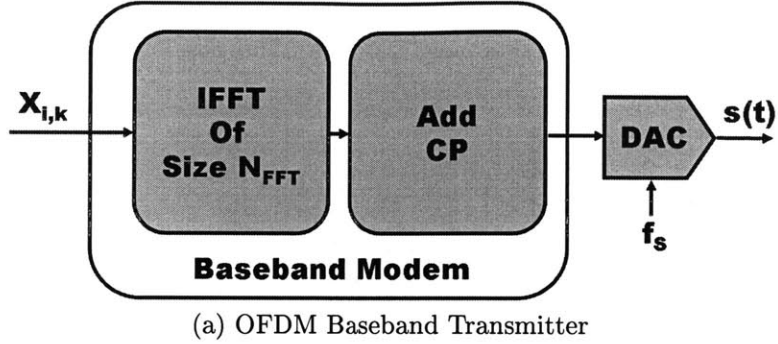
$$T_{FFT} = N_{FFT}/f_s \quad (2.6)$$

$$\Delta_f = 1/T_{FFT} \quad (2.7)$$

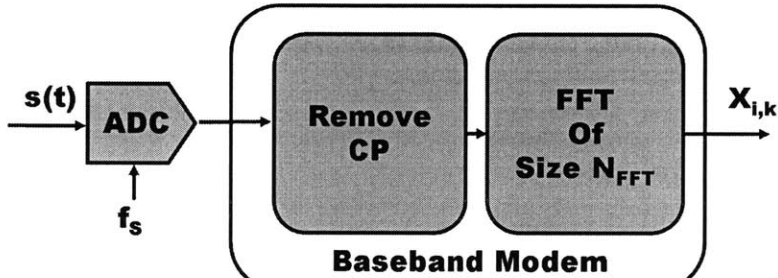
$$T_{SYM} = T_{FFT} + T_{CP} \quad (2.8)$$

where

- i is the time symbol index.
- k is the frequency index.
- K is the number of sub-carrier used.
- $X_{i,k}$ are the data symbols.
- Δ_f is the sub-carrier spacing.
- T_{FFT} is the IFFT/FFT period.
- N_{FFT} is the maximum of sub-carriers.
- f_s is the sampling frequency of the system.
- T_{CP} is the length of the cyclic prefix.



(a) OFDM Baseband Transmitter



(b) OFDM Baseband Receiver

Figure 2-2: Simple Implementation of OFDM Baseband Modem

- T_{SYM} is the period of a OFDM symbol inclusive of the CP.

Based on Equation 2.4, the OFDM baseband transceiver can be implemented as shown in Figure 2-2.

In addition, the insertion of the CP converts linear channel convolution into circular convolution. If $s_i(t)$ is the transmitted i^{th} OFDM symbol and $r_i(t)$ is the received i^{th} OFDM symbol, $r_i(t)$ has the following relationship

$$s_i(t) \xrightarrow{FFT} S_i(f) \quad (2.9)$$

$$h(t) \xrightarrow{FFT} H(f) \quad (2.10)$$

$$r_i(t) \xrightarrow{FFT} R_i(f) = S_i(f)H(f) \quad (2.11)$$

The demodulated data symbol $R_{i,k}$ can be expressed as a multiplication of the original data symbol $X_{i,k}$ and a constant factor H_k . Hence to recover the data symbol,

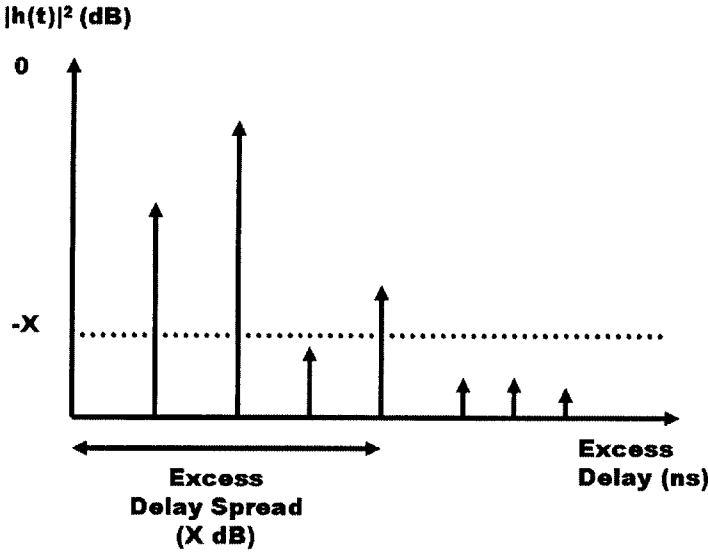


Figure 2-3: Example of the excess delay spread on a Power Delay Profile

a simple one-tap equalizer is required.

$$R_{i,k} = R_i \left(\frac{k}{T_{FFT}} \right) \quad (2.12)$$

$$X_{i,k} = S_i \left(\frac{k}{T_{FFT}} \right) \quad (2.13)$$

$$H_k = H \left(\frac{k}{T_{FFT}} \right) \quad (2.14)$$

$$R_{i,k} = X_{i,k} H_k \quad (2.15)$$

2.2.2 CP Length

The length of CP needs to be longer than the length of the channel response. The length of the channel response can be quantified using excess delay spread (X dB) of the channel.

Definition 2.2.1. The excess delay spread is defined to be the time delay during which multipath energy falls to X dB below the maximum [5].

An example of the excess spread can be found in Figure 2-3

The value of X should be based on the noise floor faced by the receiver. Multipath components below the noise floor do not contribute significantly to ISI and therefore

can be discounted. A conservative way of choosing X is to determine the maximum noise floor the system can tolerate with its most efficient modulation scheme without compromising the Bit Error Rate (BER). In the context of the WiGLAN, the most efficient modulation scheme is 256 Quadrature Amplitude Modulation (QAM) with a target BER of 10^{-3} . The minimum signal-to-noise ratio (SNR) required for this is 28.42 dB which corresponds to $X = 28.42$ dB [8].

Another fact to note is that as the link distance increases, the excess delay spread (X dB) increases. Physically, it means that the difference between shortest path and the longest path from the transmitter and receiver increases as a function of link distance. In the WiGLAN system, the maximum link distance is 10m. As reported in [8], for a link distance up to 10m, $X = 30$ dB and a center frequency of 5 GHz, the excess delay spread is bounded by 70 ns.

However, in a practical OFDM system, having the length of CP be exactly the excess delay spread (30 dB) leaves no room for timing estimation errors. Hence, in the conservative design of the WiGLAN system, the length of CP used is 200 ns. It's noted that the data rate of the system decreases as the length of CP increases. The exact relationship of the effective data rate R_{eff} can be expressed as the following

$$R_{eff} = \frac{T_{FFT} \cdot \text{Bits Per OFDM Symbol}}{T_{CP} + T_{FFT}} \quad (2.16)$$

2.3 Frequency Diversity Order of WiGLAN

Recall from Section 1.3, the goodness of Frequency Adaptive Modulation of the WiGLAN system is dependent on the frequency diversity order of the system which can be expressed as the ratio of the signal bandwidth W to the coherence bandwidth W_c . In the literature, the W_c is normally not explicitly stated. However, W_c can be derived from the rms delay spread σ_τ reported in papers with channel measurements.

<i>Link Distance</i>	σ_τ [8]	$W_c/2\pi$ (Equation 2.17)
1 m	2 ns	10 MHz
10 m	10 ns	2 MHz

Table 2.1: Coherence Bandwidth in Indoor Conditions

The equations for W_c [5] and σ_τ [8] are as follows

$$W_c \approx \frac{2\pi}{50\sigma_\tau} \quad (2.17)$$

$$\sigma_\tau = \sqrt{\sum_i (\tau_i - \tau_m)^2 |h(\tau_i)|^2} \quad (2.18)$$

$$\sigma_m = \sum_i \tau_i \cdot |h(\tau_i)|^2 \quad (2.19)$$

The coherence bandwidth in indoor conditions is summarized in Table 2.1.

For any given W_c , to obtain the maximum frequency diversity order, the signal bandwidth would be as large as possible. The signal bandwidth W in an OFDM system is bounded by the sampling frequency f_s . With today's technology of prototyping the baseband modem on Field Programmable Gate Array (FPGA), it is found that the fastest sampling frequency without having to resort to intensive pipelining of the system is 128 MHz.

For the WiGLAN system where $f_s = 128$ MHz and W_c in Table 2.1, the frequency diversity order ($= W/W_c$) can range from 12.8 to 64. For Frequency Adaptive Modulation to show an improvement compared to today's wireless standards [2, 3, 4] where the same modulation for all sub-carriers is used, frequency diversity order needs to be greater than 2 (i.e. at least two independent fading frequency paths).

2.4 N_{FFT} based on Frequency Diversity Order and CP length

The N_{FFT} selected for the WiGLAN is 128. There are several design considerations to arrive at this final number:

1. To enable a simple implementation of the Inverse Fast Fourier Transform (IFFT) and fast fourier transform (FFT), N_{FFT} should be a power of 2 [9].
2. To fully utilize the frequency diversity order in the WiGLAN system, the number of sub-carriers should be at least the maximum frequency diversity order available to the system (i.e. $N_{FFT} = 64$). Increasing N_{FFT} further will not yield better frequency diversity order.
3. For faster data rate, the T_{cp}/T_{FFT} should be kept as low as possible where $T_{FFT} = \frac{N_{FFT}}{f_s}$ (i.e. keeping the ratio of overhead to payload small). A good rule of the thumb from wireless standards [2, 3, 4] is the following:

$$T_{cp}/T_{FFT} < 0.3 \quad (2.20)$$

From Section 2.2.2 and 2.3, it is determined that $T_{cp} = .2$ ns and $f_s = 128$ MHz. Under these conditions, it is found from equation 2.20 that $N_{FFT} > 85.3$.

2.5 Key Parameters in the WiGLAN

From previous sections, several key parameters of the WiGLAN has been computed:

- From Section 2.2.2, $T_{cp} = .2$ ns for a maximum link distance of 10m.
- From Section 2.3, $f_s = 128$ MHz.
- From Section 2.4, $N_{FFT} = 128$.

From the above information and Equations 2.6 to 2.8, the other key parameters of the system can also be derived

- $T_{FFT} = 1 \text{ } \mu\text{s.}$
- $T_{SYM} = 1.2 \text{ } \mu\text{s.}$
- $\Delta_f = 1 \text{ } \text{MHz.}$

<i>Specification</i>	<i>Value</i>
Coherence Time	24 ms
Excess Delay Spread(30 dB)	70 ns
Coherence Bandwidth	2 to 10 MHz

Table 2.2: Summary of Indoor Channel Characteristics for Link Distance up to 10m

<i>Variable</i>	<i>Value</i>
FFT Size, N_{FFT}	128
CP Length, T_{CP} ,	.2 μ s
IFFT/FFT Period, T_{FFT}	1 μ s
OFDM Symbol Period, T_{SYM}	1.2 μ s
Inter sub-carrier spacing, Δ_f	1 MHz
Maximum transmission Time	10 ms
Maximum Link Distance	10m
Frequency Diversity Order	12.8 to 64

Table 2.3: Summary of Key System Parameters based on the Channel

2.6 Summary

Table 2.2 summarizes the indoor channel characteristics for link distance up to 10m.

Table 2.3 summarizes the key system parameters based on the channel. Several key points are made in this chapter:

- Continuous data transmission is confined to at most 10 ms so that the channel can be treated as an LTI system. An algorithm catering to a time-varying channel can be difficult to implement.
- A conservative CP of 200ns is inserted per OFDM symbol to prevent ISI.
- The WiGLAN system has a frequency diversity order of 12.8 to 64 which indicates that frequency adaptive modulation is ideal for this system.
- N_{FFT} is selected to be 128.
 - It is big enough to exploit the frequency diversity order available in the channel.

- It is small enough so that the resultant degradation to data rate due to insertion of CP is kept minimal.

Chapter 3

An OFDM Baseband Transceiver

From Chapter 2, a simple Orthogonal Frequency Division Multiplexing (OFDM) transceiver in the presence of a wireless channel is presented. However, the OFDM transceiver is more complex due to non-idealities from the radio-frequency (RF) Front End. In this Chapter, the entire OFDM baseband transceiver chain with the transmission model as seen in Figure 3-1 will be explored.

Bits transmitted are first Quadrature Amplitude Modulation (QAM)-modulated to symbols $X_{i,k}$. Each symbol is designated to frequency bin of index k and an OFDM symbol of time index i . Conversion of $X_{i,k}$ from the frequency domain to the time domain is performed by the OFDM transmitter. The time domain signal is sent through the transmission model. The transmission model models the wireless channel as well as the RF Front End non-idealities. The signal from the output of the transmission model is then processed by the OFDM receiver. The receiver will compensate for the effects of the transmission model. The output of the receiver is $\hat{X}_{i,k}$ which is the estimate of the QAM-modulated symbol $X_{i,k}$ sent. The QAM demodulator will then convert $\hat{X}_{i,k}$ to bits. Note that in the entire OFDM transceiver,

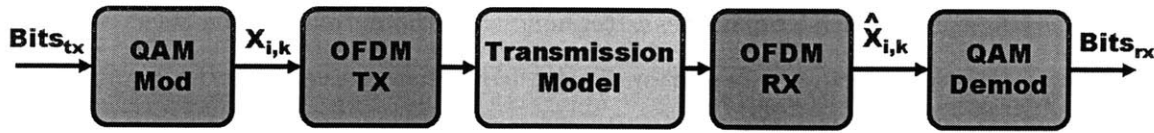


Figure 3-1: Entire OFDM Baseband Transceiver

not all the frequency bins are capable of being used due to the design and non-idealities of the RF Front End.

In the next few sections, the effect of the RF Front End on sub-carrier usage as well as the elements of the OFDM transceiver chain such as the QAM blocks, the transmission model, the OFDM receiver and transmitter will be explored in more details.

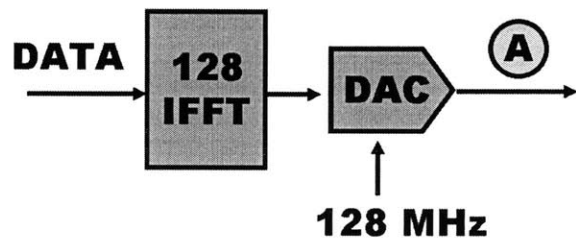
3.1 Effect of RF Front End on sub-carrier usage

In a practical implementation, not all the sub-carriers are used. As shown in Figure 3-2b, when all the sub-carriers are used, the bandwidth of the signal will be f_s and the signal and the mirror images will be next to each other. Hence, a brickwall reconstruction filter is required to filter out the mirror images. Brickwall reconstruction filters are impossible to construct as there is no transition region from the passband frequencies to the stopband frequencies. The constraints on reconstruction filter can be more relaxed by increasing the separation between the signal and the mirror images. This can be accomplished by not using some sub-carriers at the higher frequencies which is depicted in Figure 3-2c.

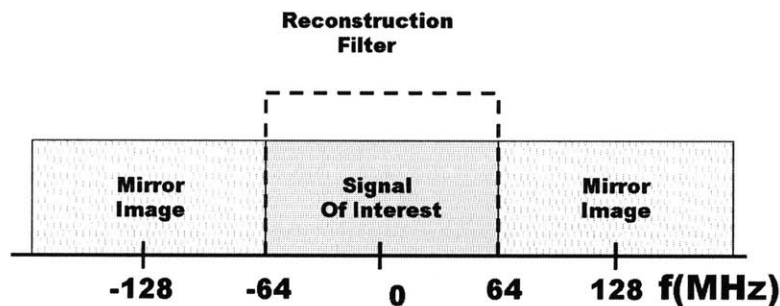
In addition, the DC sub-carrier is not used. There are intrinsic DC offsets occurring in the RF Front End which are removed by DC-coupling capacitors to achieve optimal swing in RF components. As a result, if a signal is sent at the DC sub-carrier, DC-coupling capacitors will either remove or highly attenuate that signal.

As later discussed in Section 4.3, during the stage of WiGLAN transmission when Channel State Information (CSI) per sub-carrier is unknown,

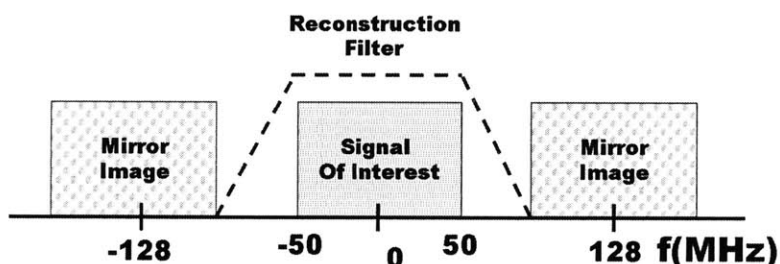
- DC sub-carrier is never used.
- 27 sub-carriers with the highest frequency components are not used to send when synchronization information is sent from the receiver and the transmitter because these sub-carriers lead into the transition band of the reconstruction. These sub-carriers might be heavily attenuated leading to high errors if data is



(a) 'A' Indicates where Frequency Plot is taken



(b) $f_s = 128$ MHz with all subcarriers used.



(c) $f_s = 128$ MHz with some subcarriers used.

Figure 3-2: Ease of Reconstruction Filter based on number of subcarriers used

<i>Modulation</i>	<i>N_{bits}</i>	<i>K_{mod}</i>
BPSK	1	1
4-QAM	2	$1/\sqrt{2}$
16-QAM	4	$1/\sqrt{10}$
64-QAM	6	$1/\sqrt{42}$
256-QAM	8	$1/\sqrt{170}$

Table 3.1: Modulation dependent variables

<i>Input bit(b₀)</i>	<i>I</i>	<i>Q</i>
0	-1	0
1	1	0

Table 3.2: BPSK Encoding Table

sent on them.

It is possible that the signal-to-noise ratio (SNR) of those sub-carriers is high enough to carry some data. Once CSI is available to the transmitter and receiver, the frequency adaptive modulation algorithm can assign data to those sub-carriers that are data-capable despite being in the transition band of the reconstruction filter.

3.2 QAM

At the transmitter, each k^{th} sub-carrier can either not be used or be modulated using Binary Phase-Shift Keying (BPSK), 4-QAM, 16-QAM, 64-QAM or 256-QAM. Depending on the modulation scheme, each modulated symbol can represent N_{bits} of data bits as shown in Table 3.1. The bits are first converted to I/Q pairs according to the encoding tables shown in Table 3.2 to Table 3.6 with the input bit, b_0 , being

<i>Input bit(b₀)</i>	<i>I</i>	<i>Input bit(b₁)</i>	<i>Q</i>
0	-1	0	-1
1	1	1	1

Table 3.3: 4-QAM Encoding Table

<i>Input bit(b_0b_1)</i>	<i>I</i>	<i>Input bit(b_2b_3)</i>	<i>Q</i>
00	-3	00	-3
01	-1	01	-1
11	1	11	1
10	3	10	3

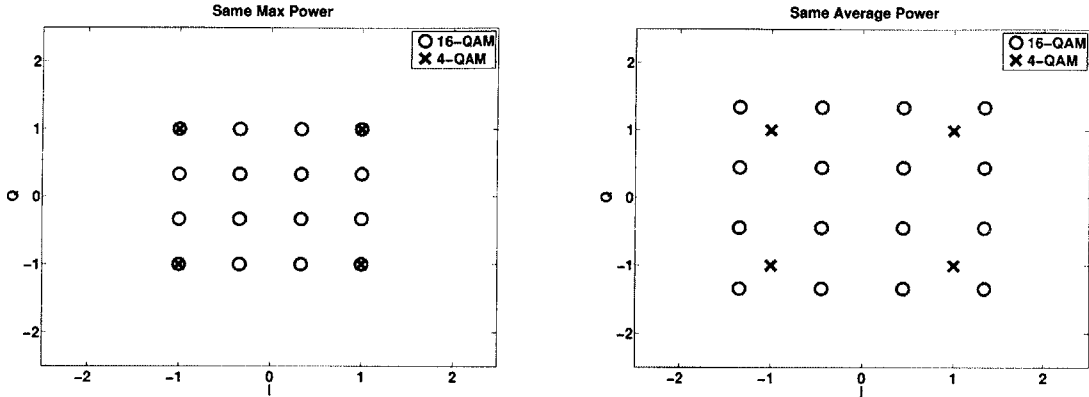
Table 3.4: 16-QAM Encoding Table

<i>Input bit($b_0b_1b_2$)</i>	<i>I</i>	<i>Input bit($b_3b_4b_5$)</i>	<i>Q</i>
000	-7	000	-7
001	-5	001	-5
011	-3	011	-3
010	-1	010	-1
110	1	110	1
111	3	111	3
101	5	101	5
100	7	100	7

Table 3.5: 64-QAM Encoding Table

<i>Input bit($b_0b_1b_2b_3$)</i>	<i>I</i>	<i>Input bit($b_4b_5b_6b_7$)</i>	<i>Q</i>
0000	-15	0000	-15
0001	-13	0001	-13
0011	-11	0011	-11
0010	-9	0010	-9
0110	-7	0110	-7
0111	-5	0111	-5
0101	-3	0101	-3
0100	-1	0100	-1
1100	1	1100	1
1101	3	1101	3
1111	5	1111	5
1110	7	1110	7
1010	9	1010	9
1011	11	1011	11
1001	13	1001	13
1000	15	1000	15

Table 3.6: 256-QAM Encoding Table



(a) Constellations with same maximum power (b) Constellations with same average power

Figure 3-3: Different in Constellations with same maximum power and same average power

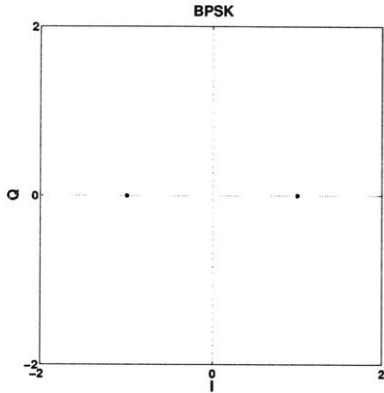
the earliest in the stream. With the I/Q pairs, the output of the QAM Modulator, X is given by

$$X = (I + jQ) \times K_{MOD} \quad (3.1)$$

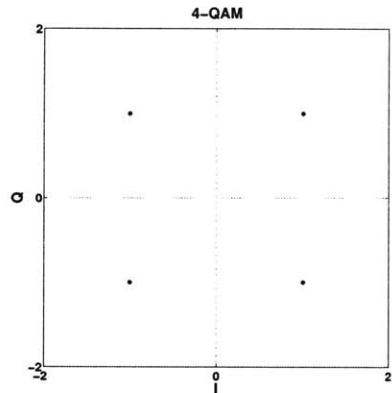
where K_{MOD} is given by Table 3.1. The purpose of K_{MOD} is to achieve the same average power for all mappings (i.e. an average power of 1). An example of constellations with the same maximum power and same average power is shown in Figure 3-3. The QAM modulator is implemented as a symbol lookup table based on the input bits.

Note that the bits are gray-coded (i.e. adjacent values of I or Q only differ by a bit). The symbol error that is most common is when a sent symbol gets demodulated as an adjacent symbol. Gray coding limit the bit error of such an occurrence to 1 bit per symbol.

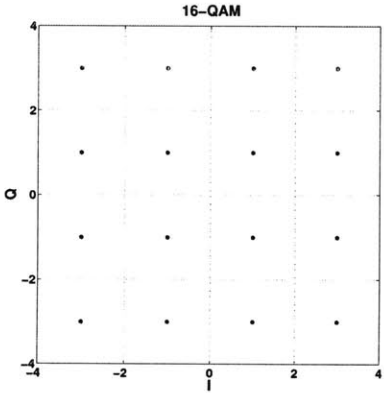
At the receiver, the input to the QAM demodulator is \hat{X} , an estimate of the sent X provided by the OFDM receiver. Assuming that getting a bit 0 or 1 is equiprobable, the optimal detection algorithm is to decode the bits of sent symbol that is nearest to the received \hat{X} . In Figure 3-4, each sent symbol X is visually associated with a square area that \hat{X} must lie in for \hat{X} to get decoded as X . The QAM demodulator is been implemented as a series of boundary comparisons to isolate the square area that



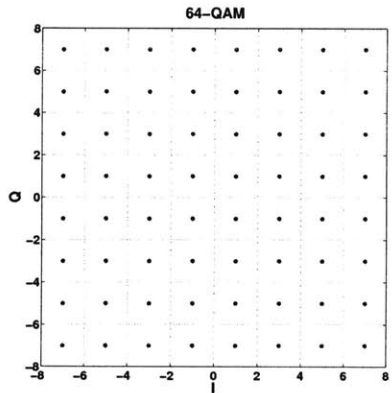
(a) BPSK Constellation Map



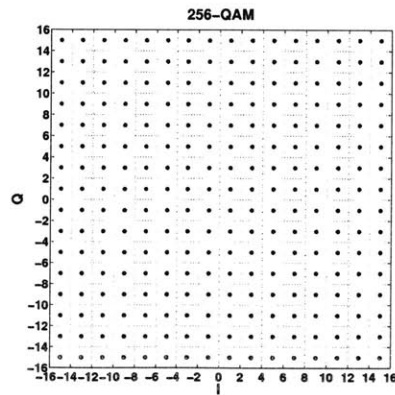
(b) 4-QAM Constellation Map



(c) 16-QAM Constellation Map



(d) 64-QAM Constellation Map



(e) 256-QAM Constellation Map

Figure 3-4: QAM Constellation Map

\hat{X} lies in. Upon locating the square area, the associated decoded bits are produced at the output of the QAM demodulator block.

3.3 Practical Transmission Model

A practical transmission system can be modeled as shown in Figure 3-5 [10]. The parameters shown in Figure 3-5 in relation to RF Front End are the following:

1. The sampling frequency of the Digital-to-Analog Converter (DAC) at the transmitter f_s and the sampling frequency of the Analog-to-Digital Converter (ADC) at the receiver f'_s are different. The Sampling Frequency Offset (SFO) ζ is defined as follows:

$$\begin{aligned}\zeta &= \frac{T'_s - T_s}{T_s} \\ T_s &= \frac{1}{f_s} \\ T'_s &= \frac{1}{f'_s}\end{aligned}\tag{3.2}$$

2. At the transmitter, there is an oscillator which modulates the baseband signal to passband. Similarly, at the receiver, there is an oscillator which demodulates the passband signal to baseband.
 - (a) δf is the Carrier Frequency Offset (CFO) between the transmitter and the receiver oscillator.
 - (b) $\Theta(t)$ represents the phase noise in the oscillators. The frequency generated by practical oscillators varies over time. This variation can be modeled as noise in the phase of the received signal.
3. $n(t)$ is the Additive White Gaussian Noise seen by the receiver. The thermal noise faced by the RF front end as well as the quantization noise of the data converters contributes to $n(t)$.

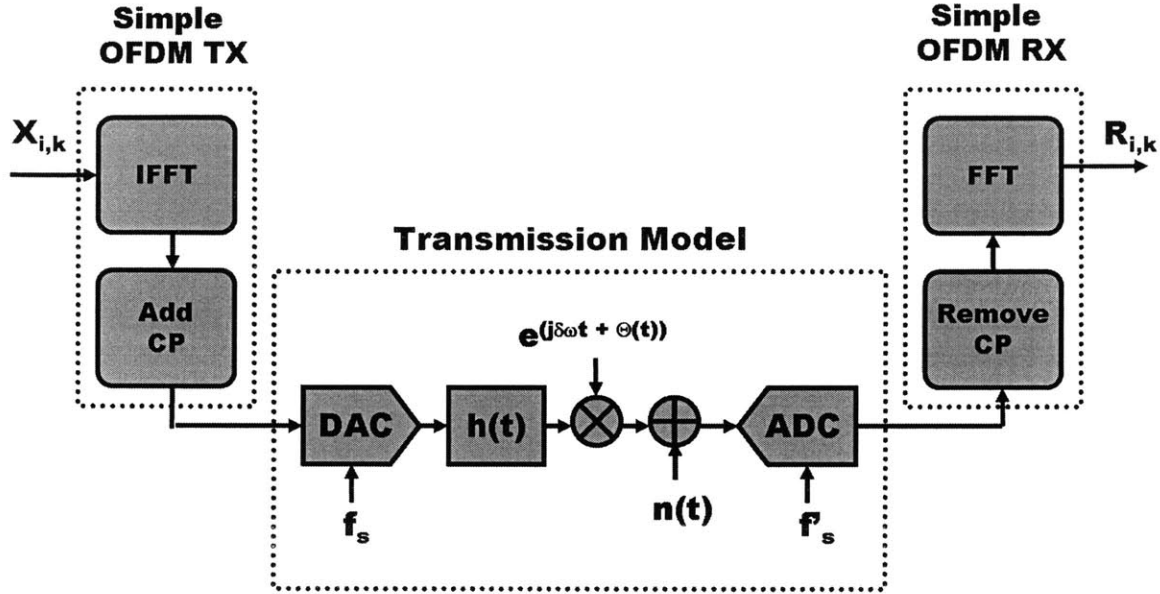


Figure 3-5: Complete baseband transmission model

The subsequent subsections will discuss the effects of the transmission model on the OFDM system.

3.3.1 Effects of Carrier and Sampling Frequency Offsets

Recall from Section 2.2.1, that in the presence of the channel $h(t)$, $R_{i,k} = H_k X_{i,k}$ (Equation 2.15). $R_{i,k}$ with respect to Figure 3-5 (in the absence of $\Theta(t)$) can be expressed as [10]

$$R_{i,k} = (e^{j\pi\phi_k} \cdot e^{j2\pi\phi_k(iN_{SYM}+N_{CP})/N_{FFT}}) \cdot si(\pi\phi_k) H_k X_{i,k} + ICI + n_{i,k} \quad (3.3)$$

where

- ICI is defined as the Inter-carrier Interference.
- $n_{i,k}$ is the complex-valued Additive White Gaussian Noise (AWGN) resulting from $n(t)$ with variance σ_N^2 .
 - $\sigma_N^2 = E[|n_{i,k}|^2]$

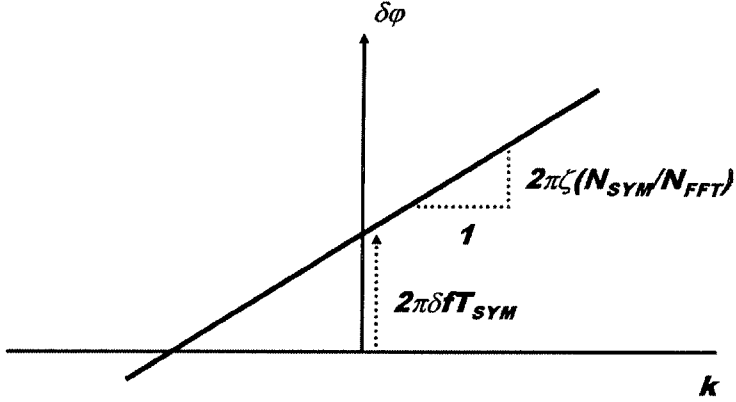


Figure 3-6: Subcarrier symbol rotation due to SFO and CFO

- $N_{CP} = \lceil T_{CP}/T_S \rceil$
- $N_{SYM} = N_{CP} + N_{FFT}$
- $si(x) = \frac{\sin(x)}{\sin(x/N_{FFT})}$
- $\phi_k \approx \delta f T_{FFT} + \zeta k$

There are three effects from CFO and SFO in the system as indicated in Equation 3.3:

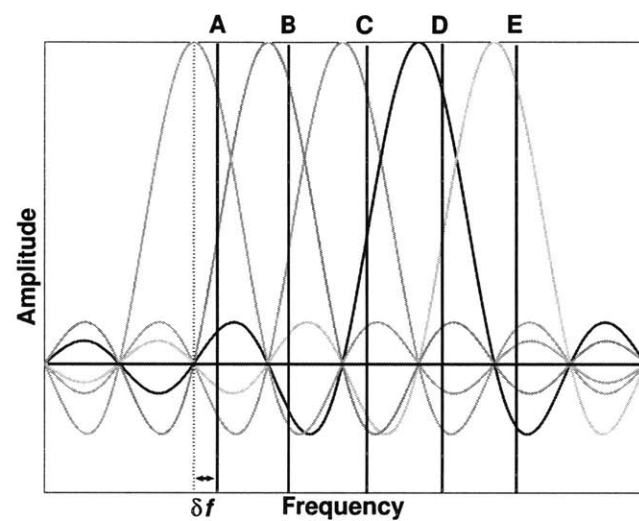
1. *Time-variant Symbol Rotation:* $e^{j2\pi\phi_k(iN_{SYM}+N_{CP})/N_{FFT}}$ is the time-variant component in the equation. Going from one OFDM symbol to the next in time will yield a phase increment of $\delta\varphi_k$.

$$\delta\varphi_k = 2\pi\phi_k N_{SYM}/N_{FFT} \quad (3.4)$$

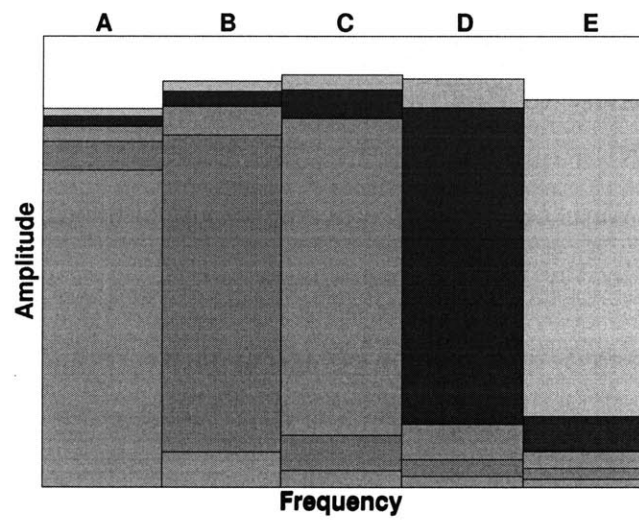
There is a linear relationship between $\delta\varphi_k$ and k as shown in Figure 3-6.

2. SNR Degradation:

- *ICI from CFO:* As shown in Figure 3-7, CFO causes sampling of data to be off from the ideal points. This results in the reduction of the desired signal's amplitude and introduces interference from other carriers. The



(a) Sampling of data in the frequency domain off by δf



(b) Non-ideal sampling of data in frequency domain causes ICI

Figure 3-7: ICI resulting from CFO δf

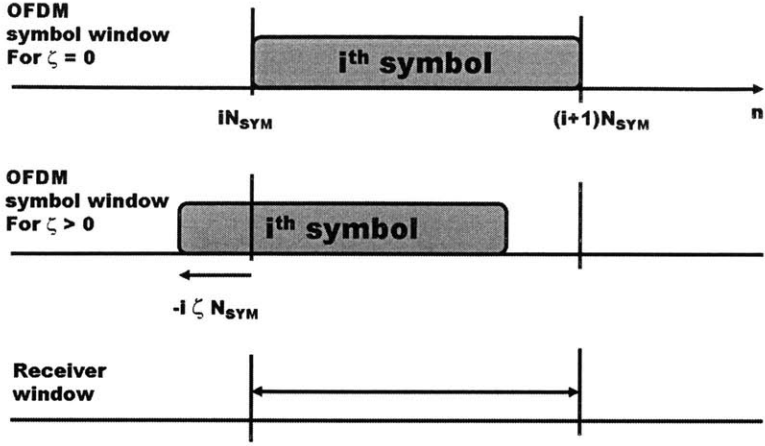


Figure 3-8: OFDM symbol window drift due to sampling frequency offset

degradation D_{CFO} in dB to the current SNR caused by CFO δf can be expressed as the following[11]

$$D_{CFO} = \frac{10}{3 \ln 10} (\pi \delta f T_{FFT})^2 SNR \quad (3.5)$$

From equation 3.5, it can be seen that as the SNR requirement is higher, the sensitivity to CFO increases. In the context of the WiGLAN, the highest SNR requirement occurs when 256-QAM is used (28.6 dB for BER = 10^{-3}). With D_{CFO} set to a negligible loss of 0.5 dB, the maximum CFO tolerated by the WiGLAN system is 6 kHz.

- *ICI from SFO:* The SNR degradation $D_{SFO;k}$ from SFO on the k^{th} subcarrier with SNR_k is given by [12]

$$D_{SFO;k} = 10 \log_{10} \left(1 + \frac{1}{3} SNR_k \cdot \left(\frac{\pi k (f'_s - f_s)}{f_s} \right)^2 \right) \quad (3.6)$$

From Equation 3.6, the degradation increases when k increases or SNR_k increases. To obtain the maximum degradation $D_{SFO;k}$, the highest SNR requirement of 28.6 dB for the use of 256-QAM and k of -64 are considered. Hence for the WiGLAN with f_s of 128 MHz and the sampling clocks of 100 parts per million (PPM), the maximum degradation D_k from Equation 3.6

is 1.4 dB. This degradation is relatively negligible.

3. Frame Drifting from SFO – Assuming the start of the 0th OFDM symbol is perfectly aligned, the drift of i^{th} OFDM symbol is $-i\zeta N_{SYM}$ as shown in Figure 3-8. The sampling clocks are specified at 100 PPM. Hence the maximum drift that can occur is 1 sample for every 5000 samples.

3.3.2 Effects of Phase Noise

Phase noise causes Inter-carrier Interference (ICI). The degradation D_{PN} in dB to the current SNR caused by phase noise can be expressed as the following[11]

$$D_{PN} = \frac{10}{ln10} \frac{11}{60} (4\pi T_{FFT} \beta) \cdot SNR \quad (3.7)$$

where β is the oscillator linewidth. Besides ICI, phase noise causes each sub-carrier in an OFDM symbol to be rotated by Common Phase Error (CPE) [13]. CPE only varies from one OFDM symbol to the next. If the CPE is slowly varying over time, it can be estimated and corrected for.

3.3.3 Bit Resolution of ADC and DAC

The ADC quantizes the signal and sends it to the digital baseband for processing. The act of quantization introduces noise to the system. Considering the quantization noise and the signal's PAPR, the SNR of a B bit ADC can be calculated as follows [14]

$$SNR(dB) = 6.02(B - 1) + 10.8 - PAPR(dB) \quad (3.8)$$

where the PAPR(dB) is the peak-to-average power ratio of the signal.

As it is later discussed in Section 3.5.1, the PAPR of the signal is at 16 dB. The ADC used in the WiGLAN is 8 bits. Using Equation 3.8, the SNR due to quantization noise is calculated to be 36.9 dB. This SNR also serves as an upper bound for the achievable SNR in an actual system where there are more noise sources.

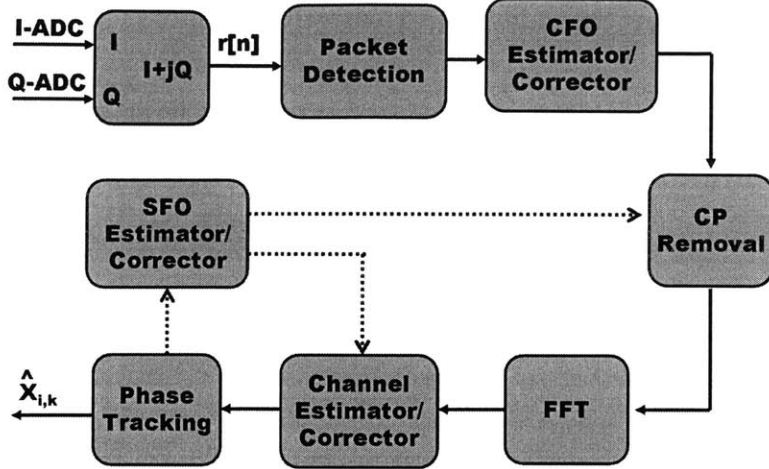


Figure 3-9: Receiver Design

Empirically, it is found that using a 10-bit DAC over 8-bit DAC yields approximately 3 dB worth of SNR improvement. In general, DAC of higher bit resolution are easier to find than ADC with equivalent bit resolution. For the conservative design of the WiGLAN, a 10-bit DAC and a 8-bit ADC is used.

3.4 Receiver Design

In consideration of the transmission model from Section 3.3, the receiver design is presented in Figure 3-9. To recover the sub-carrier data to be passed into the QAM demodulator, the received signal $r[n]$ is passed through the following sequence of blocks:

- *Packet Detection*: This module is responsible for detecting the start of the packet.
- *CFO Estimator/Corrector*: Once the packet is detected, the CFO is estimated and corrected to minimize the effects of ICI in the later stages.
- *CP Removal*: The Cyclic Prefix (CP) that is inserted to guard against Inter-symbol Interference (ISI) is removed prior to the FFT.

- *FFT*: Perform a transform on each OFDM symbol in time to obtain the sub-carrier symbols.
- *Channel Estimator/Corrector*: Estimate and correct the channel-induced attenuation and phase rotation on the sub-carrier symbols.
- *Phase Tracking*: Estimate and correct for time variant phase rotation on the sub-carrier symbols caused by CFO, SFO and phase noise.
- *SFO Estimator/Corrector*: Estimate the SFO by processing side-products of phase tracking. This module will correct for the OFDM Symbol Window Drift by indicating to the CP Removal Module to advance or delay by a sample when appropriate. This module also indicates to the channel corrector module to compensate the phase changes in the Frequency domain from the advance or delay of a sample.

3.4.1 Packet Detection

The algorithm employed is the double sliding window packet detection shown in Figure 3-10 [15]. The variables A_n and B_n are obtained from the received signal $r[n]$ by

$$A_n = \sum_{i=0}^{N_{FFT}-1} |r[n-i]|^2 \quad (3.9)$$

$$B_n = \sum_{i=1}^{N_{FFT}} |r[n+i]|^2 \quad (3.10)$$

The peak $E[M_n]$ occurs when index n is exactly the start of the packet (i.e. A_n would consist of signal and noise and B_n would consist purely of noise).

$$E[M_n]_{peak} = SNR + 1 \quad (3.11)$$

Thus, locating the peak of M_n would provide the expected start point of the packet.

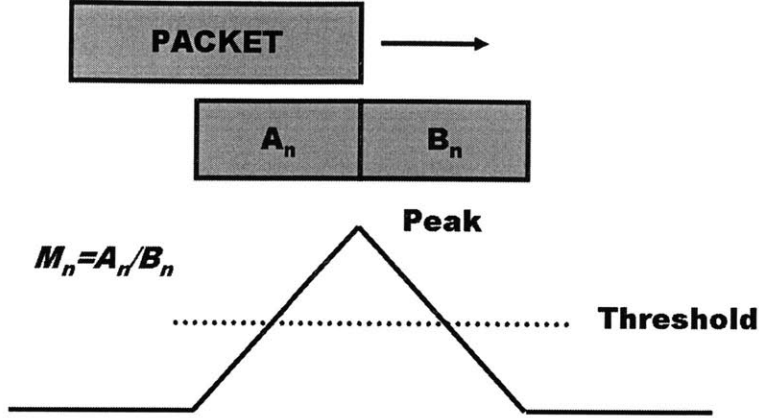


Figure 3-10: Double Sliding Window Packet Detection Algorithm

In a practical implementation, the peak finder is limited to a particular window size. The peak finder commences the search for the peak when M_n passes a certain threshold. From Equation 3.11, this threshold should be set to $SNR_{min} + 1$ where SNR_{min} is the minimum SNR the system is expected to support. The $SNR_{min} = 7$ dB in the context of the WiGLAN system. This comes from the fact that the minimum required SNR for least efficient modulation BPSK to meet the targeted BER is 7 dB. From Figure 3-10, it is observed that the peak occurs at most N_{FFT} samples (the window size of A) after the threshold is detected. Hence the peak finder has a window size of N_{FFT} .

The WiGLAN implementation of the packet detection is shown in Figure 3-11. Essentially, the packet detection algorithm senses for a large power increase to search for a packet. A DC offset in the system will diminish this power jump decreasing the efficiency of this packet detection algorithm. Hence inherent DC offset in the RF Front End necessitates the need of a DC Bias Removal filter.

The DC Bias Removal Filter used has a structure shown in Figure 3-11c[16]. The α factor is set to 0.5 as a multiplication by a power of two involves only bit shifting which is simpler than having to use an actual multiplier with built-in latency. Though ideally, the higher alpha factor will be better as seen from comparing Figure 3-11d and Figure 3-11e. All alpha factors will remove the DC component completely. However, a higher alpha factor will attenuate lower frequency bins less and the amplification

on the higher frequency bins are closer to unity gain.

3.4.2 CFO Estimation and Correction

If there are two identical symbols each of N_{FFT} samples, the Maximum Likelihood (ML) CFO estimate δf can be represented as a function of the cross-correlation z between these two symbols[15]

$$\begin{aligned} -2\pi\hat{\delta f}T_s &= \frac{\angle z}{N_{FFT}} \\ z &= \sum_{n=0}^{N_{FFT}-1} r^*[n]r[n - N_{FFT}] \\ &= \sum_{n=0}^{N_{FFT}-1} |r[n]|^2 e^{-j2\pi\delta f T_s n N_{FFT}} \end{aligned} \quad (3.12)$$

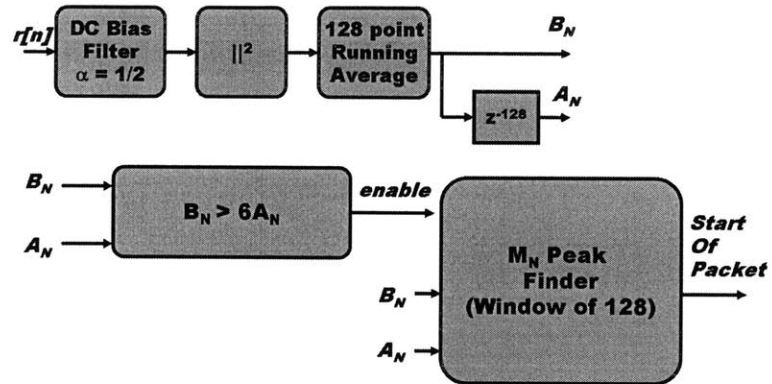
At high SNR, the performance of this algorithm can be quantified by the following[17]

$$\begin{aligned} Var(-2\pi\hat{\delta f}T_s) &= Var\left(\frac{\angle z}{N_{FFT}}\right) \\ &= \frac{1}{(N_{FFT})^2} \cdot \frac{1}{N_{FFT} \cdot SNR} \\ &= \frac{1}{(N_{FFT})^3 \cdot SNR} \end{aligned} \quad (3.13)$$

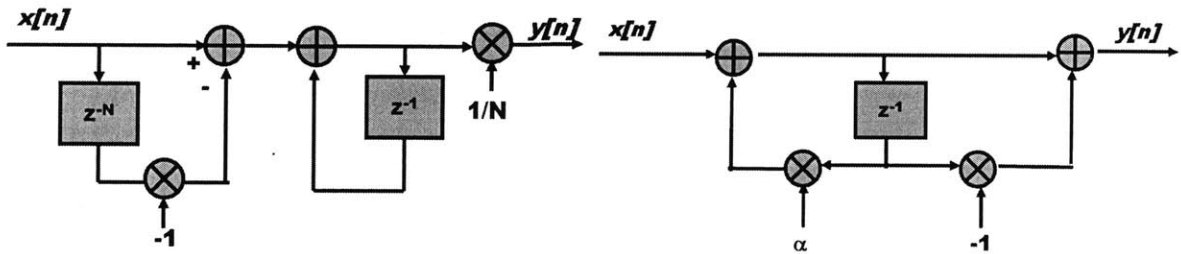
One limitation in this algorithm is that $2\pi\delta f T_s N_{FFT}$ must lies between $[-\pi, \pi]$. Hence the acquisition range of δf is as follows

$$\delta f < \frac{1}{2T_s N_{FFT}} \quad (3.14)$$

In the context of the WiGLAN, the maximum tolerable CFO is 500kHz. The maximum error on the carrier oscillator is at 50 PPM. In the 802.11a standard [2], the carrier oscillator is specified at 20 PPM. Hence, the maximum CFO arising from the 802.11a oscillators are 209.6kHz which is easily corrected by the CFO algorithm. Due to cost issues, the cheaper WiGLAN oscillators used is at 50 PPM, giving a maximum possible CFO of 524 kHz. To circumvent a large uncorrectable CFO, the prototypes

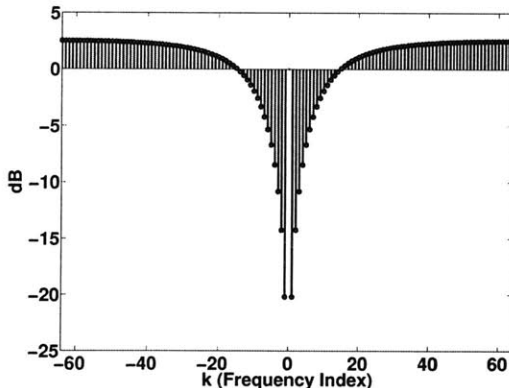


(a) Block Diagram Implementation of Packet Detection

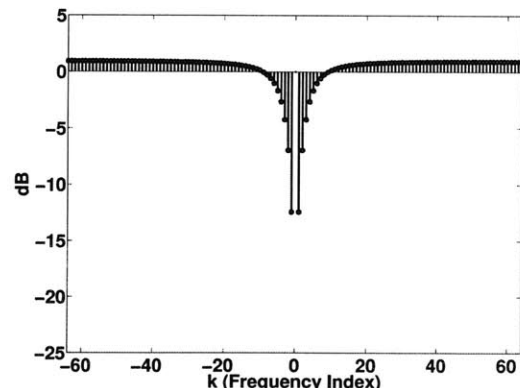


(b) N-point Moving Average Filter

(c) DC Bias Removal Filter



(d) Frequency Response of DC Bias Removal Re-(e) Frequency Response of DC Bias Removal
moval Filter $\alpha = 0.5$



(e) Frequency Response of DC Bias Removal Re-
moval Filter $\alpha = 0.8$

Figure 3-11: WiGLAN Implementation of Packet Detection

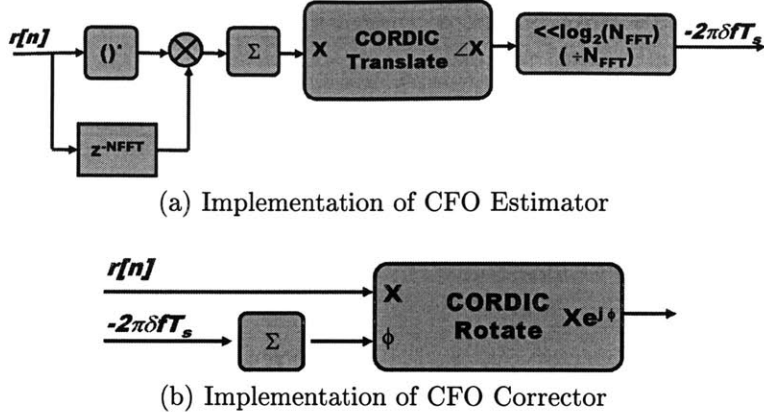


Figure 3-12: Implementation of CFO Estimator and Corrector

are measured with a spectrum analyzer before use.

After estimating the CFO, the correction can be performed by multiplying $r[n]$ by $e^{-j2\pi\delta f T_s n}$. The implementation of CFO estimator and corrector can be found in Figure 3-12, where the Coordinate Rotation Digital Computer (CORDIC) rotate and translate blocks from Xilinx are used [18]. More information about the CORDIC algorithm can be found in [19]. To facilitate easy phase wrapping, the phase output of CORDIC block is set to scaled radians (i.e. expressing π as a power of 2). In the WiGLAN, phase components are represented on the scale of [-1 1] which corresponds to $[-\pi \pi]$. When presented with another phase component greater than [-1 1], truncating the high order bits will result in phase wrapping. A more mathematical understanding of this type of truncation can be found in [20].

3.4.3 Channel Estimation and Correction

The channel estimation stage occurs after the CFO correction as the effect of ICI is minimized. However, since the CFO estimation is not perfect, there will be a residual CFO on the signal. Equation 3.3 can be re-expressed as

$$R_{i,k} = H_{eff;k} \cdot X_{i,k}^{\varphi_{i,k}(t)} + n_{eff;i,k} \quad (3.15)$$

where

- $H_{eff;k}$ represents a time-invariant multiplicative factor.
- $n_{eff;i,k}$ represents all the possible noise sources inclusive of ICI.
- $X_{i,k}^\varphi$ represents the sent symbol $X_{i,k}$ with timing varying rotation $\varphi_{i,k}$ caused by residual CFO, SFO and the CPE.

Channel Estimation seeks to estimate $H_{eff;k}$. If a pilot OFDM symbol at $i = -1$ is sent before the data OFDM symbols (corresponding to $i = 0, 1, 2\dots$), $R_{-1,k}$ can be expressed as the following

$$R_{-1,k} = H_{eff;k} \cdot X_{-1,k} + n_{eff;-1,k} \quad (3.16)$$

$H_{eff;k}$ can be estimated from the Least Squares (LS) method

$$\hat{H}_{eff;k} = \frac{R_{-1,k}}{X_{-1,k}} \quad (3.17)$$

The LS estimator is favored as it is computationally simple [21]. The LS estimator, also known as the zero-forcing estimator, amplifies noise excessively for sub-channels with low SNR but performs well for sub-channels with high SNR [5].

The estimator can be improved through averaging by sending the same pilot OFDM symbol twice at $i = -1$ and -2

$$\hat{H}_{eff;k} = \frac{1}{2} \cdot \frac{R_{-1,k} + R_{-2,k}}{X_{-1,k}} \quad (3.18)$$

This assumes that the residual CFO and the SFO is relatively small such that that the time varying rotation can be ignored when comparing $R_{-1,k}$ and $R_{-2,k}$. Hence care must be taken when averaging is done over more than 2 symbols. 802.11a [2] wireless standard uses two identical OFDM symbols to perform channel estimation.

Once $\hat{H}_{eff;k}$ has been estimated, channel correction can be performed to obtain an estimate of $X_{i,k}^\varphi$

$$\hat{X}_{i,k}^\varphi = \frac{R_{i,k}}{\hat{H}_{eff;k}} \quad (3.19)$$

To simplify the implementation, pilot symbols sent will be BPSK-modulated with an average power of 1 (i.e. $X_{-1,k} \in \{-1, 1\}$). In the WiGLAN, the implementation is shown in Figure 3-13. For the channel estimation implementation as seen in Figure 3-13a, the choice of $X_{-1,k}$ has prevented the use of multiplication and division.

For the channel correction seen in Figure 3-13b, the complex division indicated in Equation 3.19 is performed in polar form. A pipelined divider from Xilinx is used for division of the magnitude components[22]. The various binary divider algorithms can be found in [19]. Also, note that the magnitude of a number X given by the CORDIC translate block is $c|X|$ where c is referred to as the CORDIC scale factor [18]. The CORDIC scale factor might not be the same for different CORDIC blocks. The magnitude component of $\hat{X}_{i,k}^\varphi$ can be expressed as the following

$$|\hat{X}_{i,k}^\varphi| = \frac{c_1}{c_2} \cdot \frac{|R_{i,k}|}{|\hat{H}_{eff;k}|} \quad (3.20)$$

where $\frac{c_1}{c_2}$ is the amplitude mismatch factor resulting from using different CORDIC blocks to find the magnitude of $R_{i,k}$ and $H_{eff;k}$. In the WiGLAN, the amplitude mismatch factor is avoided by sharing the same CORDIC translate block for $R_{i,k}$ and $H_{eff;k}$.

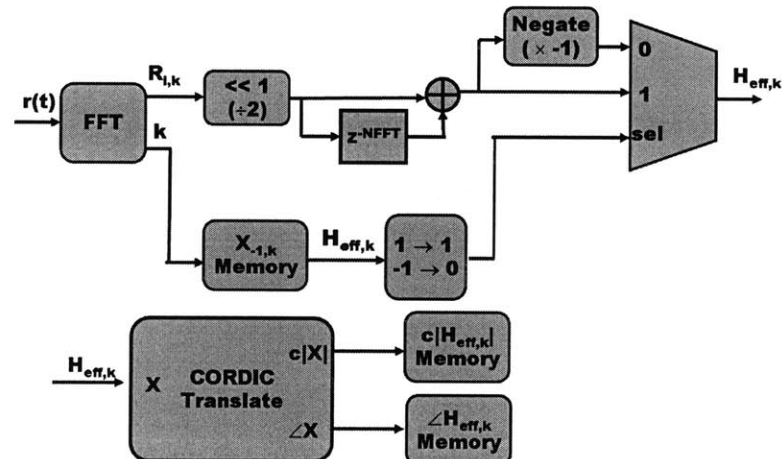
3.4.4 Phase Tracking

Looking at Equation 3.15, there remains the issue of the time-varying phase rotation $\varphi_{i,k}$ that needs to be compensated after removing the effects of $H_{eff;k}$. Let $\delta\varphi_{i,k}$ be phase accumulation that occurred going from OFDM symbol $i - 1$ to OFDM symbol i i.e.

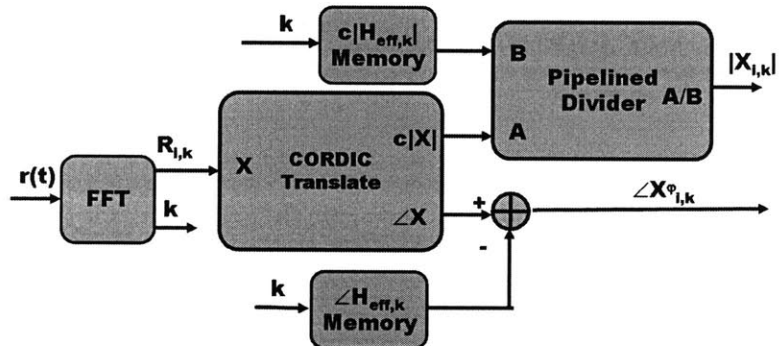
$$\delta\varphi_{i,k} = \varphi_{i,k} - \varphi_{i-1,k} \quad (3.21)$$

From Section 3.3.1 and 3.3.2, $\delta\varphi_{i,k}$ is a linear function of k where the intercept is a function of CPE and CFO and the slope is a function of the SFO.

As shown in Figure 3-14, if eight subcarriers are designated as pilots, it is possible to interpolate the values of $\varphi_{i,k}$. The pilots have the following characteristics:



(a) Implementation of Channel Estimator



(b) Implementation of Channel Corrector

Figure 3-13: Implementation of Channel Estimator and Corrector

- They are located at frequency indices $p(l)$ where $l \in \{0, 1, \dots, 7\}$.
- At the transmitter, they have known values of $X_{i,p(l)}$.
- At the receiver, they have an additional phase rotation of $\theta_{i,l}$ with respect to the $(i-1)^{th}$ OFDM symbol defined as the following

$$\theta_{i,l} = \angle X_{i,p(l)}^\varphi - \angle X_{i,p(l)} - \hat{\varphi}_{accum;i,p(l)} \quad (3.22)$$

$$\hat{\varphi}_{accum;i,p(l)} = \begin{cases} 0 & i \leq 0, \\ \sum_{m=0}^{i-1} \hat{\delta\varphi}_{m,p(l)} & \text{otherwise} \end{cases} \quad (3.23)$$

$\delta\varphi_{i,k}$ can be estimated through simple linear regression [23], also referred as the Linear Least Squares Estimator (LLSE).

$$\hat{\delta\varphi}_{i,k} = \hat{\alpha}_i + k\hat{\beta}_i \quad (3.24)$$

$$\hat{\alpha}_i = \bar{\theta}_i - \hat{\beta}_i \bar{p} \quad (3.25)$$

$$\hat{\beta}_i = \frac{S_{p\theta;i}}{S_{pp}} \quad (3.26)$$

$$S_{pp} = \sum_{l=0}^7 (p(l) - \bar{p})^2 \quad (3.27)$$

$$S_{p\theta;i} = \sum_{l=0}^7 (p(l) - \bar{p}) \theta_{i,l} \quad (3.28)$$

After estimating the additional phase rotation $\delta\varphi_{i,k}$ for each symbol, $\angle X_{i,j}$ can be estimated in the following manner

$$\angle \hat{X}_{i,k} = \angle \hat{X}_{i,k}^{\delta\varphi} - \hat{\delta\varphi}_{i,k} \quad (3.29)$$

$$\angle \hat{X}_{i,k}^{\delta\varphi} = \angle \hat{X}_{i,k}^\varphi - \varphi_{accum;i,k} \quad (3.30)$$

$X_{i,j}$ is then estimated using $\angle \hat{X}_{i,k}$ and $|\hat{X}_{i,k}|$ from the phase tracking and channel correction module respectively.

$$\hat{X}_{i,k} = |\hat{X}_{i,k}| e^{j \angle \hat{X}_{i,k}} \quad (3.31)$$

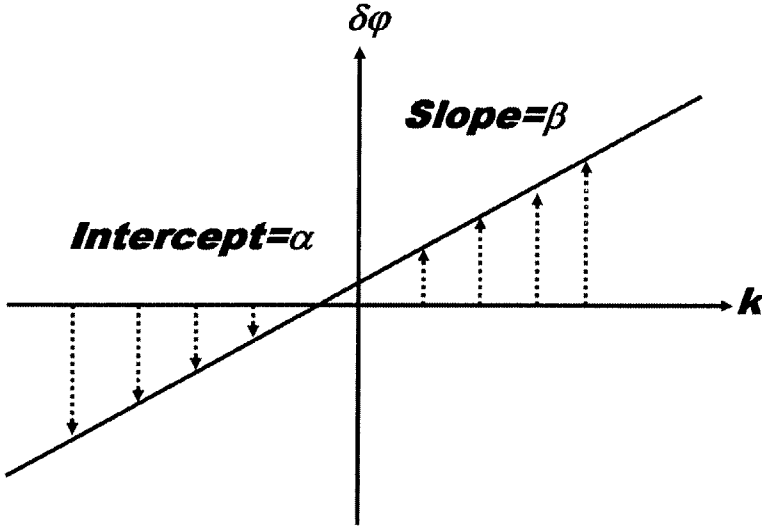


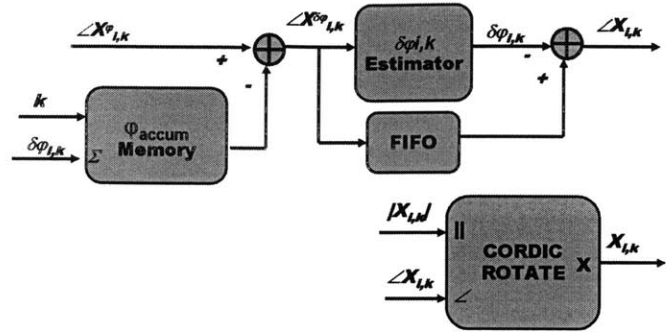
Figure 3-14: Insertion of pilot subcarriers to estimate time-varying phase rotation

The implementation of the phase tracking module is shown in Figure 3-15. Similarly to the CORDIC translate block Section 3.4.3, the CORDIC rotate block used in Figure 3-15a has a CORDIC scale factor multiplied into the output. At the expense of additional hardware, scale factor compensation should be enabled on this CORDIC block as amplitude mismatches on $\hat{X}_{i,k}$ will manifest in SNR degradation. Also note that the linear regression block is performed in two stages:

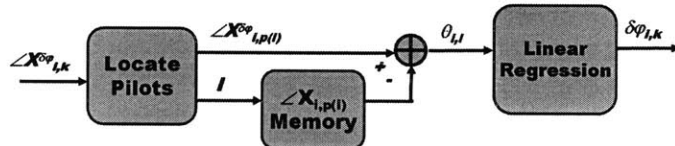
- Variables involving solely $p(l)$ are computed as seen in Figure 3-15d. These computations take place prior to data arrival as the pilot information $p(l)$ is known.
- $\varphi_{i,k}$ estimation based on $\theta_{i,l}$ given the variables involving $p(l)$ are computed as seen in Figure 3-15c. These computations take place during the processing of the data OFDM symbols.

3.5 OFDM Transmitter

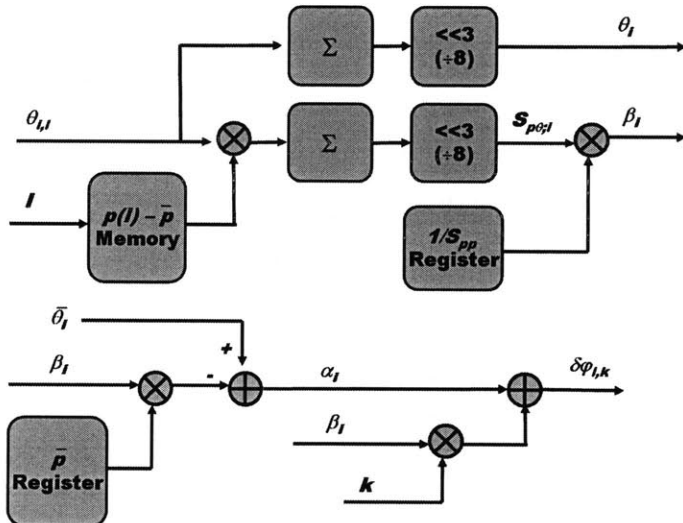
The transmitter design, in consideration of the receiver design in Section 3.4 is presented in Figure 3-16. Upon receiving the modulated symbols from the QAM Modulator, the following blocks are needed to perform the OFDM modulation:



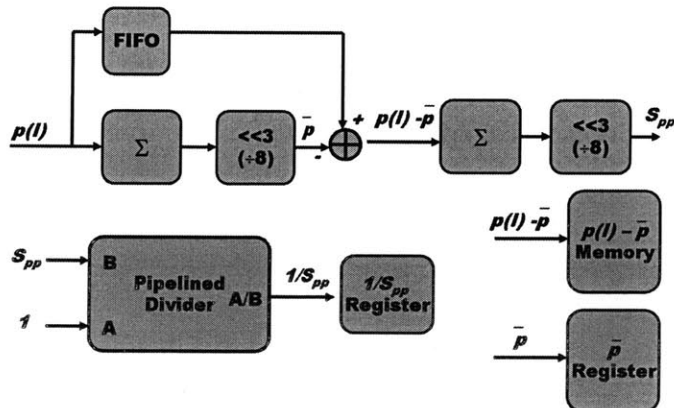
(a) Implementation of Phase Tracking Corrector



(b) Implementation of $\varphi_{i,k}$ Estimator



(c) Implementation of Linear Regression



(d) Initialization of Linear Regression Module

Figure 3-15: Implementation of Phase Tracking Module

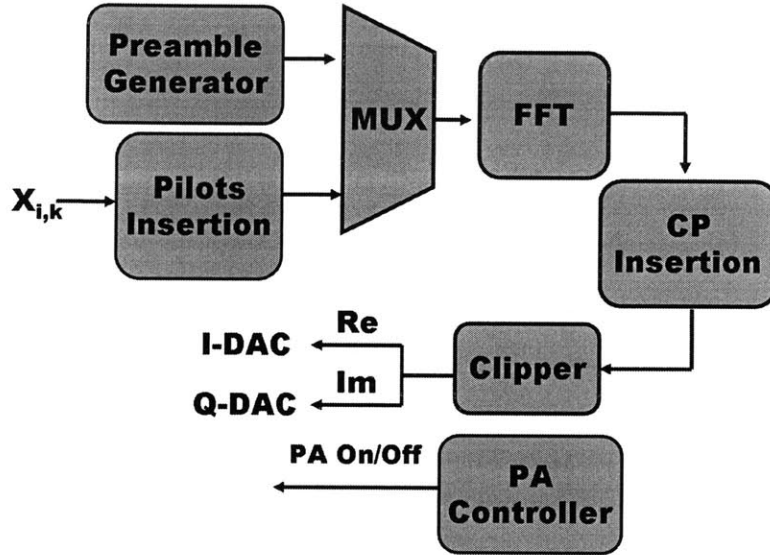


Figure 3-16: OFDM Transmitter

- *Preamble Generator:* This module generates the preamble which consists of pilot symbols to be sent before the data symbols. These pilot symbols are to be used for CFO and channel estimation.
- *Pilot Insertion:* This module inserts the pilot sub-carriers in the data OFDM symbols used for phase tracking.
- *MUX:* Ensures that the preamble is sent before the data symbols.
- *FFT:* Perform a transform on sub-carrier symbols to obtain the time representation of the OFDM symbol.
- *CP Insertion:* CP is inserted on each OFDM symbol to prevent ISI from the channel.
- *Clipper:* The peak-to-average power ratio (PAPR) of an OFDM signal is large. This module reduces the PAPR through hard-limiting the input amplitude to the DACs.
- *PA Controller:* Switch the PA on only during transmission of data.

3.5.1 Clipper

The PAPR of an OFDM signal is large. From [24], having 128 available sub-carriers like in the WiGLAN can yield a PAPR of at least 21 dB. The occurrence of large peaks is statistically uncommon as shown in Figure 3-17 hence clipping can be implemented to reduce the PAPR of the signal without heavily affecting performance of the system. Other algorithms with better performance are available for reduction of PAPR [25] but clipping offers the best implementation simplicity. To mathematically express the clipping scheme, the discrete time samples of an OFDM symbol has to be formulated.

For the i^{th} OFDM symbol, $[X_{i,-\frac{N_{FFT}}{2}} \dots X_{i,\frac{N_{FFT}}{2}-1}]$ is processed by the IFFT and the resultant discrete time samples $x^i[n]$, where n ranges from 0 to $N_{FFT}-1$, can be expressed as the following

$$x^i[n] = \sum_{k=-\frac{N_{FFT}}{2}-1}^{\frac{N_{FFT}}{2}} X_{i,k} e^{j2\pi kn/N} \quad (3.32)$$

Clipping is implemented to reduce the PAPR of the signal. If $x^i[n]$ is clipped, the clipped signal $\tilde{x}^i[n]$ can be expressed as the following

$$\tilde{x}^i[n] = Re(\tilde{x}^i[n]) + j \cdot Im(\tilde{x}^i[n]) \quad (3.33)$$

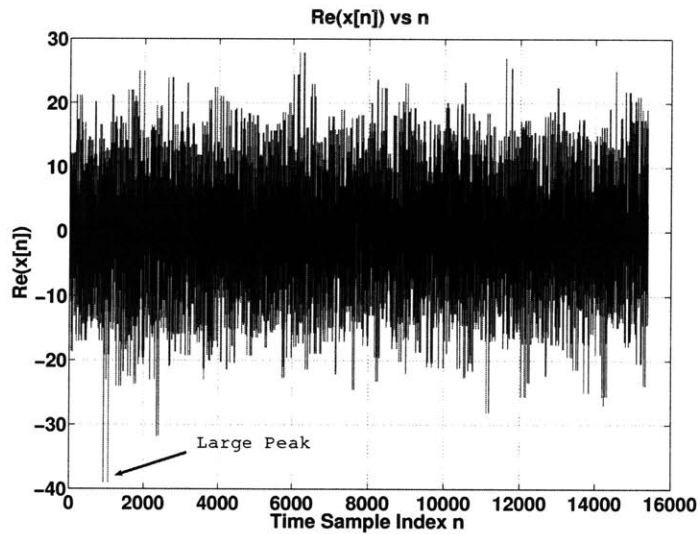
$$x^i[n] = Re(x^i[n]) + j \cdot Im(x^i[n]) \quad (3.34)$$

$$Re(\tilde{x}^i[n]) = \begin{cases} 1 & \frac{Re(x^i[n])}{A_{CLIP}} \geq 1, \\ -1 & \frac{Re(x^i[n])}{A_{CLIP}} \leq -1, \\ \frac{Re(x^i[n])}{A_{CLIP}} & \text{otherwise} \end{cases} \quad (3.35)$$

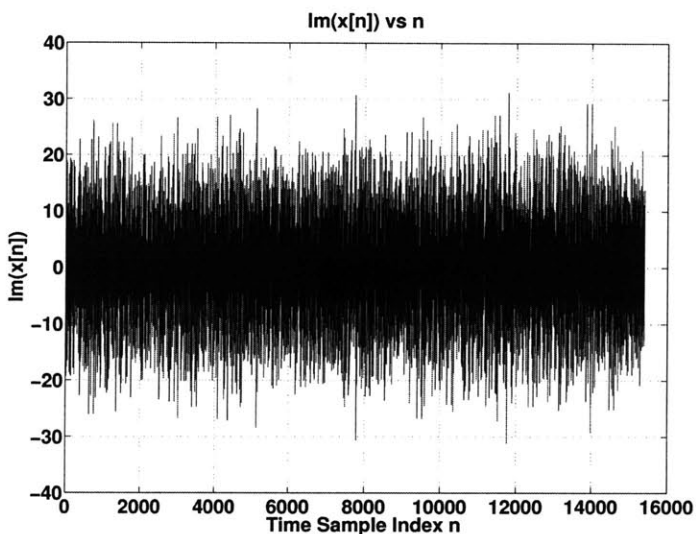
$$Im(\tilde{x}^i[n]) = \begin{cases} 1 & \frac{Im(x^i[n])}{A_{CLIP}} \geq 1, \\ -1 & \frac{Im(x^i[n])}{A_{CLIP}} \leq -1, \\ \frac{Im(x^i[n])}{A_{CLIP}} & \text{otherwise} \end{cases} \quad (3.36)$$

(3.37)

where A_{CLIP} is the clipping amplitude applied on the real and imaginary components



(a) Real Part of an OFDM Signal



(b) Imaginary Part of an OFDM Signal

Figure 3-17: Rare Occurrence of Large Peaks in OFDM Signal

of $x^i[n]$. The lower the clipping amplitude A_{CLIP} , the higher the occurrence of clipping. Let P_{CLIP} be the probability of a clip happening in an OFDM symbol of N_{FFT} samples. P_{CLIP} is a metric of interest because a clip in an OFDM symbol will raise the noise floor for all the frequency bins in that OFDM symbol. As discussed later in Section 4.1.2, the target coded BER is 10^{-5} . Conservatively assuming that a clip in OFDM symbol increases the noise floor so much that it invalidates the symbol, a reasonable P_{CLIP} selected is 10^{-7} . To determine A_{CLIP} from P_{CLIP} , the statistical characteristics of the time samples need to be derived.

If N_{FFT} is large and all the $X_{i,k}$ are independent zero mean random variables with the same variance, by Central Limit Theorem, it can be concluded that $x^i[n]$ is approximately Gaussian with zero mean and variance σ^2 expressed as

$$\sigma^2 = \sum_{k=-\frac{N_{FFT}}{2}}^{\frac{N_{FFT}}{2}-1} Var(X_{i,k}) \quad (3.38)$$

From [26], due to orthogonality of the sub-carriers, it can be also concluded that $x^i[n]$ are independent. Given the statistical attributes of $x^i[n]$, $|x^i[n]|^2$ is exponentially distributed with $\beta = \sigma^2$ [27]. More information about the exponential distribution can be found in [23].

From the clipping scheme, clipping occurs when amplitude of $Re(x^i[n])$ or $Im(x^i[n])$ exceeds A_{CLIP} . Hence the minimum $|x^i[n]|$ that might experience clipping is A_{CLIP} where either $Re(x^i[n])$ or $Im(x^i[n])$ is equal to A_{CLIP} and the other component is zero. For analysis of the derivation of A_{CLIP} , it is assumed that if $|x^i[n]|$ exceeds A_{CLIP} , clipping is experienced. Based on the statistical properties of $|x^i[n]|^2$ found earlier, the relationship between P_{CLIP} and A_{CLIP} can be formulated as the following

$$\begin{aligned} 1 - P_{CLIP} &= Pr(|x^i[n]|^2 < A_{CLIP}^2)^{N_{FFT}} \\ &= (1 - exp(-\frac{A_{CLIP}^2}{\sigma^2}))^{N_{FFT}} \\ A_{CLIP} &= \sqrt{-\sigma^2 \cdot ln(1 - (1 - P_{clip})^{\frac{1}{N_{FFT}}})} \end{aligned} \quad (3.39)$$

The maximum power $|x^i[n]|^2$ resulting from the clipping scheme described in Equation 3.33 is $2A_{CLIP}^2$. From Equation 3.39, the PAPR(dB) of the signal can be derived

$$\begin{aligned} PAPR(dB) &= 10\log_{10}\left(\frac{|x^i[n]|_{MAX}^2}{var(x^i[n])}\right) \\ &= 10\log_{10}\left(\frac{2A_{CLIP}^2}{\sigma^2}\right) \\ &= 10\log_{10}\left(-2 \cdot \ln\left(1 - (1 - P_{CLIP})^{\frac{1}{N_{FFT}}}\right)\right) \end{aligned} \quad (3.40)$$

In the WiGLAN where $N_{FFT} = 128$ and $P_{CLIP} = 10^{-7}$, the transmitted signal PAPR is 16 dB.

So far, A_{CLIP} and $PAPR(dB)$ of the signal are derived on the assumption that all $X_{i,k}$ are used to carry random data. In the WiGLAN, this is not true as some sub-carriers are allocated as known pilots and some sub-carriers are not used. However, Equation 3.39 and 3.40 give a good approximation of the A_{CLIP} and $PAPR(dB)$.

In the WiGLAN, average power of used sub-carriers is set to one. Equation 3.38 and 3.39 can be re-expressed as the following

$$\sigma^2 = N_{USED} \quad (3.41)$$

$$A_{CLIP} = \sqrt{-N_{USED} \cdot \ln\left(1 - (1 - P_{clip})^{\frac{1}{N_{FFT}}}\right)} \quad (3.42)$$

Since the $N_{FFT} = 128$ and $P_{CLIP} = 10^{-7}$ in the WiGLAN, Equation 3.42 indicates that it is possible to create a small lookup table of A_{CLIP} indexed by N_{USED} . N_{USED} ranges from 0 to 128 hence this lookup table will not be large. The clipper is implemented on the FPGA as shown in Figure 3-18.

3.5.2 PA Control at the Transmitter

The transmitter controls the switching on and off of the PA. When the transmitter is not sending data, the PA should be turned off. There are always unwanted signals at the input of PA caused from either mixer leakage or intrinsic DC offset from the DAC. Switching off the PA when the transmitter is not in use ensures that these unwanted

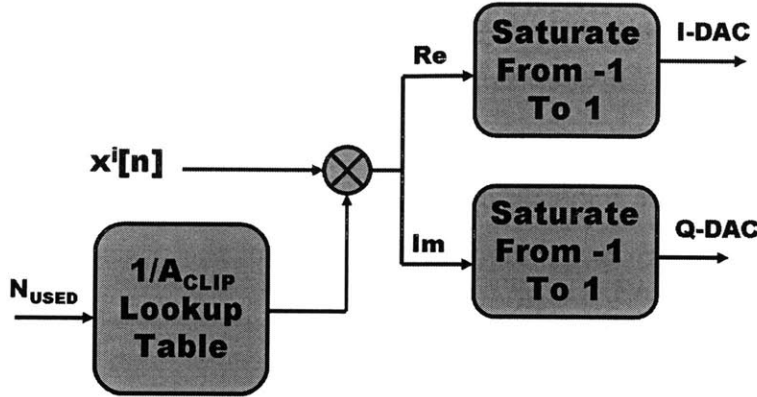


Figure 3-18: Clipper Implementation

signals would not be amplified by the PA and cause unnecessary interference to other transceivers.

For the WiGLAN, the switching on and off of the PA follows this scheme:

- Switch on the PA $1 \mu\text{s}$ before data is sent.
 - Empirically, the switching on of the PA could cause the frequencies on the oscillators in the RF Front End to fluctuate for while before settling to its natural frequency. Data should not be sent until the oscillators settle down.
- Switch off the PA $1 \mu\text{s}$ after data is sent.
 - There is a latency of data signal from the DAC to the PA. Instantaneous switching off the PA at the end of data transmission might result in the loss of data signal toward the end.

3.6 Summary

The sub-carrier modulation used can be chosen from BPSK, 4-QAM, 16-QAM, 64-QAM and 256-QAM. If Frequency Adaptive Modulation is used, each sub-carrier can be used if it is capable of transmission. If not, there are some constraints on the sub-carriers that can be used.

The RF Front End produces a lot of non-idealities such as CFO, SFO and phase noise. The main design consideration of the receiver is taking these non-idealities into account and compensating for their effects. The transmitter design is simpler than the receiver design. The main design consideration for the transmitter is the signal clipping algorithm which is required as the PAPR of the transmitted OFDM signal is quite large.

Chapter 4

Frequency Adaptive Modulation

For Frequency Adaptive Modulation to occur, the transmitter and the receiver should have partial Channel State Information (CSI) to make the sub-carrier modulation assignment. Figure 4-1 shows the Wireless Gigabit Local Area Network (WiGLAN) protocol for the Frequency Adaptive Modulation to take place. There are 3 steps to the protocol:

- *Step 1 - SNR Estimation* The receiver measures the signal-to-noise ratio (SNR) on each channel and assign an appropriate modulation scheme on each sub-carrier.
- *Step 2 - CSI Feedback* Feedbacks the assigned modulation scheme from the receiver to the transmitter.
- *Step 3 - Data* Data is sent from the transmitter to the receiver using the assigned modulation scheme.

The next few sections will discuss the following:

- look at the networking aspects.
- explore the frequency adaptive modulation protocol to more detail.

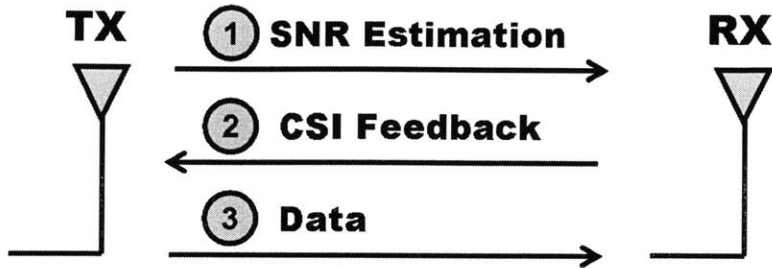


Figure 4-1: Protocol for Frequency Adaptive Modulation

4.1 Networking Aspects on the WiGLAN

4.1.1 Integration of the Physical Layer with the MAC layer

Packet Flow required for the proposed protocol is similar to 802.11a Media Access Control (MAC) protocol. In 802.11a, Request To Send (RTS) packet and Clear To Send (CTS) packet is used to reserve access to the channel [28].

1. When the transmitter wants to send a packet, it sends an RTS packet to the receiver.
2. The receiver will respond with CTS packet giving the transmitter the permission to send.
3. The transmitter would then send the data packet.

If the 802.11a MAC protocol is used, integration of the proposed frequency adaptive modulation protocol will be relatively simple.

4.1.2 Bit Error Rate

In a wireless network like 802.11a, the maximum Packet Error Rate (PER) is 0.1 given a packet length of 1000 bytes (8000 bits). [2] This translates to a Bit Error Rate (BER) of 1.32^{-5} .

$$1 - PER = (1 - BER)^{BitsPerPacket} \quad (4.1)$$

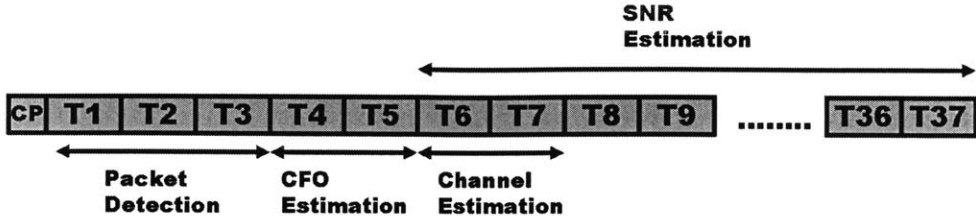


Figure 4-2: Packet Structure during SNR Estimation

BER of that magnitude is usually obtained using channel coding. For sake of simplicity, the frequency adaptive modulation targets for maximum uncoded BER of 10^{-3} . Given that frequency adaptive modulation reduces the Rayleigh channel to Gaussian sub-channels, it's not difficult to find a channel code with moderate complexity to obtain a coded BER of 1.32^{-5} . Two such possible channel codes are Bose, Ray-Chaudhuri, Hocquenghem (BCH) Code(127,99) and BCH Code(15,5). Theory behind BCH codes can be found in [29].

4.2 Step 1: SNR Estimation

The SNR of each sub-carrier should be estimated and an appropriate sub-carrier modulation assignment is assigned to each sub-carrier. To initiate this process, the transmitter sends a packet as shown in Figure 4-2 to the receiver. The packet consist of 37 identical Orthogonal Frequency Division Multiplexing (OFDM) training symbols. The packet uses all the sub-carriers excluding the DC bin. The OFDM training

symbols is the Fourier Transform of the sequence S given by

$$\begin{aligned}
S_{-64,63} = & (-1, -1, -1, -1, -1, -1, -1, 1, 1, -1, -1, -1, 1, 1, -1, \\
& 1, -1, 1, 1, -1, 1, -1, -1, -1, -1, -1, 1, -1, 1, -1, 1, \\
& 1, -1, 1, -1, -1, 1, -1, -1, -1, -1, 1, -1, -1, 1, 1, \\
& 1, -1, -1, 1, 0, 1, 1, 1, 1, -1, -1, -1, 1, -1, -1, -1, \\
& 1, -1, -1, 1, 1, -1, 1, 1, -1, -1, 1, 1, 1, -1, 1, 1, -1, \\
& 1, 1, -1, -1, 1, 1, 1, -1, 1, -1, -1, -1, 1, -1, 1, -1, \\
& 1, 1, 1, 1, 1, -1, -1, 1)
\end{aligned} \tag{4.2}$$

where the sub-indices of S indicates the indices of frequency bins S is assigned to. Pilot sub-carriers used for phase tracking at the receiver are fixed at Frequency bin indices $k = \{-39, -28, -17, -6, 6, 17, 28, 39\}$

As mentioned in Section 3.1, the higher frequency bins in the transition region of the reconstruction filter as well as the DC bin are not used. Not using the higher frequency bins might be pessimistic as it might be possible to send data despite the higher degree of attenuation compared to bins in the passband region of the reconstruction filter. One advantage of performing frequency adaptive modulation is the SNR of each sub-carrier is measured and used to send data if its SNR permits it. It is expected that most of the throughput gain would be the result of adapting the bins in the passband region. The reason for adapting the bins in the transition region is that there will be some throughput gain and the added complexity is minimal.

Given that the signal power of all the used sub-carriers is normalized to 1 at the receiver, the SNR of the k^{th} bin is given by

$$SNR_k = \frac{1}{\sigma_k^2} \tag{4.3}$$

where σ_k^2 is the variance of the noise in the k^{th} bin.

The next two subsections will cover SNR estimation and sub-carrier modulation

assignment.

4.2.1 SNR Estimation

As shown at Figure 3-9, $\hat{X}_{i,k}$ are the recovered sub-carrier data symbols from the output of the OFDM receiver. In this SNR Estimation step, $\hat{X}_{i,k}$ can be expressed as the following

$$\hat{X}_{i,k} = S_k + n_{i,k} \quad (4.4)$$

where

- S_k is the k^{th} element in the sequence given by Equation 4.2.
- $n_{i,k}$ is circular symmetric complex Gaussian noise with mean 0 and variance σ_k^2 (i.e. $n_{i,k} \sim CN(0, \sigma_k^2)$). Thermal noise, quantization and estimation errors in the digital baseband all contributes to this term.

SNR_k can be estimated in the following manner

$$S\hat{N}R_k = \frac{1}{\hat{\sigma}_k^2} \quad (4.5)$$

$$\hat{\sigma}_k^2 = \frac{1}{N} \sum_{i=1}^N |\hat{X}_{i,k} - S_k|^2 \quad (4.6)$$

$$(4.7)$$

where N is the number of OFDM symbols used to perform the SNR estimation.

After computing $S\hat{N}R_k$, an $100(1-\chi)\%$ confidence interval for the true SNR_k can be derived.

$$\frac{N\hat{\sigma}_k^2}{\sigma_k^2} \sim gamma(N, 1) \quad (4.8)$$

$$Pr\left[\frac{N\hat{\sigma}_k^2}{\sigma_k^2} > \gamma_{N,1}\right] = 1 - \chi$$

$$Pr\left[SNR_k > \frac{S\hat{N}R_k \gamma_{N,1}}{N}\right] = 1 - \chi \quad (4.9)$$

where

- $\text{gamma}(\alpha, \beta)$ indicated a gamma distribution with its defining parameters α and β . More information about the gamma distribution can be found in [23].
- $(1-\chi)$ is the probability that SNR_k lie in the interval $(\frac{S\hat{N}R_k\gamma_{N,1}}{N}, \infty)$.

Obtaining this confidence interval is important as the sub-carrier modulation decision should be based on the true SNR_k . There are two parameters that should be decided before the confidence interval can be computed:

1. χ : As χ is an important parameter in determining the confidence interval, it's imperative that an appropriate χ is chosen for the WiGLAN. In the context of the WiGLAN, χ is the probability of making a wrong sub-carrier modulation decision (i.e. assigning a sub-carrier modulation based on the confidence interval but SNR_k does not lie within the interval). Frequency Adaptive modulation is currently performed on a per packet basis. The target PER from Section 4.1.2 is 0.1. Assuming the worst case that any wrong sub-carrier modulation decision will cause a packet error, a maximum probability of making a modulation error that can be reasonably tolerated would be 10^{-3} . To achieve this probability, the upper bound for the allowable χ occurs when all 127 sub-carriers in the WiGLAN system is used and is found to be 7^{-6} using the following equation

$$1 - 10^{-3} = (1 - \chi)^{127} \quad (4.10)$$

2. N : A Figure of Merit (FOM) is needed to evaluate the right N . The FOM appropriate to this would be $SNR_{margin}(dB)$ shown in Figure 4-3. The true SNR_k can dip below $SNR_{margin}(dB)$ of $S\hat{N}R_k$ with probability of χ . From Equation 4.9, the $SNR_{margin}(dB)$ can be expressed as the following

$$SNR_{margin}(dB) = -10\log_{10}\frac{\gamma_{N,1}}{N} \quad (4.11)$$

Intuitively, the larger the N , the variance from the true SNR_k exhibited by

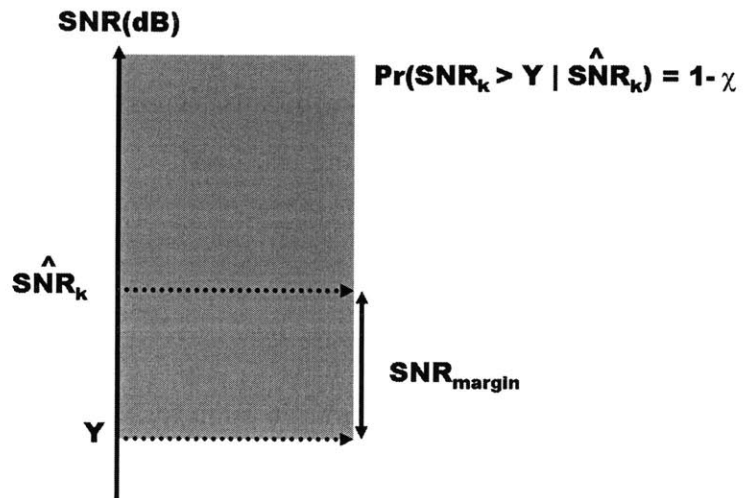


Figure 4-3: SNR Margin

N	$SNR_{margin}(dB)$
1	51.54
2	27.27
4	15.35
8	9.26
16	5.89
32	3.89
64	2.62
128	1.79

Table 4.1: $SNR_{margin}(dB)$ for different N given $\chi = 7^{-6}$

\hat{SNR}_k will decrease which translates to a smaller SNR_{margin} . Table 4.1 shows the $SNR_{margin}(dB)$ for various N given the previously determined $\chi = 7^{-6}$. For implementation simplicity, only powers of 2 are considered for N .

Though increasing N provides a better SNR_{margin} , it comes at the cost of processing overhead. A N of 32 is chosen because it gives a good compromise between SNR_{margin} of 3.89 and processing overhead.

Hence in the WiGLAN where

- Pilot OFDM symbols used for SNR estimation $N=32$.
- Probability of making a wrong modulation decision for a sub-carrier is 7^{-6} .

an interval for the true SNR_k based on \hat{SNR}_k can be determined and a modulation decision can be made based on the lower bound of this interval given by

$$SNR_{k,LB}(dB) = \hat{SNR}_k(dB) - 3.89 \quad (4.12)$$

4.2.2 Sub-carrier Modulation Assignment

The sub-carrier modulation assignment is determined based on SNR_k , the signal-to-noise ratio of each k^{th} sub-carrier, . The adaptive modulation scheme picks the most efficient modulation capping the maximum BER at 10^{-3} as show in Figure 4-4. For optimal data rate, true water filling power algorithm should be used where power in sub-carrier can be varied. However, for the WiGLAN, constant average power is assigned to each used sub-carrier. The data rate loss compared to the true water filling power algorithm is negligible while the complexity reduction is significant [30].

From Section 3.5.1, the peak-to-average power ratio (PAPR) of the signal is fixed through the clipping algorithm. Since the maximum power of the PA is also fixed, it would imply that the total average power is fixed which is then distributed equally to the used sub-carriers. In Step 1: SNR Estimation, all 127 sub-channels are used. After performing adaptive modulation, it is possible that in Step 3: Data, some null sub-channels might be allocated leading to less than 127 sub-channels being used.

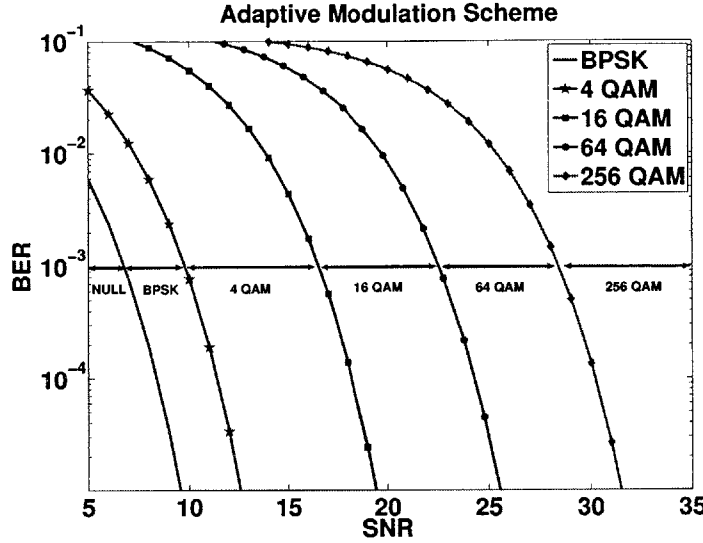


Figure 4-4: Adaptive Modulation Assignment with target BER of 10^{-3}

This means that the average power on these sub-carriers in Step 3 have increased effectively increasing the SNR_k in Step 3 over the SNR_k in Step 1. Rightfully, for optimal performance, the SNR_k in Step 3 should be used to make the modulation decision. As the sub-carrier modulation decisions are made in Step 1, an algorithm could be developed to estimate the SNR_k in Step 3 from the SNR_k obtained in Step 1. This is an area for further investigation. For now, SNR_k in Step 1 is used to make the modulation decisions.

The true value of SNR_k which the modulation decision should be based, is unknown at the receiver but statistical inference can be made about the true SNR_k . From Section 4.2.1, it is determined that the adaptive modulation decision should be made based on $SNR_{k;LB}(dB)$ given by Equation 4.12. In implementation, $\hat{\sigma}_k^2$ which is the reciprocal of \hat{SNR}_k , is computed based on Equation 4.6 and decision on the sub-carrier modulation assignment is based on $\hat{\sigma}_k^2$ as shown in Table 4.2.

The pilot sub-carriers used for phase tracking would remain unchanged. Intuitively, if the pilot-sub-carrier is located in a frequency bins with low SNR, it would be good to reassign that pilot sub-carrier in another frequency bin. However, empirically, it is found that the SNR of each sub-carrier is dependent on the positions of pilot sub-carriers. Hence, in order to perform reassignment of pilot sub-carriers,

<i>Modulation Assignment</i>	$SNR_k(dB)$ (Figure 4-4)	$\hat{SNR}_k(dB)$ (Equation 4.12)	$\hat{\sigma}_k^2$ (Equation 4.5)
Null	Below 6.79	Below 10.68	Above 8.55^{-2}
BPSK	6.79 to 9.80	10.68 to 13.69	4.28^{-2} to 8.55^{-2}
4-QAM	9.80 to 16.55	13.69 to 20.44	9.04^{-3} to 4.28^{-2}
16-QAM	16.55 to 22.55	20.44 to 26.44	2.27^{-3} to 9.04^{-3}
64-QAM	22.55 to 28.42	26.44 to 32.31	5.87^{-4} to 2.27^{-3}
256-QAM	Above 28.42	Above 32.31	Below 5.87^{-4}

Table 4.2: Making Modulation Assignment based on $\hat{\sigma}_k^2$

these steps needs to be adhered to:

1. Coarse SNR Estimation to determine the usable bins.
 - OFDM Receiver used pre-determined pilot sub-carriers for phase tracking.
2. Reassignment of the pilot sub-carriers among usable bins.
3. Fine SNR Estimation which the adaptive modulation decision is based on.
 - OFDM Receiver used newly-assigned pilot sub-carriers for phase tracking.

Note that in order to reassign the pilot sub-carriers, there is an additional cost of performing another round of SNR estimation. It is not clear if the data rate increase resulting from the SNR improvement from pilot reassignment would be greater than the data rate decrease resulting from the additional processing overhead. This is an area of further investigation. For this version of the implementation, the pilot sub-carriers are fixed throughout all the steps of transmission.

4.3 Step 2: CSI Feedback

After the sub-carrier modulation assignment has been determined at the receiver in Step 1, the information has to be shipped back to the transmitter. The packet containing this information has a structure shown in Figure 4-5.

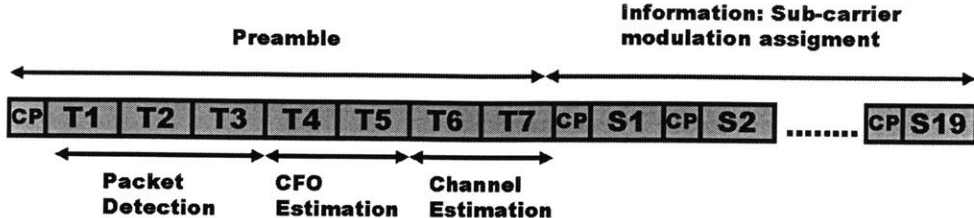


Figure 4-5: Packet Structure during CSI Feedback

For the OFDM preamble symbols, it is formed by taking the Fourier Transform of the sequence $S_{PREAMBLE}$. $S_{PREAMBLE,k}$, the element of $S_{PREAMBLE}$ assigned to the k^{th} frequency bin is determined in the following manner

$$S_{PREAMBLE,k} = \begin{cases} S_k & \text{if } k^{th} \text{ frequency bin is used,} \\ 0 & \text{otherwise} \end{cases} \quad (4.13)$$

where S_k is the k^{th} element from Equation 4.2. Having the same number of frequency bins used in the preamble and the data symbols would result in the same average power throughout the packet. This is particularly important for a real-time Automatic Gain Controller (AGC) where power is adjusted during the preamble assuming the average power of the preamble and the data is same.

Pilot sub-carriers are reserved in the OFDM data symbols. They are used for phase tracking and are fixed at frequency bin indices $k = \{-39, -28, -17, -6, 6, 17, 28, 39\}$. Note that the pilot assignment is the same as Step 1. Let P_k be the value of the pilot sub-carrier at the k^{th} frequency bin is determined in the following manner

$$P_k = \begin{cases} S_k & k = \{-39, -28, -17, -6, 6, 17, 28, 39\}, \\ N/A & \text{otherwise} \end{cases} \quad (4.14)$$

As the sub-carriers are not yet adapted to sub-carrier conditions, the synchronization data sent from the receiver to the transmitter faces a Rayleigh fading channel. In this scenario, only frequency bins indices k from -50 to -1 and 1 to 50 are used. Sub-carriers in the transition band of the anti-aliasing filters are avoided as mentioned

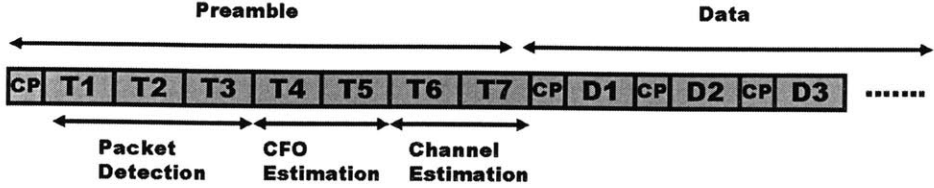


Figure 4-6: Packet Structure during Data Transmission

in Section 3.1. Excluding the pilot sub-carriers, 92 sub-carriers are used to carry data. As the synchronization information is important and Rayleigh fading channel is experienced, the following design choices are made to minimize and detect errors:

- The data-bearing sub-carriers are BPSK-modulated.
- The data bits are first coded by Cyclic Redundancy Check (CRC)(48,32) for error detection capabilities (i.e. 32 bits are used to form a 48 codeword). The implementation structure of the CRC can be found in [29].
- Following the CRC(48,32), BCH(15,5) is then subsequently applied to the bits for error correction capabilities. Empirically, at max link distances of 10m, BCH(15,5) gives no errors. The implementation structure of the BCH codes can be found in [19].

It would take 19 OFDM data symbols to send the synchronization information in Step 2. From the above information, it can be inferred that 92 bits are sent per OFDM symbol. From Table 4.2, each sub-carrier has 6 possibilities for a modulation decision. It would translate to 3 bits of synchronization data per sub-carrier. In total, 384 data bits needs to be sent. However, after the CRC(48,32) and BCH(15,5), the number of bits to be sent has increased to 1728. This means that 19 OFDM data symbols are needed to ship the information from the receiver to the transmitter.

4.4 Step 3: Data

After the CSI information is received in Step 2, data is sent in the packet structure shown in Figure 4-6. The data OFDM symbols are modulated using the sub-carrier

modulation assignment obtained. Based on the frequency bins used in the data symbols, the OFDM preamble symbols are formed by taking the Fourier Transform of the sequence $S_{PREAMBLE}$ where $S_{PREAMBLE,k}$ is determined in Equation 4.13. Pilot sub-carriers in the data symbols used for phase tracking fixed at the same locations as in Step 1 and 2 (i.e. frequency bin indices $k = \{-39, -28, -17, -6, 6, 17, 28, 39\}$). Values of these pilot sub-carriers P_k is determined in Equation 4.14.

4.5 Summary

In order for Frequency Adaptive Modulation to work, the transmitter and receiver needs to be synchronized. A packet is sent from the transmitter to the receiver to estimate the SNR and make modulation decisions on a per sub-carrier basis. The information is sent back from the receiver to the transmitter. This information has to be heavily coded as a Rayleigh fading channel is faced. Once the transmitter and receiver is synchronized, frequency adaptive modulation can take place.

In systems that are coded, a BER of 10^{-5} is targeted. For the WiGLAN where data is not coded, a targeted uncoded BER of 10^{-3} is chosen. After coding, an uncoded BER of 10^{-3} can easily be driven down to 10^{-5} .

Chapter 5

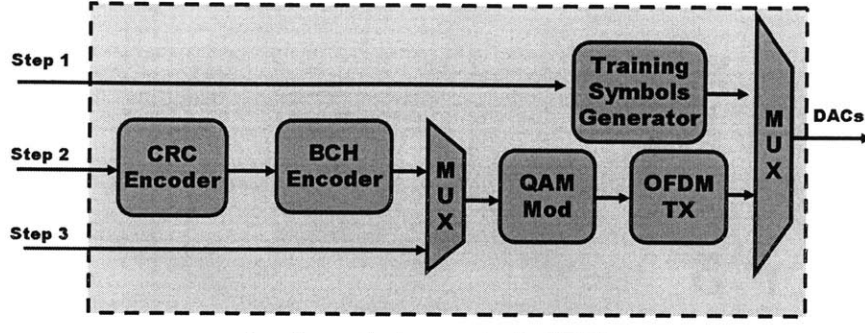
Results and Analysis

In this chapter, results will be presented. The first section will report logic utilization of implemented transmitter and receiver on the Field Programmable Gate Array (FPGA) and analyze it. The second section will present the test setup performed with the Wireless Gigabit Local Area Network (WiGLAN) prototype in a real-time wireless environment. The third section will cover the experimental data collected and the subsequent sections will analysis the experimental data.

5.1 Logic Utilization of the WiGLAN Baseband Node

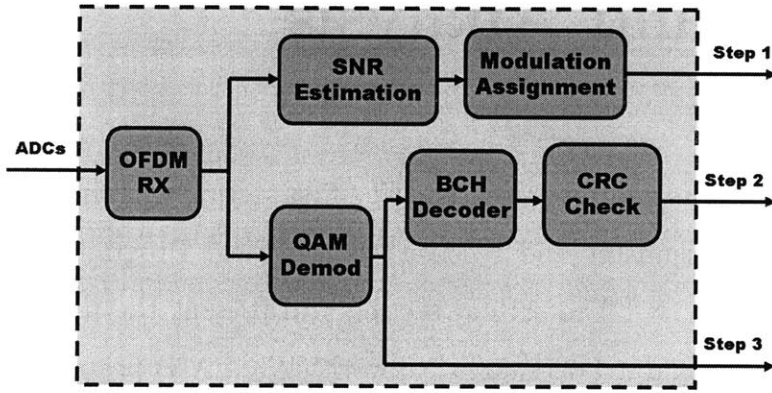
The baseband modem is implemented on the Xilinx Virtex 4 FPGA. The resources available on this FPGA are as follows:

- *Flip-Flops (FF)*: These are storage elements.
- *Look-up Table (LUT)*: These are 4-input look-up tables which are capable of implementing any arbitrarily defined 4-input Boolean function.
- *RAMB16*: These are 18kbits memory blocks.
- *DSP48*: These are multipliers capable of multiplying two 18 bits numbers.



Implemented on a single FPGA

(a) Transmitter Implementation on FPGA



Implemented on a single FPGA

(b) Receiver Implementation on FPGA

Figure 5-1: Baseband Modem Implementation on FPGA

In addition to reporting the device utilization of the design in terms of these resources, the FPGA synthesis and implementation tool also reports the total equivalent gate count for the design which is the number of 2-input NAND gates required for the design if all utilized FPGA resources are decomposed to 2-input NAND gates. More information about the Xilinx Virtex 4 FPGA can be found in [31].

FPGA implementation of the transmitter and receiver capable of supporting the Frequency Adaptive Modulation specified in Chapter 4 is shown in Figure 5-1. The design on the FPGA is capable of running at the desired clock frequency of 128 MHz. The device utilization of the transmitter and receiver is found in Table 5.1. For the Frequency Adaptive Modulation to fully function, the transmitter and receiver needs to be integrated on a single FPGA. It is noted that the IFFT/FFT module required by the transmitter and the receiver is one of the most resource-intensive

<i>Resources</i>	<i>Transmitter</i>	<i>Receiver</i>
<i>FFs (/30,720)</i>	2,883 (9%)	12,486 (40%)
<i>LUTs (/30,720)</i>	3,350 (10%)	12,354 (40%)
<i>RAMB16s (/192)</i>	12 (6%)	37 (19%)
<i>DSP48s (/192)</i>	11 (11%)	44 (22%)
<i>Gate Count</i>	82,984	273,491

Table 5.1: Number of 2-input NAND gates of Transmitter and Receiver

<i>Resources</i>	<i>FFT/IFFT</i>
<i>FFs (/30,720)</i>	2,260 (7%)
<i>LUTs (/30,720)</i>	1,918 (6%)
<i>RAMB16s (/192)</i>	7 (3%)
<i>DSP48s (/192)</i>	9 (4%)
<i>Gate Count</i>	61,536

Table 5.2: Number of 2-input NAND gates of IFFT/FFT Module

<i>Resources</i>	<i>Transceiver</i>
<i>FFs (/30,720)</i>	13,107 (42%)
<i>LUTs (/30,720)</i>	13,786 (46%)
<i>RAMB16s (/192)</i>	42 (21%)
<i>DSP48s (/192)</i>	46 (23%)
<i>Gate Count</i>	294,939

Table 5.3: Estimated Number of 2-input NAND gates of Transceiver

<i>Resources</i>	<i>Frequency Adaptive Modulation Blocks</i>
<i>FFs (/30,720)</i>	650 (2%)
<i>LUTs (/30,720)</i>	1112(3%)
<i>RAMB16s (/192)</i>	13 (6%)
<i>DSP48s (/192)</i>	2 (1%)
<i>Gate Count</i>	16,499

Table 5.4: Number of 2-input NAND gates of Frequency Adaptive Modulation blocks

module. Device utilization of this module is given in Table 5.2. In terms of gate count, the IFFT/FFT modules occupy 74% and 23% of the transmitter and receiver design respectively. Hence during integration, the IFFT/FFT module will be shared between the transmitter and the receiver. Based on Tables 5.1 and 5.2, the estimated device utilization of the integrated transceiver is given in Table 5.3. Since the entire transceiver fits into a single FPGA and uses less than half of the FPGA’s resources, it can be said that the implementation size of the design is reasonable.

The Frequency Adaptive Modulation blocks in the FPGA implementation shown in Figure 5-1 are:

- SNR estimation.
- Modulation assignment.
- BCH encoder and decoder.
- CRC encoder and CRC check.

Without these blocks, Frequency Adaptive Modulation is not possible. However, normal OFDM transmission without Frequency Adaptive Modulation can still occur. Hence the Frequency Adaptive Modulation blocks are the extra overhead on a normal Orthogonal Frequency Division Multiplexing (OFDM) system to enable Frequency Adaptive Modulation. The device utilization of the Frequency Adaptive Modulation blocks is shown in Table 5.4

In [32], a OFDM baseband modem extended with adaptive loading has been implemented on a FPGA. There are two key differences from the WiGLAN node:

<i>Tx Location</i>	<i>Link Distance(m)</i>
A	1.0
B	2.8
C	4.5
D	6.3
E	4.0
F	6.3
G	8.2
H	10.2
I	5.7
J	7.2
K	8.9
L	10.8

Table 5.5: Link Distance for various measurements

1. *Bandwidth:* 20 MHz of bandwidth is utilized as opposed to 128 MHz in the WiGLAN.
2. *Frequency Adaptive Modulation:* Fischer algorithm [33] is used. The Fischer algorithm is an optimal adaptive modulation algorithm but requires an expensive \log_2 computation. The WiGLAN, as elaborated in Chapter 4, uses a sub-optimal low complexity adaptive modulation algorithm. This algorithm uses a series of comparisons on the estimated SNR per sub-carrier to make a modulation decision.

It is found in [32] that Frequency Adaptive Modulation using the Fischer algorithm causes a extra overhead that uses approximately 103% more gates compared to the IFFT/IFFT. From Tables 5.2, 5.3 and 5.4, the gate count for the WiGLAN's Frequency Adaptive Modulation is 27% compared to IFFT/FFT and 6% compared to the overall transceiver. It can be said that Frequency Adaptive Modulation used in WiGLAN is of low implementation complexity.

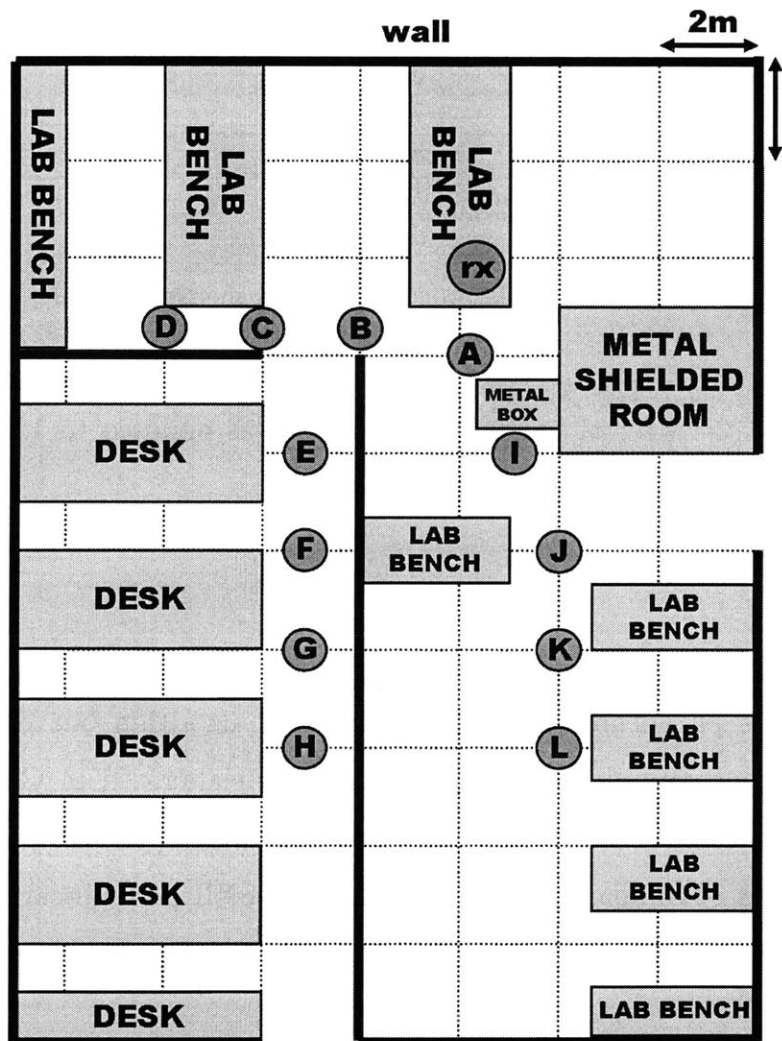


Figure 5-2: Location of transmitter-receiver pair in the Lab

5.2 Measurement Test setup

To perform measurements, two WiGLAN Nodes are used where one acts as a transmitter and the other acts as a receiver. A WiGLAN nodes consist of the implemented baseband modem integrated with a custom-made RF Front End [7]. The maximum transmit power of the RF Front End is 7.5 dBm. All the measurements are taken in a lab environment. Figure 5-2 shows the location of the receiver and 11 possible locations of the transmitter from A to L. These locations are chosen to obtain a diversity of channel conditions such as

- *Strong Line of Sight:* Locations A to D which are unobstructed.
- *Weak Line of Sight:* Locations E to H which are obstructed by a metal box.
- *No Line of Sight:* Locations I to L which are obstructed by concrete wall.

The link distance of these locations are presented in Table 5.5. During the test, a packet is sent from the transmitter to the receiver. The preamble structure of this packet and pilot sub-carrier assignment is the same as Step 3:Data of the Frequency Adaptive Modulation Protocol documented in Section 4.4. The pre-determined configuration of this packet is as follows:

- All the sub-carriers are used to send data and are BPSK-modulated except the DC bin and 8 pilot sub-carriers.
- The packet contains 524,195 randomly generated data bits with each sub-carrier transmitting 4,405 data bits.

The receiver will process the packet and decode the bits real-time. Bit Error Rate (BER) for each sub-carrier is calculated by taking the ratio of the number of bit errors received to the total number of bits sent on each sub-carrier. Also, the first 100 OFDM data symbols are acquired on the FPGA and are processed in the Matlab to:

- Estimate the channel attenuation $|H|^2$ per sub-carrier as described in Equation 3.18.

- Estimate the signal-to-noise ratio (SNR) per sub-carrier as described in Equation 4.5 where $N = 100$.
- Make an adaptive modulation decision from the estimated SNR using Table 4.2.

$|H|^2$ is of interest because a variation in $|H|^2$ results in an equal variation in the *SNR* (i.e. a drop of X dB in $|H|^2$ would result in a drop of X dB in *SNR*). The assumption here is that the noise power contribution for different frequencies is the same at the input of the baseband. This is characteristic of the thermal noise of the RF Front End and quantization noise which are the major sources of noise.

Performance of a OFDM system without Frequency Adaptive Modulation will be evaluated. This system could be referred to as a normal OFDM system for the rest of the thesis. The normal OFDM system uses the WiGLAN hardware but with the following constraints:

- 27 higher frequency bins in the transition band of the analog filters and the DC bin are not used as discussed in Section 3.1.
- All remaining 100 sub-carriers are used but the modulation scheme for these sub-carriers, while can be adapted, is chosen the same for all bins.

These constraints are typical in today's wireless standards [2, 3, 4]. After measuring the BER and SNR per sub-carrier, the following variables are obtained for the normal OFDM system using BPSK:

- *Mean SNR of the system*: This is calculated as the average SNR of the 100 sub-carriers used.
- *System BER*: This is calculated as the ratio of number of bit errors received to the total number of bits sent on the 100 sub-carriers used.

5.3 Channel Measurements

The measured channel attenuation $|H|^2$, SNR, adaptive modulation decisions and BER for location A to F can be found in Figure 5-3 to 5-8. The adaptive modulation

A		B	
Modulation Scheme	Number	Modulation Scheme	Number
256-QAM	0	256-QAM	0
64-QAM	7	64-QAM	16
16-QAM	62	16-QAM	72
4-QAM	40	4-QAM	20
BPSK	8	BPSK	3
Null	3	Null	2
Pilot	8	Pilot	8
C		D	
Modulation Scheme	Number	Modulation Scheme	Number
256-QAM	0	256-QAM	0
64-QAM	5	64-QAM	4
16-QAM	32	16-QAM	37
4-QAM	30	4-QAM	42
BPSK	6	BPSK	9
Null	46	Null	28
Pilot	8	Pilot	8

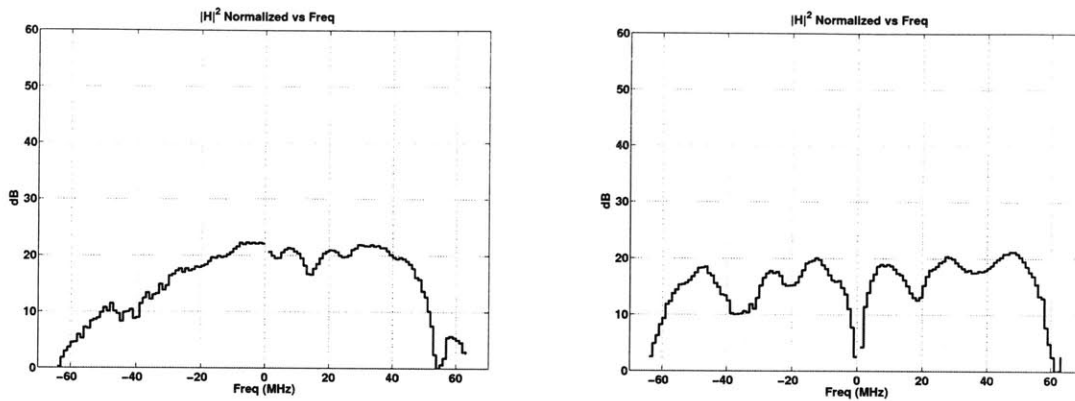
Table 5.6: Adaptive Modulation Assignment for Location A to D

assignments for each location is tabulated in Table 5.6 to Table 5.8. The measured mean SNR and system BER for a normal OFDM system described in Section 5.2 can be found in Table 5.9

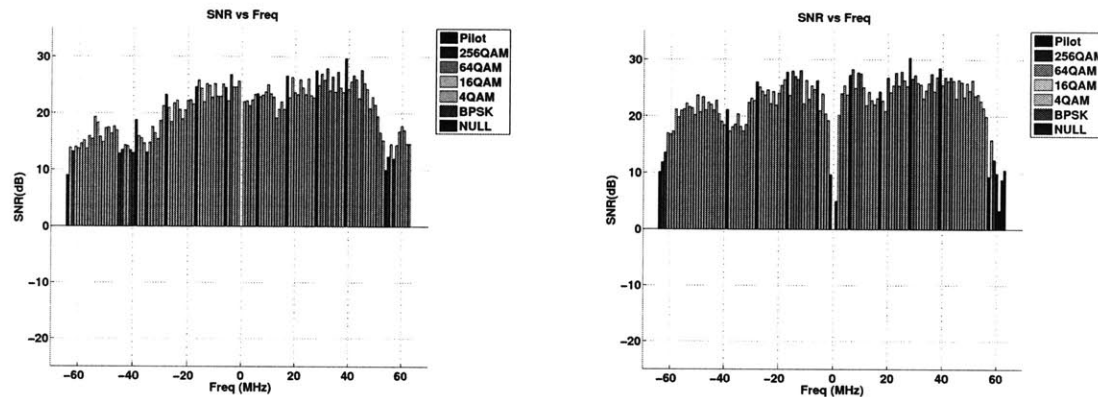
5.4 Analysis

Upon visual inspection of Figure 5-3 to 5-8, the $|H|^2$ variations matches up with the *SNR* variations. Also, the BER is inversely proportional to the SNR. Based on the channel measurements taken, the subsequent sections will describe an in-depth analysis on the following:

- Path Loss Exponent in the Lab.
- Verification that a Rayleigh Channel decompose to Gaussian sub-channels.
- Data Rate of the WiGLAN ignoring synchronization overhead from Frequency Adaptive Modulation.

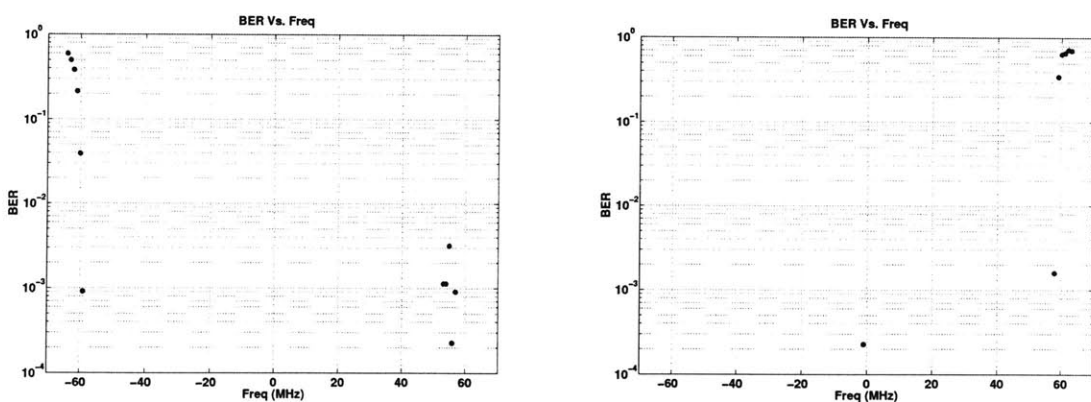


(a) A: Channel Attenuation $|H|^2$ vs. Frequency (b) B: Channel Attenuation $|H|^2$ vs. Frequency



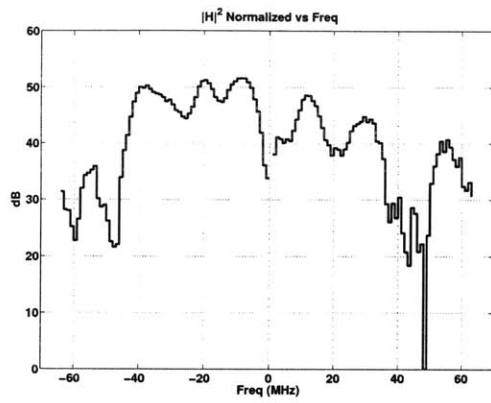
(c) A: SNR vs. Frequency

(d) B: SNR vs. Frequency

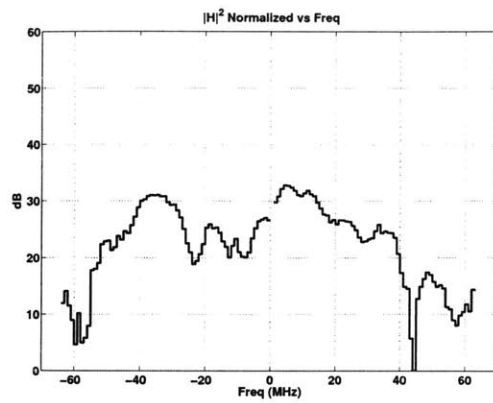


(e) A: BER vs. Frequency ($\text{BER} \geq 2.2 \times 10^{-4}$ shown)
(f) B: BER vs. Frequency ($\text{BER} \geq 2.2 \times 10^{-4}$ shown)

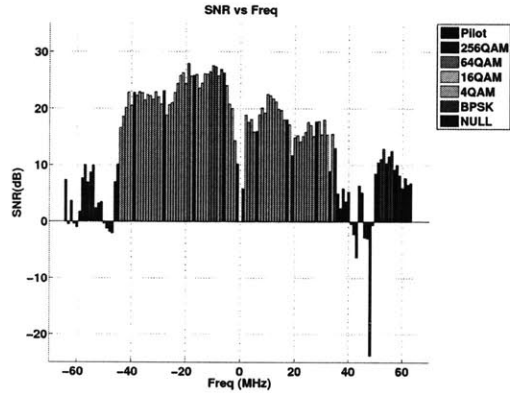
Figure 5-3: Measurements for Location A-B



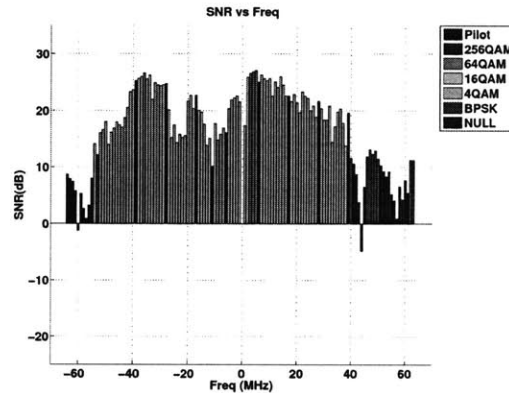
(a) C: Channel Attenuation $|H|^2$ vs. Frequency



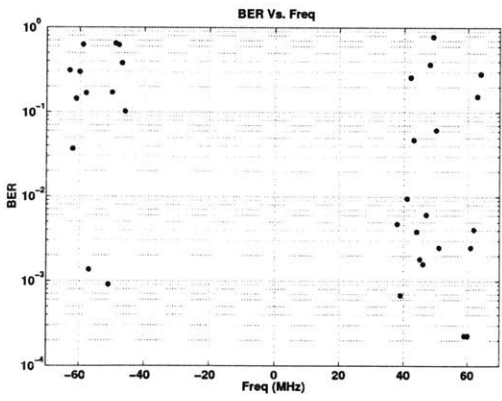
(b) D: Channel Attenuation $|H|^2$ vs. Frequency



(c) C: SNR vs. Frequency



(d) D: SNR vs. Frequency



(e) C: BER vs. Frequency($\text{BER} \geq 2.2 \times 10^{-4}$ shown)

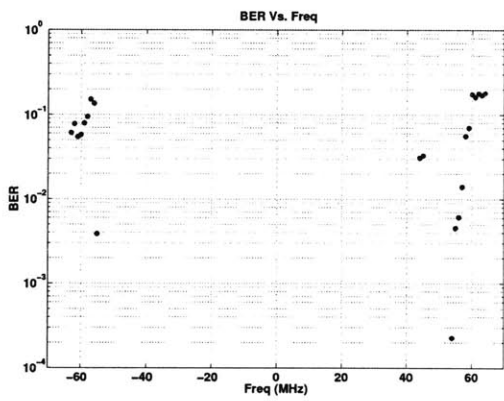
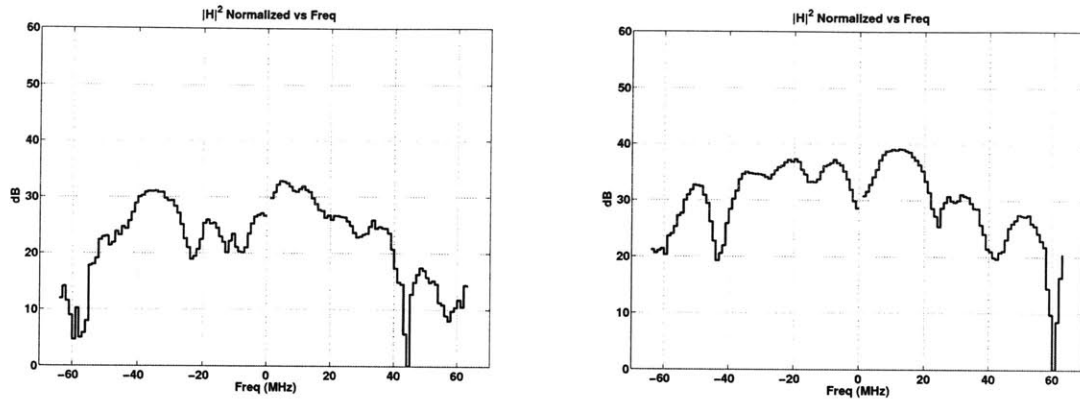
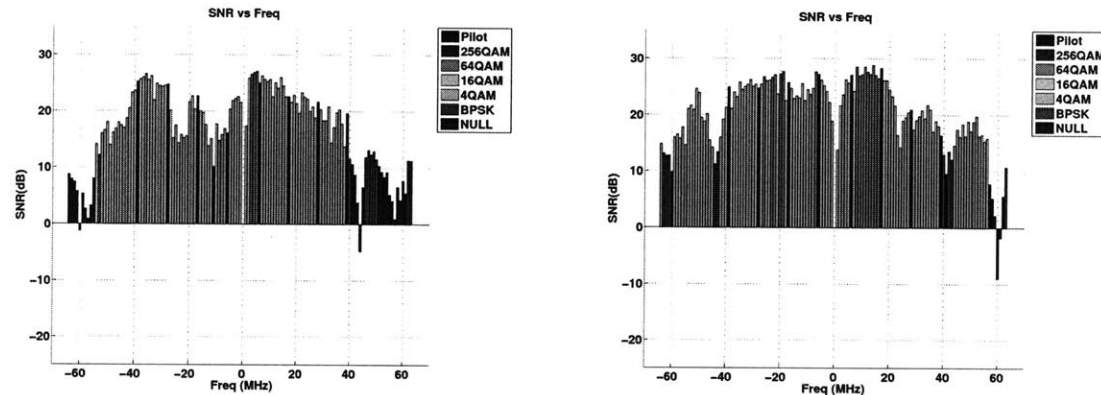


Figure 5-4: Measurements for Location C-D

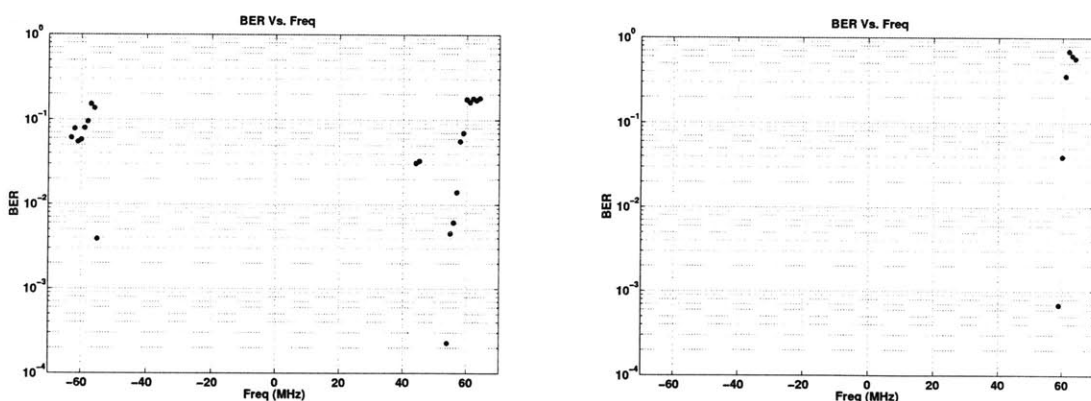


(a) D: Channel Attenuation $|H|^2$ vs. Frequency (b) E: Channel Attenuation $|H|^2$ vs. Frequency



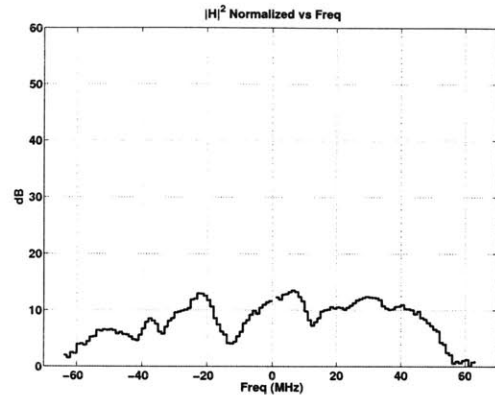
(c) D: SNR vs. Frequency

(d) E: SNR vs. Frequency

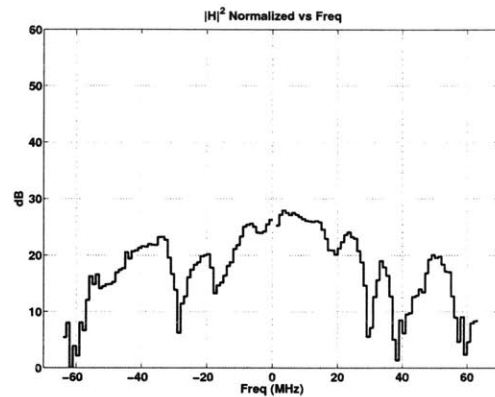


(e) D: BER vs. Frequency($\text{BER} \geq 2.2 \times 10^{-4}$ shown)
(f) E: BER vs. Frequency($\text{BER} \geq 2.2 \times 10^{-4}$ shown)

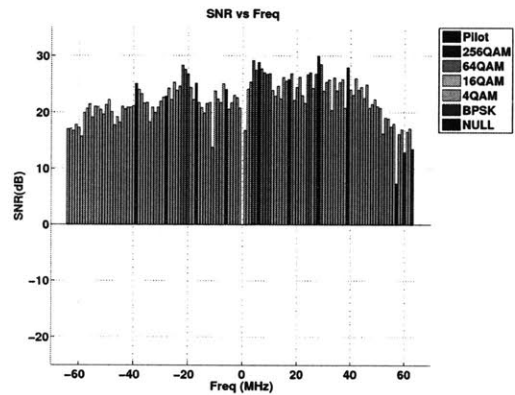
Figure 5-5: Measurements for Location D and E



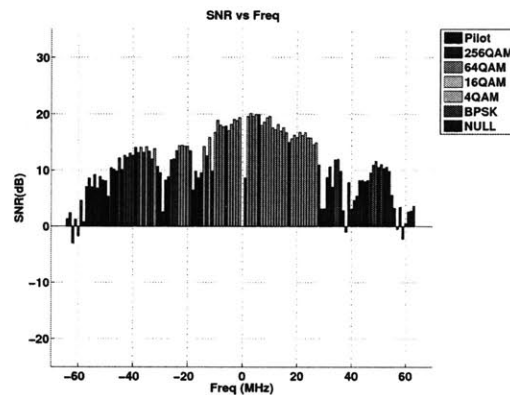
(a) F: Channel Attenuation $|H|^2$ vs. Frequency



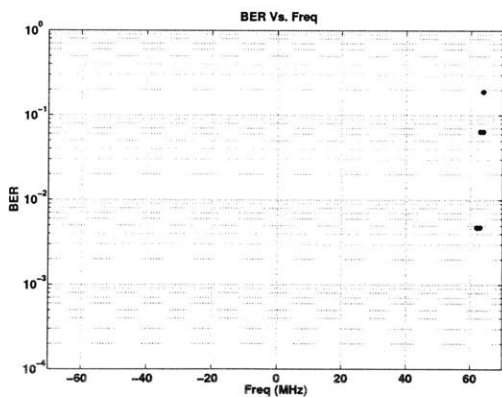
(b) G: Channel Attenuation $|H|^2$ vs. Frequency



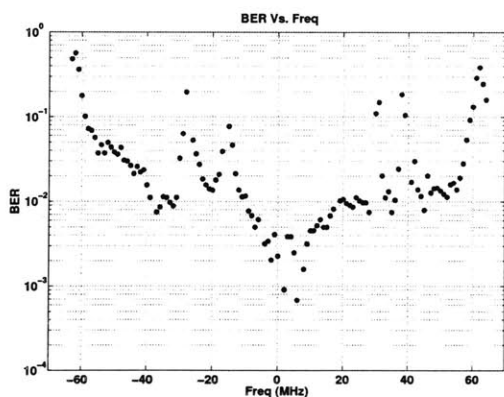
(c) F: SNR vs. Frequency



(d) G: SNR vs. Frequency

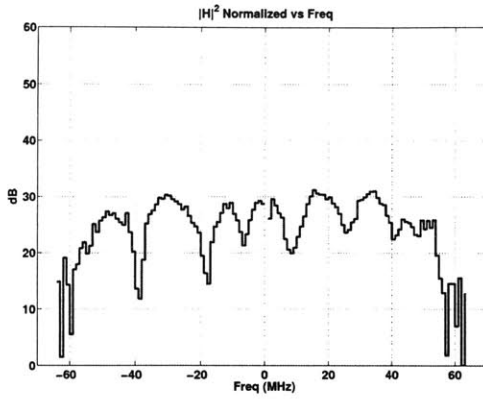


(e) F: BER vs. Frequency($\text{BER} \geq 2.2 \times 10^{-4}$ shown)

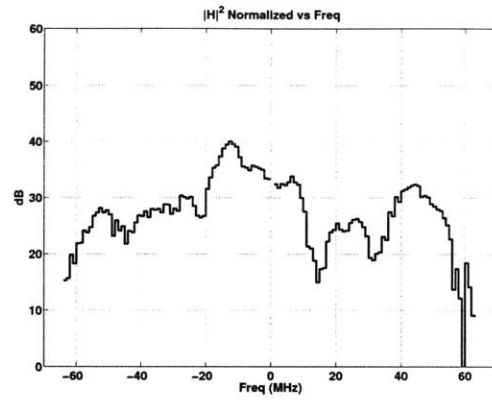


(f) G: BER vs. Frequency($\text{BER} \geq 2.2 \times 10^{-4}$ shown)

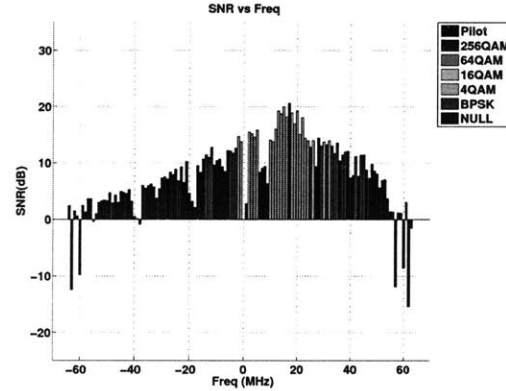
Figure 5-6: Measurements for Location F and G



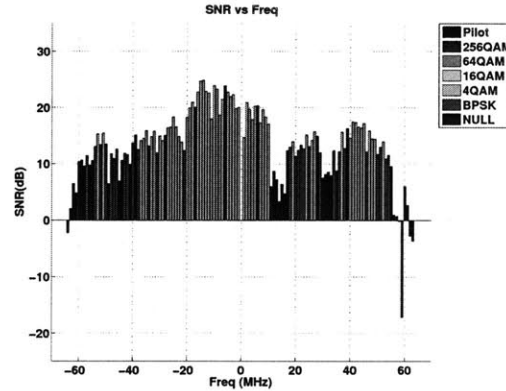
(a) H: Channel Attenuation $|H|^2$ vs. Frequency



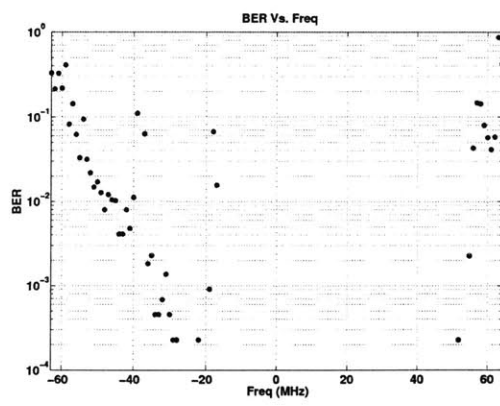
(b) I: Channel Attenuation $|H|^2$ vs. Frequency



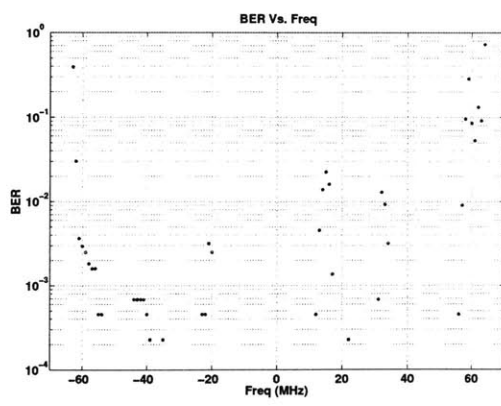
(c) H: SNR vs. Frequency



(d) I: SNR vs. Frequency



(e) H: BER vs. Frequency($\text{BER} \geq 2.2 \times 10^{-4}$ shown)



(f) I: BER vs. Frequency($\text{BER} \geq 2.2 \times 10^{-4}$ shown)

Figure 5-7: Measurements for Location H and I

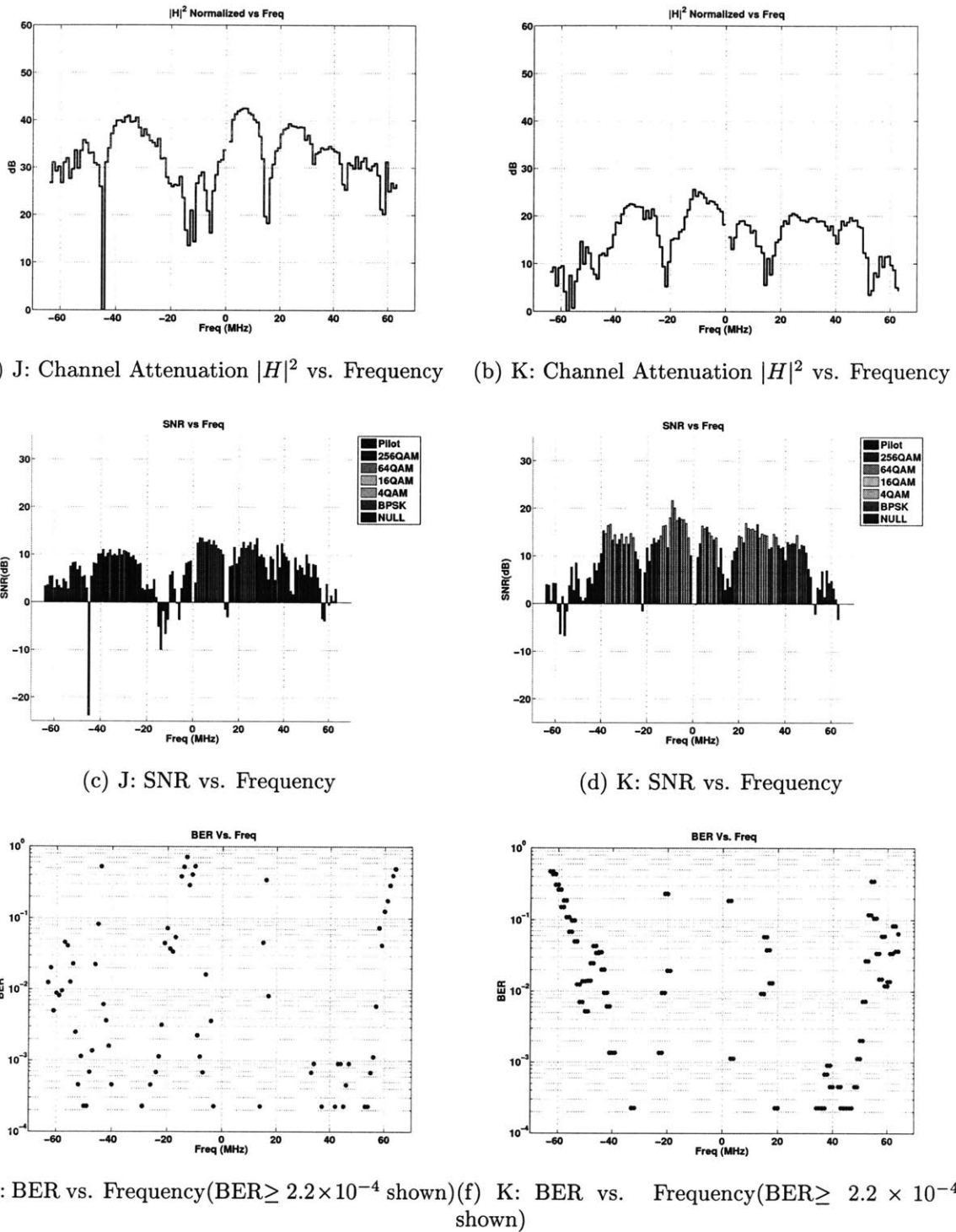


Figure 5-8: Measurements for Location J and K

E	
Modulation Scheme	Number
256-QAM	0
64-QAM	15
16-QAM	48
4-QAM	39
BPSK	9
Null	9
Pilot	8

F	
Modulation Scheme	Number
256-QAM	0
64-QAM	14
16-QAM	74
4-QAM	28
BPSK	2
Null	2
Pilot	8

G	
Modulation Scheme	Number
256-QAM	0
64-QAM	0
16-QAM	0
4-QAM	42
BPSK	19
Null	59
Pilot	8

H	
Modulation Scheme	Number
256-QAM	0
64-QAM	0
16-QAM	0
4-QAM	23
BPSK	17
Null	80
Pilot	8

Table 5.7: Adaptive Modulation Assignment for Tx Location E to H

I	
Modulation Scheme	Number
256-QAM	0
64-QAM	0
16-QAM	13
4-QAM	44
BPSK	29
Null	33
Pilot	8

J	
Modulation Scheme	Number
256-QAM	0
64-QAM	0
16-QAM	0
4-QAM	0
BPSK	22
Null	98
Pilot	8

K	
Modulation Scheme	Number
256-QAM	0
64-QAM	0
16-QAM	1
4-QAM	37
BPSK	28
Null	54
Pilot	8

L	
Modulation Scheme	Number
256-QAM	0
64-QAM	0
16-QAM	0
4-QAM	0
BPSK	13
Null	107
Pilot	8

Table 5.8: Adaptive Modulation Assignment for Tx Location I to L

<i>Transmitter Location</i>	<i>Mean SNR(dB)</i>	<i>System BER</i>
A	21.78	-
B	23.47	2.46×10^{-6}
C	15.82	3.59×10^{-2}
D	19.20	6.96×10^{-4}
E	21.87	-
F	23.19	-
G	12.77	2.27×10^{-2}
H	9.96	3.80×10^{-3}
I	14.88	1.04×10^{-3}
J	7.05	4.55×10^{-2}
K	11.79	8.42×10^{-3}
L	4.92	1.11×10^{-1}

Table 5.9: Measured Mean SNR and System BER of a normal OFDM System in various locations ($\text{BER} \geq 2.4 \times 10^{-6}$ shown)

- Data Rate of the WiGLAN considering synchronization overhead from Frequency Adaptive Modulation.
- Data Rate of a normal OFDM system.
- Comparison of the WiGLAN with a normal OFDM system.

5.4.1 Path Loss Exponent In the Lab

An increase in link distance, d leads to a decrease in received power. This decrease in power is referred to as the path loss, PL . PL has the following relationship with d [5]

$$PL \propto d^n \quad (5.1)$$

$$PL(\text{dB}) = n(10\log_{10}(d)) + c_{PL} \quad (5.2)$$

where n is defined to be the path loss exponent [5] and c_{PL} is a constant. The path loss component is dependent on the surroundings and building type. As discussed in Section 5.3, the received SNR(dB) is a linear function of the channel attenuation(dB). The channel attenuation can also be viewed as the path loss. Hence from Equation 5.2,

the following can be said about the received SNR(dB)

$$SNR(dB) = -n(10\log_{10}(d)) + c_{SNR} \quad (5.3)$$

where c_{SNR} is a constant. From Tables 5.9 and 5.5, the measured mean SNR(dB) is plotted against $-10\log_{10}d$ in Figure 5-9. A best-fit line from linear regression can be computed and the slope of this best-fit line gives an estimated n .

Observing from Figure 5-9, the measurements tend to cluster on either side of the best-fit line and the data point at $d = 1$ seems to be an outlier. From [5], it is stated in the Ericsson Multiple Breakpoint Model that the path loss exponent varies for different ranges of link distance. It is expected that the path loss exponent is larger from longer distances than shorter distances. With respect to the measurements obtained, it is possible that the path loss exponent is not the same for the range of $1 \leq d \leq 10.8$ which explains the bad fit of the best-fit line. Another best-fit line is computed for data points with $d \geq 2.8$ and plotted. From Figure 5-9, this best-fit line provides a good fit for data points with $d \geq 2.8$

Hence in the lab environment where the measurements are taken, the path loss exponent n is estimated to be 2.80 for link distances ranging from 2.8m to 10.8m. It is reported in [5] that typical values of the path loss exponent in an indoor environment can vary from 1.6 to 3.3.

5.4.2 Decomposition of Rayleigh Channel to Gaussian sub-carriers

A typical OFDM system uses the same modulation scheme across all the sub-carriers. Assuming a packet is sent within the coherence time and large variations are experienced in channel frequency response, the system faces a Rayleigh fading across the frequency dimension. It is expected that large variations would occur due to the fact that the signal bandwidth is large. Frequency Adaptive Modulation can be used to reduce the Rayleigh channel to Gaussian sub-channels by optimizing the modulation scheme on a sub-carrier basis.

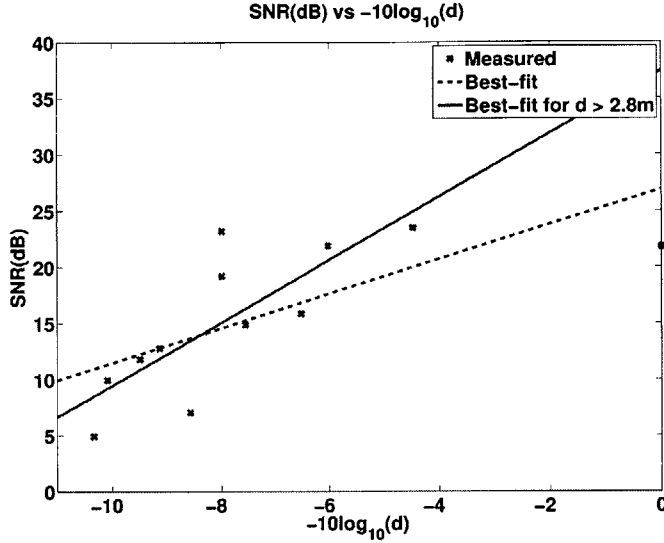


Figure 5-9: Mean SNR vs $-10\log_{10}(d)$

Measured system and the sub-carriers' BER from Section 5.3 are compared with Theoretical Rayleigh and Gaussian curves for BPSK in Figure 5-10. For $SNR \leq 15dB$, the system BER follows the Rayleigh curve. At higher SNR, the system BER deviates from the Rayleigh curve and gets closer to the Gaussian curve. Based on the number of bits sent, a system BER greater than 2.4×10^{-6} can be detected. From Table 5.5, locations with $21 \geq SNR(dB) \geq 24$ has no bit error when the Rayleigh curve predicts a system BER of at least 10^{-4} in that SNR range.

The measurements indicate that as the mean SNR increases, the system is getting increasingly less Rayleigh in nature. This can be explained in the following manner. From Section 2.3, as the link distance decreases, the coherence bandwidth will decrease leading to less variations in the channel frequency response. It is expected that as link distance decreases, the degree of Rayleigh fading experienced by the channel decreases. From Section 5.4.1, the mean SNR increases from a decrease in link distance. Hence, it can be inferred that as the mean SNR increases, the channel deviates from Rayleigh curve and approaches the Gaussian curve.

In addition, the results validate that while the system faces a various degree of Rayleigh fading, each of the sub-carriers is Gaussian in nature. This shows a strong case for Frequency Adaptive Modulation. The processing gain of reducing a Rayleigh

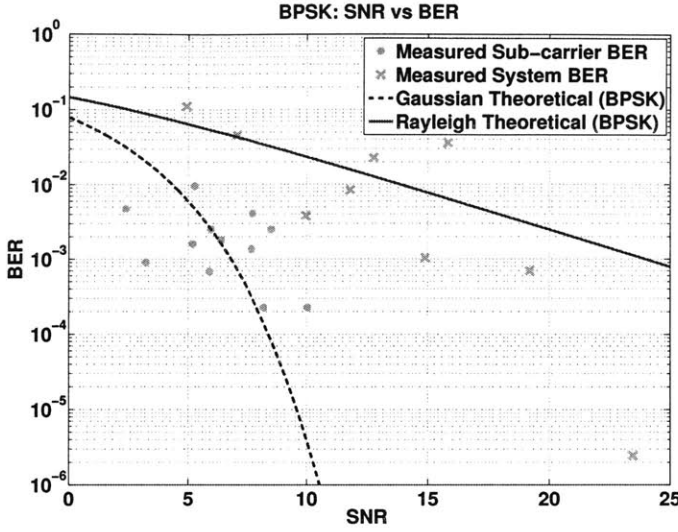


Figure 5-10: Rayleigh Fading Channel decomposed to Gaussian sub-carriers (System BER $\geq 2.4 \times 10^{-6}$ and Sub-carrier BER $\geq 2.2 \times 10^{-4}$ shown)

channel to Gaussian sub-carriers can be used to:

- Increase data rate.
- Improve BER.
- Reduce channel coding requirements.

5.4.3 Data Rate of the WiGLAN ignoring Frequency Adaptive Modulation Overhead

From Chapter 2, the symbol period of each OFDM period, T_{SYM} is $1.2 \mu s$. For each transmitter location, the number of bits per OFDM symbol N_{BPS} can be derived using Tables 3.1 and 5.6 to 5.8. The N_{BPS} and the data rate R_{WiGLAN} for location A to K can be found in Table 5.10.

From Tables 5.5 and 5.10, the Link Distance vs. Data Rate R is plotted in Figure 5-11. It shows that generally as the link distance increases, R decreases. This is expected as the link distance increases, the received signal power gets increasingly attenuated. There is no line of sight for location I to L. As expected, it does generally do poorly compared to other measurements at comparable link distances. For

<i>Transmitter Location</i>	N_{BPS}	$R_{WiGLAN} = N_{BPS}/T_{SYM} (Mbps)$
A	378	315
B	427	355
C	224	186
D	265	220
E	396	330
F	438	365
G	103	85
H	63	52
I	169	140
J	22	18
K	106	88
L	13	10

Table 5.10: WiGLAN Data Rate for location A to L

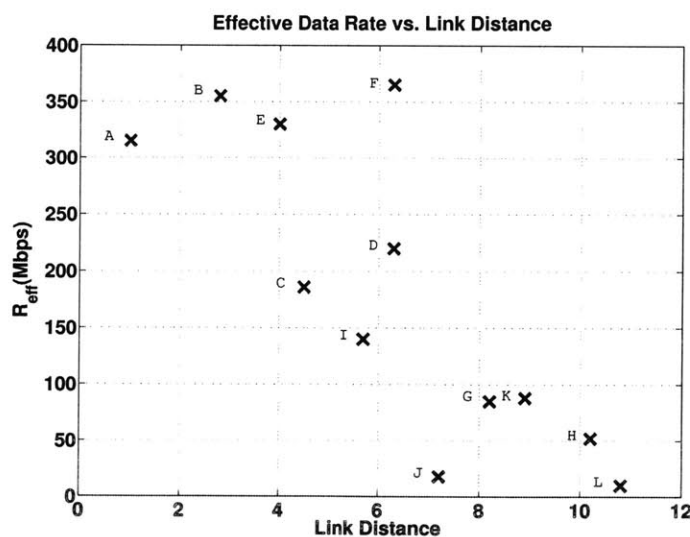


Figure 5-11: Data Rate vs Link Distance

Location A to D where there is a strong line of sight, it is expected to perform better than Location E to H where there is a weak line of sight. Location D and F are at comparable distances but the data rate from Location F is 1.83 times of Location D. When there is line of sight between the transmitter and receiver, the link quality is indicated by Ricean K factor which is the relative strength of the direct to the scattered components of the signal [34]. Therefore, even Location D has a stronger line of sight compared Location F, the strength of the scattered components is unknown.

5.4.4 Data Rate of WiGLAN with Frequency Adaptive Modulation Overhead

Before data is sent, the adaptive modulation protocol in Chapter 4 requires that

1. A packet of 37 OFDM symbols be sent from transmitter to receiver for SNR estimation seen in Figure 4-2. This introduces an overhead of $37.2 \mu\text{s}$.
2. A packet of 26 OFDM symbols to be sent from receiver to transmitter for CSI feedback seen in Figure 4-5. This introduces an overhead of $30 \mu\text{s}$.

Now including the computational latency of processing these synchronization packets, the synchronization overhead, T_{sync} is approximately $100\mu\text{s}$.

As long as the transmission is within the coherence time of the channel, it is possible to have a networking protocol that incurs the synchronization overhead for a window of packets sent. For a conservative analysis, it is assumed that the synchronization overhead is incurred for per packet sent. Intuitively, if the packet size is large, the synchronization overhead could be negligible. In wireless standards[2], the maximum number of bits per packet, N_{BPP} , is 32,760 bits (4,095 bytes). The effective data rate $R_{WiGLAN;eff}$ and the loss of data rate due to overhead L_{OH} can be

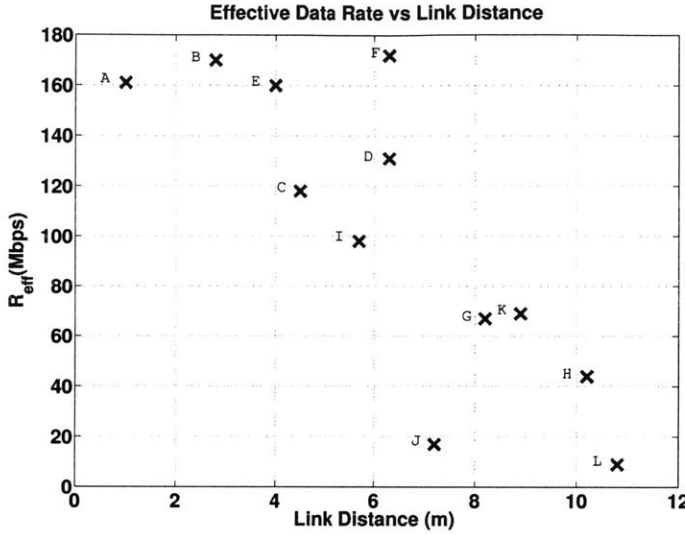


Figure 5-12: Effective Data Rate vs. Link Distance

found in the following manner

$$R_{WiGLAN;eff} = \frac{N_{BPP}}{T_{sync} + T_{data}} \quad (5.4)$$

$$T_{data} = \frac{N_{BPP}}{R_{WiGLAN}} \quad (5.5)$$

$$L_{OH} = \frac{R_{WiGLAN} - R_{WiGLAN;eff}}{R_{WiGLAN}} \quad (5.6)$$

where

- T_{data} is the time to sent the data packet.
- R_{WiGLAN} is the data rate of sending the data packet as determined in Section 5.4.3.

Using $T_{sync} = 100 \mu s$, N_{BPP} to 32760 and R_{WiGLAN} values in Table 5.10, the $R_{WiGLAN;eff}$ and L_{OH} are calculated and tabulated in Table 5.11. It is observed that L_{OH} is proportional to the R_{WiGLAN} . When the R_{WiGLAN} is larger, the time to send the data packet decreases. However, the overhead time, T_{sync} remains the same. This means as R_{WiGLAN} increases, the overhead becomes a larger percentage of the packet which in turns increases L_{OH} . The $R_{WiGLAN;eff}$ vs. Link Distance can be found in Figure 5-12.

<i>Transmitter Location</i>	R_{WiGLAN} (Table 5.10)	$R_{WiGLAN;eff}$ (Mbps) (Equation 5.4)	L_{OH} (Equation 5.6)
A	315	161	0.49
B	355	170	0.52
C	186	118	0.36
D	220	131	0.40
E	330	160	0.51
F	365	172	0.53
G	85	67	0.21
H	52	44	0.15
I	140	98	0.30
J	18	17	0.6
K	88	69	0.21
L	10	9	0.10

Table 5.11: Effective WiGLAN Data Rate And Data Loss from Overhead for location A to K

5.4.5 Data Rate of a normal OFDM System

A normal OFDM system can adapt its modulation scheme but the same modulation scheme must be used for all sub-carriers. For the measurements, only BPSK is being used. The data rate of this system should be based on the highest QAM modulation that yield the targeted uncoded BER of 10^{-3} . Based on the estimated SNR of the k^{th} sub-carrier from Section 5.3, the probability of symbol error for each sub-carrier using M-ary QAM, $P_{M;k}$ can be calculated using the following [6]

$$P_{M;k} = 1 - (1 - P_{\sqrt{M}})^2 \quad (5.7)$$

$$P_{\sqrt{M};k} = 2 \left(1 - \frac{1}{\sqrt{M}} \right) Q \left(\sqrt{\frac{3}{M-1} SNR} \right) \quad (5.8)$$

As mentioned in Section 3.2, the QAM bit assignments are gray-coded. It can be assumed that a symbol error corresponds to a bit error where each symbol contains $\log_2 M$ bits. The BER for the k^{th} sub-carrier using M-ary QAM can be calculated

Location	BPSK(Measured)	BER		
		4-QAM	16-QAM	64-QAM
A	-	1.76×10^{-7}	1.26×10^{-3}	×
B	2.47×10^{-6}	4.17×10^{-4}	2.14×10^{-3}	×
C	3.59×10^{-2}	×	×	×
D	6.96×10^{-4}	1.95×10^{-3}	×	×
E	-	1.51×10^{-5}	2.30×10^{-3}	×
F	-	5.71×10^{-9}	1.30×10^{-4}	3.60×10^{-3}
G	2.27×10^{-2}	×	×	×
H	3.80×10^{-3}	×	×	×
I	1.03×10^{-3}	×	×	×
J	4.55×10^{-2}	×	×	×
K	8.41×10^{-3}	×	×	×
L	1.11×10^{-1}	×	×	×

Table 5.12: Finding the highest QAM modulation that yield a $\text{BER} \leq 10^{-3}$ for a normal OFDM System at Locations A to L (BPSK $\text{BER} \geq 2.4 \times 10^{-6}$ shown)

using the probability of symbol error per sub-carrier, $P_{M;k}$

$$\text{BER}_{M;k} = \frac{P_{M;k}}{\log_2 M} \quad (5.9)$$

The expected BER of this system for M-ary QAM would be the mean $\text{BER}_{M;k}$ of all the sub-carriers used. Using Equations 5.7 to 5.9, Table 5.12 finds the highest QAM modulation that yields a $\text{BER} \leq 10^{-3}$.

Based on Table 5.12, the highest QAM modulation that gives BER less than 10^{-3} is selected and its data rate, R_{NORM} is computed. Bits per OFDM packet N_{BPS} and R with respect to each location A to K are given in Table 5.13 where T_{SYM} is $1.2\mu\text{s}$.

5.4.6 Comparison of WiGLAN to a normal OFDM system

The throughput gain of the WiGLAN system compared to a normal OFDM system is computed. The upper bound on this gain, G_{UB} and the effective gain G_{eff} are

<i>Transmitter Location</i>	Modulation	N_{BPS}	$R_{NORM} = N_{BPS}/T_{SYM} (Mbps)$
A	4-QAM	184	153
B	4-QAM	184	153
C	-	0	0
D	BPSK	92	77
E	4-QAM	184	153
F	16-QAM	368	307
G	-	0	0
H	-	0	0
I	-	0	0
J	-	0	0
K	-	0	0
L	-	0	0

Table 5.13: Data Rate for normal OFDM System at location A to K

calculated like the following

$$G_{UB} = \frac{R_{WiGLAN}}{R_{NORM}} \quad (5.10)$$

$$G_{eff} = \frac{R_{WiGLAN;eff}}{R_{NORM}} \quad (5.11)$$

where

- R_{WiGLAN} is the data rate of the WiGLAN where synchronization overhead is not taken into account shown as determined in Section 5.4.3.
- R_{NORM} is the data rate of a normal OFDM System as determined in Section 5.4.5.
- $R_{WiGLAN;eff}$ is the effective data rate of the WiGLAN when the synchronization overhead is taken into account as determined in Section 5.4.4.

Table 5.14 shows the G_{eff} and G_{UB} for locations where the normal OFDM system is capable of transmission. Without considering the synchronization overhead, the average data rate of the WiGLAN system is 2.57 times the average data rate of a normal OFDM system. Realistically, the average data rate of the WiGLAN system is 1.44 times the average data rate of a normal OFDM system.

<i>Transmitter Location</i>	R_{NORM} (Mbps)	R_{WiGLAN} (Mbps)	$R_{WiGLAN;eff}$ (Mbps)	G_{UB}	G_{eff}
A	153	315	161	2.06	1.05
B	153	355	170	2.32	1.11
C	0	186	118	-	-
D	77	220	131	2.86	1.70
E	153	330	160	2.16	1.05
F	307	365	172	1.19	0.56
G	0	85	67	-	-
H	0	52	44	-	-
I	0	140	98	-	-
J	0	18	17	-	-
K	0	88	69	-	-
L	0	10	9	-	-
Average	180	101	70	2.57	1.44

Table 5.14: Throughput gain of WiGLAN compared to Normal OFDM System

It is noted that the normal OFDM system and the WiGLAN system used for comparison both target uncoded BER of 10^{-3} . It might be argued that the throughput gain should be compared when the systems are coded to meet a coded BER of 10^{-5} . It is not difficult to find an appropriate code to drive the BER of the normal OFDM system from 10^{-3} down to 10^{-5} . The same code can be applied to the WiGLAN and the BER performance will be better than the normal OFDM system. This is due to the fact that the WiGLAN does not face a Rayleigh channel as opposed to the normal OFDM system. Hence comparing the throughput gain for the WiGLAN system to a normal OFDM system for a targeted uncoded BER of 10^{-3} actually produces conservative value as it implicitly assumes that the same coding scheme will be used. In reality, it is expected that the throughput gain to be greater because a simpler coding scheme can be applied to the WiGLAN which minimizes the data rate loss due to coding.

5.5 Summary

Several key observations are mentioned in this chapter:

1. The entire baseband design of the WiGLAN node is an implementation of a reasonable size as it fits easily onto one FPGA. The 2-input NAND gate count of the entire transceiver is estimated to be 294,939. This design is clocked at 128 MHz.
2. The Frequency Adaptive Modulation algorithm is shown to be of low complexity as it is only 6% of entire transceiver in terms of gate count.
3. The baseband design is integrated with a custom-made RF Front End with a maximum transmitter power of 7.5 dBm and measurements are taken in a lab environment. The key measurement results are as follows:
 - (a) For link distances of 2.8m to 10.8m in the lab environment, the path loss exponent is 2.80.
 - (b) Frequency Adaptive Modulation reduces the Rayleigh Channel to several Gaussian sub-channels.
 - (c) At a range of 1.0m to 10.8m, the WiGLAN system is capable of:
 - 10 Mbps to 355 Mbps not considering the overhead from Adaptive Modulation.
 - 6 Mbps to 172 Mbps after considering the overhead from Adaptive Modulation.
 - (d) The data rate decreases as a function of link distance.
 - (e) Without considering the synchronization overhead, the average data rate of the WiGLAN system is 2.57 times the average data rate of a normal OFDM system. Realistically, the average data rate of the WiGLAN system is 1.44 times the average data rate of a normal OFDM system. If coding is to be incorporated, the throughput gain would be even higher as simpler codes can be used in the WiGLAN compared to normal OFDM system. This is the result of the WiGLAN not facing a Rayleigh channel.

Chapter 6

Conclusions and Future Research

In this Chapter, conclusions of the thesis are presented and future research directions are explored.

6.1 Conclusions

The goal of the Wireless Gigabit Local Area Network (WiGLAN) project is to characterize empirically the throughput gain from adaptive modulation in wideband wireless environment. To achieve this goal, an Orthogonal Frequency Division Multiplexing (OFDM) baseband modem as documented in Chapter 3 is built on Xilinx Virtex 4 Field Programmable Gate Array (FPGA). This baseband modem is interfaced with a RF Front End. Specifications of this baseband modem and radio-frequency (RF) Front End can be found in Tables 6.1 and 6.2. This prototype is used to explore the Frequency Adaptive Modulation algorithm in Chapter 4. Chapter 5 reports that the entire transceiver design which is clocked at 128 MHz, uses 294,939 2-input NAND gates. This design fits into a single FPGA which means that the design is of a reasonable size. The Frequency Adaptive Modulation algorithm occupied 6% of the entire transceiver baseband design in terms of gates. This means that the logic overhead added on to a normal OFDM system to enable Frequency Adaptive Modulation is small.

Chapter 5 also documents the channel measurements with the WiGLAN nodes of

<i>Parameter</i>	<i>Value</i>
Sampling Frequency	128 MHz
Sub-carrier Frequency Spacing	1 MHz
Number of data sub-carriers	119
Number of pilot sub-carriers	8
IFFT/FFT Period	1 μ s
Cyclic Prefix	.2 μ s
Symbol Period	1.2 μ s
Uncoded BER	10^{-3}
Modulation Per Bin	BPSK, 4, 16, 64, 256 QAM
Max Link Distance	10 m

Table 6.1: Summary of Baseband Specifications

<i>Parameter</i>	<i>Value</i>
Bandwidth	128 MHz
Carrier Frequency	5.25 GHz
Maximum Output Power	7.5 dBm
Noise Figure	4 dB
Bit Resolution of DAC	10 bits
Bit Resolution of ADC	8 bits
Sampling Frequency	128 MHz

Table 6.2: Summary of RF Front End Specifications

a maximum transmit power of 7.5 dBm. The analysis shows that for the WiGLAN system

- it is capable of transmitting from 10 Mbps to 355 Mbps at distances of 1.0m to 10.8m with a target uncoded Bit Error Rate (BER) of 10^{-3} .
- The average data rate from Frequency Adaptive Modulation is 2.57 times the average data rate without Frequency Adaptive Modulation.

However, in order to perform Frequency Adaptive Modulation, there is a synchronization setup time between the transmitter and receiver. When this is taken into account, Chapter 5 reports that for the WiGLAN

- it is capable of transmitting from 6 Mbps to 172 Mbps at distances of 1.0m to

10.8m with a target uncoded BER of 10^{-3} .

- the average data rate from Frequency Adaptive Modulation is 1.44 times the average data rate without Frequency Adaptive Modulation.

It is verified experimentally, that Frequency Adaptive Modulation can decompose a Rayleigh Fading Channel into Gaussian sub-carriers. The WiGLAN system is better than normal wideband OFDM systems because it does not face a Rayleigh fading channel. It relaxes the coding requirements on the Gaussian WiGLAN system.

In addition, the bandwidth in the WiGLAN is better utilized. The sub-carriers in the transition band of anti-aliasing filters are not used in normal OFDM systems. In the WiGLAN, these sub-carriers are used if any one is capable of data transmission.

6.2 Future Research

Future work involves running the entire WiGLAN Frequency Adaptive Modulation Protocol described in Chapter 4 on the FPGA and verify its performance. Subsequently, the topic of immediate interest is to verify the WiGLAN's resilience to narrowband interferer. Since the WiGLAN estimates the signal-to-noise ratio (SNR) of all the sub-carriers independently, it can detect the sub-carriers affected by interferer and avoid transmission in them while continuing transmission on other bins. Without Frequency Adaptive Modulation, the system would have stop transmission in the presence of interferer only in a few bins. Hence Frequency Adaptive Modulation opens up the grounds for cognitive radio where the spectrum is shared between various transceivers. In addition, there are multiple directions that can be explored within the context of WiGLAN that might be of academic interest.

6.2.1 Adaptive CP

Recall from Section 2.2.2 that the length of the Cyclic Prefix (CP) is based on the excess delay spread(X dB). Currently, in the implementation, the CP guards against the worst case for 10 meter with $X = 30$ dB. If a short pulse is sent from the transmitter

to the receiver, it is possible to estimate the excess delay spread(30 dB) and adjust the CP appropriately. As link distance decreases, the excess delay spread(30 dB) would decrease. Hence using this scheme, it is expected that the shorter the link distance, the higher throughput gain compared to our current system.

Another improvement that can be made is to adapt the threshold X in determining the excess delay spread. When the link distance increases, the noise floor increases in relation to the signal. Ideally, the noise floor should determine the threshold X used in the excess delay spread estimate. For this added feature, as the link distance increases, the throughput gain would increase compared to adjusting the CP based on $X=30$ dB. Since Frequency Adaptive Modulation involves computations of the SNR, it should be fairly straightforward to derive the threshold X.

One of the drawbacks of using OFDM is loss of data rate from the insertion of CP. The effects of the CP is kept to the minimum by adaptively adjusting the CP to channel conditions. Admittedly, there is a cost of synchronizing the CP between the transmitter and receiver but this will be negligible compared to synchronizing the modulation schemes assigned to each sub-carrier. If the CP is halved in the WiGLAN system where the symbol period is $1.2\mu s$ and the CP length is $0.2\mu s$, there will be 9% increase in data rate.

6.2.2 Reduction of PAPR

One characteristic of the WiGLAN system is that there might be null channels if the SNR of those sub-channels are bad. Tone Reservation[26] can be used where appropriate tones at the transmitter can be inserted into the null channels to reduce the transmitted signal's PAPR. If the peak power is fixed, a reduction in PAPR would correspond to an increase in average signal power. This allows an increase in the received SNR which will result in either a throughput gain or BER improvement.

However, since the PAPR reducing tones are sent on null channels, it means that at the receiver, these tones are highly attenuated. These tones will then have no effect on the receiver PAPR. Given some channel information at the transmitter, Tone Injection method [26] can be used to inject tones into data channels to reduce the

received PAPR. When the received PAPR is reduced, the Analog-to-Digital Converter (ADC) SNR would increase leading to BER improvement. Note that reducing the transmitted PAPR is not synonymous to reducing the received PAPR. Intuitively, to optimize the reduction of the transmitted and received PAPR, these two steps are performed in sequence:

- Tone injection is performed on data channels to reduce received PAPR.
- Tone reservation is performed on null channels to reduce transmitted PAPR.
As the tones on the null channels are not seen at the receiver, this will have minimal change on the received PAPR.

6.2.3 Adaption of Pilot Sub-carriers

There are 8 pilot sub-carriers to perform phase tracking in the WiGLAN. However, at high SNR, 4 pilot sub-carriers might be sufficient to perform phase tracking. Reducing pilot sub-carriers will increase throughput gain. A scheme can be in place to allocate the number of pilot sub-carriers based on channel conditions.

Another variable that can be adjusted with pilot sub-carriers is its frequency index position. Currently, the locations of these 8 pilot sub-carriers are fixed. The quality of phase tracking is a function of the spacing between sub-carriers and the SNR of the pilot sub-carriers. If the pilot sub-carriers placement occurs at sub-carriers with the best SNR, the quality of the phase tracking is improved at the expense of data rate. Hence a placement algorithm can be developed that gives the best compromise between the quality of phase tracking and data rate.

6.2.4 Development of Better SNR Estimation Scheme

In the WiGLAN, the total power budget is distributed equally between all sub-carriers. During SNR estimation step, all sub-carriers except the DC bin are used hence the power of each sub-carrier is at its minimal. During modulation assignment, as some bins might be null, there will be less sub-carriers transmitting compared to

the SNR Estimation step. This means that if the SNR Estimation was redone with the new (now less) sub-carriers, as each sub-carrier has more power than previously, they will have higher SNR and hence will be assigned higher modulation.

6.2.5 Use of OOK

In the WiGLAN system, each data sub-carrier is Quadrature Amplitude Modulation (QAM)-modulated (i.e. the phase and the amplitude of the sub-carrier are indicative of the bits sent). As the SNR decreases, the channel estimate gets increasingly unreliable. At some point, it might be better to go with other modulation scheme that is less dependent on the channel estimate.

According to [35], for low SNR and no Channel State Information (CSI) is available, the data sub-carrier should be modulated using On-Off Keying (OOK). OOK sends power for a bit 1 and sends nothing for a bit 0. Only the amplitude component needs to be detected for OOK and the phase can be disregarded. Investigation can be performed in real channel conditions to find the SNR region where OOK should be used over QAM. Adding additional granularity would improve throughput gain and quality of reception.

Appendix A

Acronyms

ADC	Analog-to-Digital Converter
AGC	Automatic Gain Controller
AWGN	Additive White Gaussian Noise
BCH	Bose, Ray-Chaudhuri, Hocquenghem
BER	Bit Error Rate
BPSK	Binary Phase-Shift Keying
CFO	Carrier Frequency Offset
CORDIC	Coordinate Rotation Digital Computer
CP	Cyclic Prefix
CPE	Common Phase Error
CRC	Cyclic Redundancy Check
CSI	Channel State Information
CTS	Clear To Send
DAC	Digital-to-Analog Converter

DSP	Digital Signal Processing
FOM	Figure of Merit
FFT	Fast Fourier Transform
FFT	fast fourier transform
FIR	Finite Impulse Response
FPGA	Field Programmable Gate Array
ICI	inter-carrier interference
IFFT	Inverse Fast Fourier Transform
iid	Independently and Identically Distributed
ICI	Inter-carrier Interference
ISI	Inter-symbol Interference
LS	Least Squares
LTI	linear and time-invariant
LLSE	Linear Least Squares Estimator
MAC	Media Access Control
ML	Maximum Likelihood
OFDM	Orthogonal Frequency Division Multiplexing
OOK	On-Off Keying
PA	power amplifier
PAPR	peak-to-average power ratio
PPM	parts per million

PER	Packet Error Rate
QAM	Quadrature Amplitude Modulation
RF	radio-frequency
RTL	Register Transfer Level
RTS	Request To Send
SFO	Sampling Frequency Offset
SNR	signal-to-noise ratio

WiGLAN Wireless Gigabit Local Area Network

Bibliography

- [1] A. P. Chandrakasan, H.S. Lee, and C. G. Sodini. Wireless gigabit local area network. *Microsystems Technology Laboratories Annual Report*, Cambridge, Massachusetts, 2002.
- [2] IEEE Standard 802.11a 1999. *Supplement to Information Technology - Telecomm. And Information Exchange between Technology - Telecomm. and Information Exchange between Systems - Local And Metropolitan Area Networks - Specific Requirements - Part 11: Wireless LAN Medium Access Control (MAC) and Physical Layer (PHY) Specifications High-speed Physical Layer in the 5 GHz Band*, 1999.
- [3] EWC. *HT Physical Specifications - Enhanced Wireless Consortium publication*, v1.29 edition, Dec 2005. 802.11n Draft Standard.
- [4] Anuj Batra. *Multi-band OFDM Physical Layer Proposal for IEEE 802.15 Task Group 3a*, 10 November 2003.
- [5] Theodore S. Rappaport. *Wireless Communications Principles and Practice*. Prentice Hall Communications Engineering and Emerging Technologies Series. Prentice Hall, Upper Saddle River, NJ, second edition, 2002.
- [6] John Proakis. *Digital Communications*. McGraw-Hill, New York, NY, fourth edition, 2000.

- [7] Nir Matalon. An implementation of a 5.25 ghz transceiver for high data rate wireless applications. Master's thesis, Massachusetts Institute of Technology, Department of Electrical Engineering and Computer Science, July 2005.
- [8] S.S. Ghassemzadeh, R. Jana, C.W. Rice, W. Turin, and V Tarokh. Measurement and modeling of an ultra-wide bandwidth indoor channel. *IEEE Transactions on Communications*, 52(10):1786 – 1796, October 2004.
- [9] Xilinx Logicore. *Fast Fourier Transform v3.2*, 11 January 2006. DS260.
- [10] M Speth, SA Fechtel, G Fock, and H Meyr. Optimum receiver design for wireless broad-band systems using ofdmpart i. *IEEE Transactions on Communications*, 47(11):1668 – 1677, November 1999.
- [11] T Pollet, M Van Bladel, and M Moeneclaey. Ber sensitivity of ofdm systems to carrier frequency offset and wiener phase noise. *IEEE Transactions on Communications*, 43(234):191 – 193, February-April 1995.
- [12] T. Pollet, P. Spruyt, and M. Moeneclaey. The ber performance of ofdm systems using non-synchronized sampling. In *Proc. IEEE Globecom.*, volume 1, pages 253 – 257, San Francisco, CA, June 1994.
- [13] P. Robertson and S. Kaiser. Analysis of the effects of phase-noise in orthogonal frequency division multiplex (ofdm) systems. In *Proc. IEEE International Conference on Communications(ICC95)*, pages 1652 – 1657, Seattle, June 1995.
- [14] Alan V. Oppenheim, Ronald W. Schafer, and John R. Buck. *Discrete-Time Signal Processing*. Prentice Hall Signal Processing Series. Prentice Hall, Upper Saddle River, NJ, second edition, 1999.
- [15] John Terry and Juha Heiskala. *Wireless OFDM LANs: A Theoretical And Practical Guide*. Sam Publishing, Upper Saddle River, NJ, 2002.
- [16] R Lyons and A Bell. The swiss army knife of digital networks. *IEEE Signal Processing Magazine*, pages 90 – 100, May 2004.

- [17] T.M. Schmidl and D.C. Cox. Low-overhead, low-complexity [burst] synchronization for ofdm. In *Proc. IEEE ICC'96*, volume 3, pages 1301–1306, Dallas, TX, June 1996.
- [18] Xilinx Logicore. *Cordic v3.0 Product Specification*, 21 May 2004. DS249.
- [19] U. Meyer-Baese. *Digital Signal Processing with Field Programmable Gate Arrays*. Prentice Hall Communications Engineering and Emerging Technologies Series. Springer-Verlag, Berlin Heidelberg, second edition, 2004.
- [20] Randal E. Bryant and David O'Hallaron. *Computer Systems A Programmer's Perspective*. Prentice Hall, Upper Saddle River, NJ, 2003.
- [21] J.-J. van de Beek, O. Edfors, M. Sandell, S.K. Wilson, and P.O Borjesson. On channel estimation in ofdm systems. In *Proc. IEEE Vehicular Technology Conf'95*, volume 2, pages 815–819, Chicago, IL, July 1995.
- [22] Xilinx Logicore. *Pipelined Divider v3.0 Product Specification*, 28 April 2005. DS305.
- [23] Dennis D. Wackerly and William Mendenhall III. *Mathematical Statistics with Applications*. Duxbury Advanced Series. Duxbury, Pacific Grove, CA, sixth edition, 2002.
- [24] Charles J. Meyer. *Measuring the peak-to-average power of digitally modulated signals*. Boonton Electronics, 1 April 1993. Application Note AN-50.
- [25] S.H. Lee and J.H. Lee. An overview of peak-to-average power ratio reduction techniques for multicarrier transmission. *IEEE Wireless Communications*, pages 56 – 65, April 2006.
- [26] Jose Tellado. *Multicarrier Modulation with Low PAR Applications to DSL and Wireless*. Kluwer Academic Publishers, Norwell, MA, 2000.
- [27] Athanasios Papoulis and S. Unnikrishna Pillai. *Probability, Random Variables and Stochastic Processes*. McGraw-Hill, New York, NY, fourth edition, 2002.

- [28] James F. Kurose and Keith W. Ross. *Computer Networking A Top-Down Approach Featuring the Internet*. Pearson Education, Inc, second edition, 2002.
- [29] Bernard Sklar. *Digital Communications Fundamentals and Applications*. Prentice Hall, Upper Saddle River, NJ, second edition, 2001.
- [30] W. Yu and M. Cioffi. Constant-power waterfilling: Performance bound and low-complexity implementation. *IEEE Transactions on Communications*, pages 23 – 28, January 2006.
- [31] Xilinx. *Virtex-4 User Guide*, 10 September 2004.
- [32] M. Wouters, G. Vanwijnsberghe, P. Van Wesemael, T. Huybrechts, and S. Thoen. Real time implementation on fpga of an ofdm based wireless lan modem extended with adaptive loading. In *Solid-State Circuits Conference, 2002. ESSCIRC 2002. Proceedings of the 28th European*, pages 531 – 534, September 2002.
- [33] R.F.H. Fischer and J.B. Huber. A new loading algorithm for discrete multitone transmission. In *IEEE Proc. GLOBECOM'96*, pages 724–728, London, England, November 1996.
- [34] Cihan Tepedelenlioglu, Ali Abdi, and Georgios B. Giannakis. The ricean k factor: Estimation and performance analysis. *IEEE Transactions on Wireless Communications*, 2(4):56 – 65, July 2003.
- [35] S. Misra, A. Swami, and L. Tong. Cutoff rate analysis of the gauss-markov fading channel with binary inputs and partial csi at the receiver. In *Proc. 2003 Conf. Info. Sci. and Systems*, Baltimore, MD, 2003.